Small-signal Stability Analysis and Power System Stabilizer Design for Grid-Connected Photovoltaic Generation System

by

Akshay Kashyap

A thesis submitted to the Faculty of Graduate and Postdoctoral Affairs in partial fulfillment of the requirements for the degree of

Master of Applied Science

in

Electrical and Computer Engineering

Carleton University
Ottawa, Ontario

Abstract:

Solar energy is one of the emerging forms of renewable energy, and has been proved to be a potential source for generation of electricity. However, the rise in number of photovoltaic (PV) generators presents issues for electric power utilities. Thus, integration of a PV system to the grid, is an important area of research. Out of the various issues faced by the utilities, one of the main issues is related to power system stability.

The objective of this thesis is to achieve stability for a grid-connected PV system with the proposed new power system stabilizer (PSS). Stability is attained by conducting small signal analysis and time domain analysis on the investigated PV system. First, time domain analysis on detailed and average PV system models without PSS is performed. Second, small signal stability analysis on average PV system model with and without PSS is performed. It is observed that the damping effect and the dynamic stability of the investigated PV system are achieved, with the help of the proposed new PSS

Acknowledgements:

"*I am deeply grateful to my thesis supervisor for his untiring support, encouragement and guidance throughout the entire research. Thank you Sir, for sharing your passion for good research in the area of Power System Stability with me.*"

- **to Professor Xiaoyu Wang**

"A very significant thanks to you for the support and for being patient with me in our numerous discussions."

- **to Shichao (Systems and Computer Eng. Dept)**

"Thanks to my research collaborators for the thoughtful insights and helping me think with an open mind for approaching my research."

- **to Rahul Kosuru & Jian Xiong**

"Sir you provided great technical support and made sure we used the latest software for our research in Hydro Lab."

- **to Mikhail Nagui**

"Thank you for making all the administrative procedures, especially regarding registration, so easy."

- **to M/s. Anna Lee & Staff of DOE**

"Thanks for the great moral support you guys provided throughout my degree, and for being there for me always."

- **to Ashwini Sadekar & Satwik Shetty**

"I appreciate your love and patience for me and without your support, I couldn't have achieved this important step of my life."

- **to Mom, Dad & Shirin**

Contents

List of tables:

List of figures:

List of Abbreviations

PV	Photovoltaic
PV-DG	PhotoVoltaic-Distributed Generation
PSS	Power System Stabilizer
I_{SC}	Short-circuit Current
MPPT	Maximum Power Point Tracking
PLL	Phase Lock Loop
PCC	Point of Common Connection
VSI	Voltage Source Inverter
P	Active Power
Q	Reactive Power

Chapter 1

Introduction

1.1 Background

Renewable energy sources have enormous potential and are capable of generating energy levels much greater than the current world demand. The use of such sources can help to reduce pollution, increase environmental sustainability, and lower the consumption of fossil fuels. Increasing climate changes, coupled with the depletion of fossil fuels, are the main driving forces for renewable energy legislation, incentives, and commercialization. The principal types of renewable energy sources include solar, wind, and hydro. Solar power is one of the most promising renewable sources, as it is more predictable than wind energy, and less vulnerable to seasonal changes as hydro power. Power generation by hydro or wind is restricted to the sites where resources are available. Solar energy can be harnessed at the point of demand both in rural and urban areas, thus decreasing the cost of transmitting the electricity (costs of transmission). Grid connected Photovoltaic (PV) systems that are connected to the distribution level, particularly with MW capacity, are increasing at an aggressive rate, in order to meet the energy demand. However, there is less experience in the interconnection of utility-scale PV systems with the distribution network, where loads are present. The Grid or also known as the utility is an interconnected network, which supplies electricity to the consumers. This interconnected network consists of resources for transmission and distribution of power or electricity from the generation station to a distribution station, via high-voltage transmission lines. This voltage is then delivered to the customers, from the distribution stations.

Utility-scale PV systems need special attention, unlike small scale PV systems, which are limited to a few hundreds kW and are unlikely to show an impression on the distribution

system. Thus, there is a need to analyze the large scale, three-phase PV systems employed as Photovoltaic Distributed Generation (PV-DGs), in terms of performance, dynamic characteristics, and control. D.M Chapin, C.S Fuller, and G.S. Person of Bell laboratory patented the solar cell, in 1954. The next year, Hoffman Electronics' semiconductor division announced the first commercial photo- voltaic product that was 2% efficient, priced at 25$ per cell, and generating power of 14 mW each. By 1980, photovoltaics began finding many off-grid applications such as pocket calculators, highway lights, and small home applications. By 2002, worldwide photovoltaic power production reached 600 MW per year, and was increasing at a rate of over 40% per year. The continued discovery and development of silicon and other photovoltaic materials have helped increase cell efficiency and decrease cost. At present, solar PV power costs less than 2$ per watt [1]. The total global solar photovoltaic capacity is fast approaching the 100 GW milestone, as per the International Energy Agency. [4] About 37 GW was connected to the grid in 2013, and almost the same amount in 2012. Europe currently represents 59% of the world PV market, but is facing competition from the Asia-Pacific Region. In 2012, China was the second-largest PV market for new installations [3], thus placing solar power generation in second position in terms of the new sources of power generation.

Solar Photovoltaic Distributed Generation (PV-DG) systems represent one of the fastest-growing types of renewable energy sources worldwide, currently being integrated into distribution systems [2]. The most crucial aspect of the system is that the technical requirements of the utility power system need to be satisfied to ensure the safety of the PV installer and the reliability of the utility grid [5]. It is very important to understand the technical requirements when performing an interconnection between two systems. For example, critical interconnection problems such as harmonic distortion, islanding detection, and

electromagnetic interference need to be identified and solved. The interconnection of PV systems with the grid is accomplished with the help of a supply electric power to electrical equipment. The inverter plays an important role in this interconnection. There is a need for the PV arrays and inverter to be characterized based on the geographical location of the PV system and the installation configuration, but also based on the defects that occur during the operation of the system [6-10]. In a grid-interconnected PV system, the inverter plays a key role, and its reliability and safety are of the utmost importance to the system. As part of the PV-DG plant interconnection impact studies, which include the typical power flow analysis, an in-depth research is required into the potentially dynamic impacts of PV-DG units on the feeder voltages under various load conditions. The investigation into the dynamic impacts of the system lead to the development of various control strategies/techniques needed for the stability and smooth operation of the PV-DG systems.

1.2 Review of Power System Stabilizers

As the power systems evolved over time, the stability problems associated to them have increased. Power system stability, as defined in [11], is the ability of an electric power system for an initial operating condition to regain the state of operating equilibrium after being subjected to a physical disturbance. The power network system or grid is a highly changing environment, whose various parameters are subject to change continually. A stabilizer tries to keep these continually changing parameters at their original or steady states, to ensure the smooth operation of the power system. Thus, [11] & [12] show the importance of stability for a power system. This portion of the thesis will review the different types of power system stabilizers that have previously been proposed. The detailed design and description of the proposed power system stabilizer in this research is presented in Chapter 4. The PV system

designed in this thesis makes use of controllers to control the DC voltage collected at the output of the boost (DC-DC) converter, as well as the reactive power. They also control the grid's voltage and power. The power system stabilizer can be applied to either the input side of the controllers or the output terminals of the inverter, where the grid voltages and power can be stabilized. In this thesis, the power system stabilizer is connected to the output of the DC voltage controller at the input of the inner loop current controller. Reference [13] explains the modeling of various power system components, such as power system networks, loads, synchronous generators, excitation systems, and power system stabilizers (PSS). A PSS [14] is an additional block of a generator excitation control, added to improve the dynamic performance of the overall power system, particularly to damp the power/frequency oscillations.

The PSS structure employed in [13], uses the rotor angle deviation as an auxiliary stabilizing signal, which is applied at the input of the controller, based on the literature from [15-18]. The difference between this and the proposed thesis is the stabilizing signal and its point of application in the PV system. Reference [19] discusses the use of a robust controller for damping low frequency power oscillations in a PV power plant, as the PV plant is subject to various positive and negative influences caused by the oscillations in power, depending on various factors such as location and size of the PV plant. Generally, for oscillation damping or stabilizing, the real power modulation technique is considered. When damping or stabilizing, control is based on real power modulation, and renewable energy sources normally have to curtail their real power output [20-22], thus making use of reactive power modulation techniques for power oscillation damping. Reference [19] utilizes a PSS design with a rotor speed deviation as the input auxiliary stabilizing signal, and also has an additional block for the lead-lag phase compensation in the PSS. Reference [23] talks about a damping technique

that can be achieved through independent control of the flow of real power from the stabilizer and the voltage at the point of common coupling, which is positioned between the stabilizer and the grid system. Instability problems resulting from inter-area oscillations are caused by insufficient system damping and relatively weak tie-line connectors. If no appropriate action takes place, then this oscillation may endanger the power network [25-29].

The design of the intermediate bus voltage feedback controller using the frequency technique helps achieve damping. This controller uses the frequency as a stabilizing signal for the system, compared with the PSS proposed in this thesis, where no voltage feedback controller is used. Reference [30] discusses a power system stabilizer with positive voltage feedback to facilitate anti-islanding schemes in inverter-based distributed generator DG's. This research tries to detect the variations that may occur in the DG-terminal voltage to generate a positive feedback signal. The DG is a PV system to take into consideration, as the technique used to find the feedback signal is similar to that of a PSS design. The PSS design in this thesis is used for stability purposes only.

Reference [12] provides a detailed analysis of various power system stability parameters and their designs for large generating stations. The detailed analysis of the power system is essential to the identification of the various parameters that affect the system, so that a technique can be established for adequately stabilizing the system. The PSS in [30] connects to the overall system as part of an excitation system. This is a result of a machine being connected to the system, as mentioned in the reference. Reference [31] talks about a control strategy for the dynamic stability of a grid-connected PV system.

The main reason for having control techniques to support dynamic stability is the complexity of PV penetration issues. Issues such as active power variation, bus voltage fluctuation, reactive power flow, system stability etc., are all related to PV penetration. The control strategy

proposed in [31] to achieve dynamic stability includes the design components of a PSS, thus not requiring an additional PSS block; it was able to successfully dampen the signal caused by any faults occurring in the system. A reasonable amount of literature is available on the effects of PV penetration [44] on the dynamic stability of a power system. Therefore, it is important to realize the parameters that are affecting the system stability and to try and control these parameters, in order to ensure the smooth functioning of any complex power system. The functionalities of a damping controller and of a power system stabilizer are basically the same. The two try to achieve system stability by damping the signal that is identified as the critical parameter or the signal affecting system stability.

The techniques mentioned above to achieve stability in a grid-connected PV system, differ from the technique proposed in this thesis. Firstly, the thesis proposes a model with no machine. Thus, no need of an excitation system design as, mentioned in [24] and [12], [15], [29], [31]. Secondly, the network frequency is used as the auxiliary stabilizing signal, which is fed to the proposed power system stabilizer. This, PSS is applied at the input of the inner loop current controller.

Lastly, the proposed power system stabilizer helps achieve higher stability and better damping of oscillations. This is achieved, due to a better understanding of the critical parameters affecting system stability. Thus, helping in selecting an appropriate stabilizing signal. The detailed design of the PSS and its parameters are explained in Chapter 5.

1.3 Photovoltaic Systems

Solar energy can be exploited through solar thermal and solar photovoltaic systems, for a variety of applications. While solar thermal utilizes the heat energy of the sun, photovoltaic technology is enabled by the direct conversion of sunlight energy to electricity through a

semiconductor device called solar cell or photovoltaic cell. The output of a solar cell is about 2 to 3 W at 0.5 to 0.7 V, which is a level that has limited applications. Several cells are connected in a series in order to obtain useful voltage. Such series connected cells are sealed in a weatherproof package, which forms a photovoltaic (PV) module.

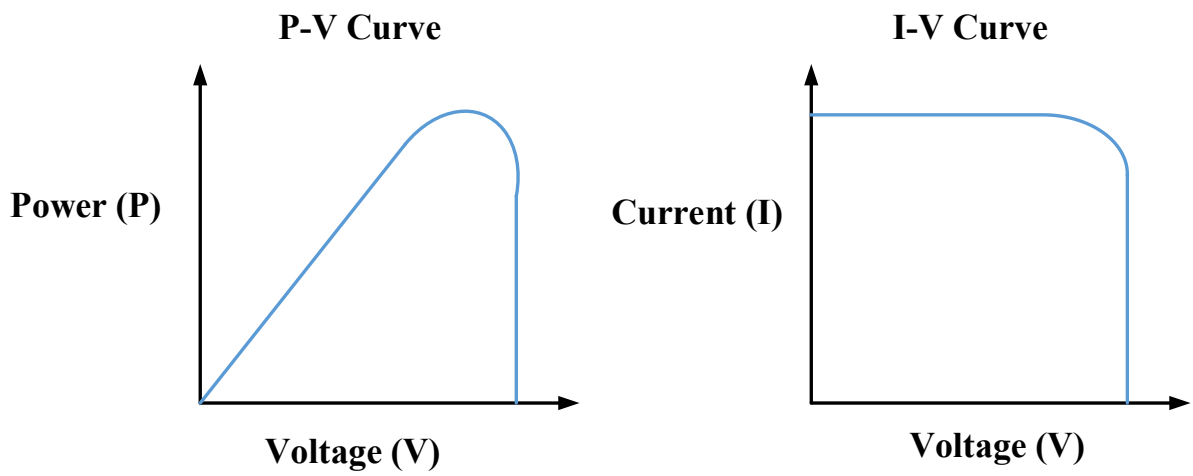

Figure 1.1: The current and power characteristic curves of PV Source.

Based on the power requirement, several PV modules are connected in series and in parallel combinations to form a PV array. General characteristics of PV sources, i.e., the current and power curves (PV array or PV module) are shown in Figure 1.1.

From the Figure 1.1 it can be observed that the power output of the PV source depends on the voltage and the current generated in the panel. In the Figure 1.1, I_{sc} and V_{oc} are the short circuit current and open circuit voltage of the PV source. V_{mp} and I_{mp} are the voltage and current at which the PV source can deliver maximum power P. Hence, a power conditioner is needed to operate the PV source at maximum power point.

Photovoltaic systems use PV sources to generate electricity, and can provide both DC and/or AC outputs. They can be operated isolated or interconnected to a utility grid. PV systems are classified according to their functional and operational requirements, their component

configuration, and how they are connected to other power sources and loads. The two basic classifications are stand-alone (off-grid) and grid connected systems.

1.3.1 Stand-alone PV system

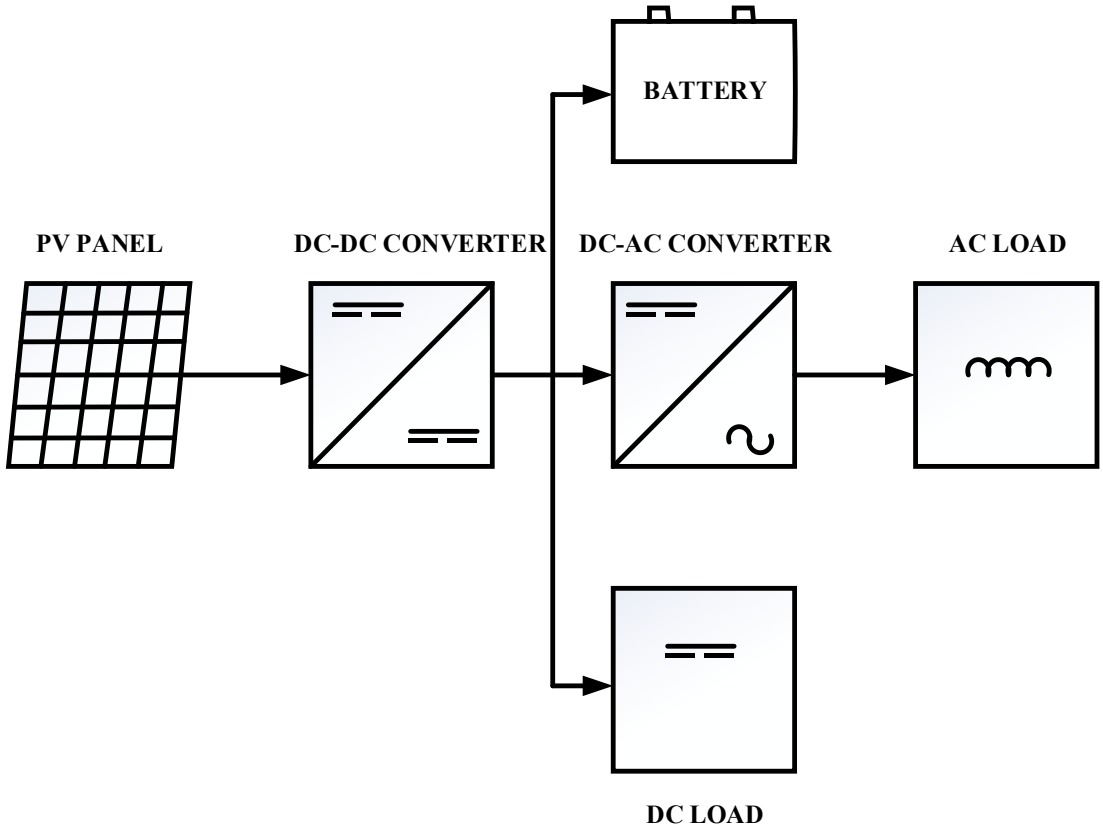

Figure 1.2: Block diagram of a PV Stand Alone system

Stand-alone systems produce power independent to the utility grid. They are appropriately suitable for remote and environmentally sensitive areas such as national parks and residences which are located remotely. Figure 1.2 shows the block diagram for a Stand Alone PV system. These PV systems are immune to system blackouts and do not rely on penetration of long distance transmission lines. Main disadvantage of this system is they only work in day light hours and battery storage is required, so that excess energy produced during day can be stored and used in night. However, with batteries it require additional cost, maintenance and increases the complexity of control.

1.3.2 Grid connected PV system

To feed the continuously increasing electric consumers, the distribution lines are generally extended beyond the acceptable lengths. Figure 1.3 shown below is the block diagram for a grid connected PV system. This results in a poor voltage profile for the customers at far end. Moreover, feeding power to various load centers through transmission lines causes a significant amount of power losses. By installing a power generating source at the distribution level overcomes these problems. Installation of a generating source at the distribution level also eliminates the need of upgrading the transmission lines and their associated switch gear.

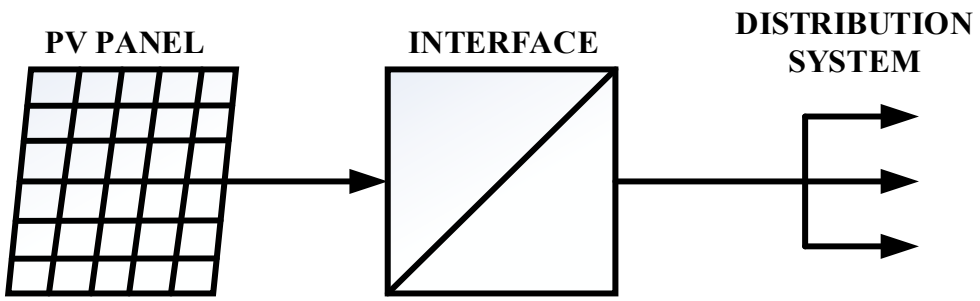

Figure 1.3: Block diagram for a Grid connected PV system

Due to these economic and regulatory factors, the vast majority of the PV systems are connected to the existing distribution network in the form of Photovoltaic Distributed Generation (PV-DG) instead of connecting to the transmission network. Unlike stand-alone systems, these do not require batteries. The interface requirement between the PV sources and utility grid depends upon size and application.

1.4 Concept of PV-DG

PV systems connected to the distribution network can be basically classified into three types, they are described in the following subsections [2].

1.4.1 Utility-scale PV-DG

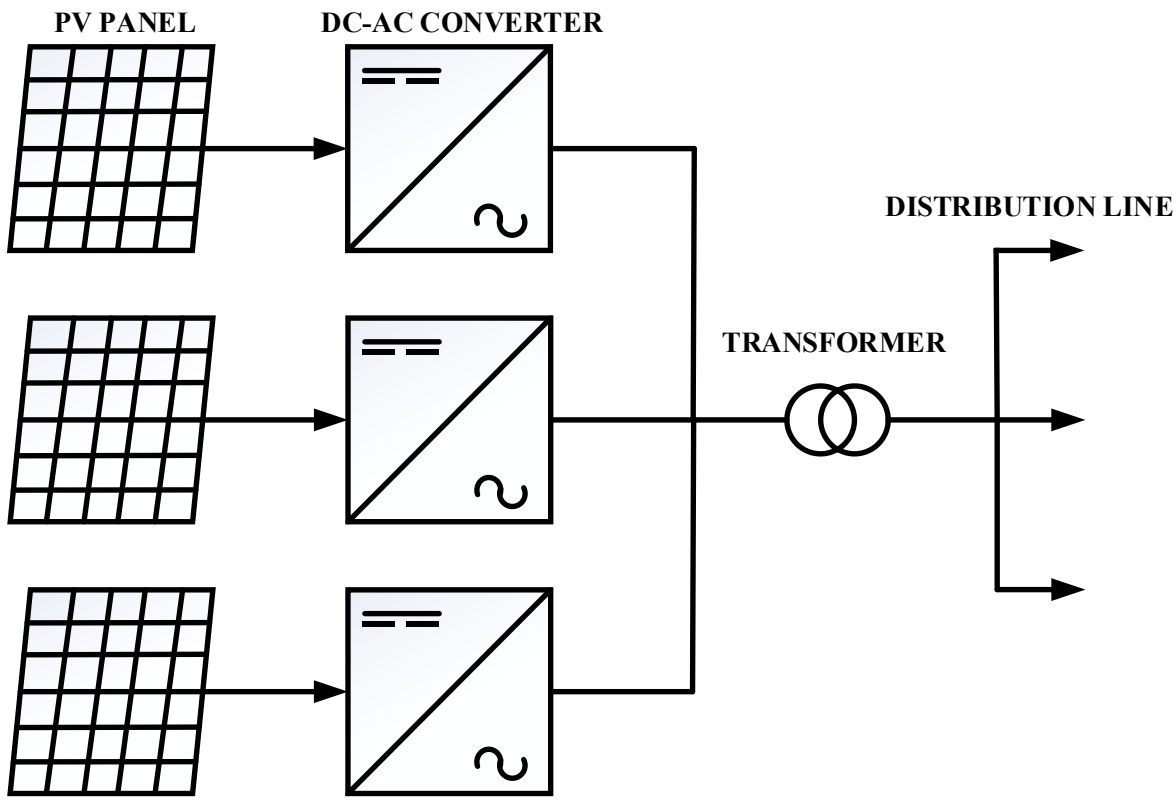

Figure 1.4: Block diagram Utility Scale PV-DG system

PV systems ranging from 1 to 10 MW are utility scale PV-DG. These are directly connected to conventional feeders or distribution substation via express feeders. Utility scale PV-DG has nominal capacities compatible with substation ratings or manageable by medium-voltage distribution feeders. These are typically three-phase and requires one or more transformers.

A MW-size PV-DG plant generally includes several power electronic DC-AC converters (inverter) modules connected in parallel that vary in size depending on the model and manufacturer as shown in the Figure 1.4.

Each inverter is equipped with both internal and external protection schemes such as fast overcurrent protection, under and over voltage and frequency safeguards, as well as active anti-island protection schemes to prevent the PV system from feeding power to the grid in

the event that the utility grid connection is lost.

1.4.2 Medium scale PV-DG

PV systems whose capacity are in the range of 10 to 1000 kW are categorized under medium-scale PV-DG. These are mainly installed on small or large buildings such as residential complexes, retail stores, government sites and other buildings. Their typical interconnection configuration depends on the capacity of the PV system. Larger plants (those with the capacity in hundreds of kW) may typically have installation similar to utility-size PV-DG, including separate interconnecting transformer, with the main difference in the nominal rating of the associated equipment (transformers, inverters and switchgears). Smaller plants in which the PV system capacity is comparable to the load may have typical installations similar to small scale PV systems, using existing customer transformers, with minor changes in the interconnection.

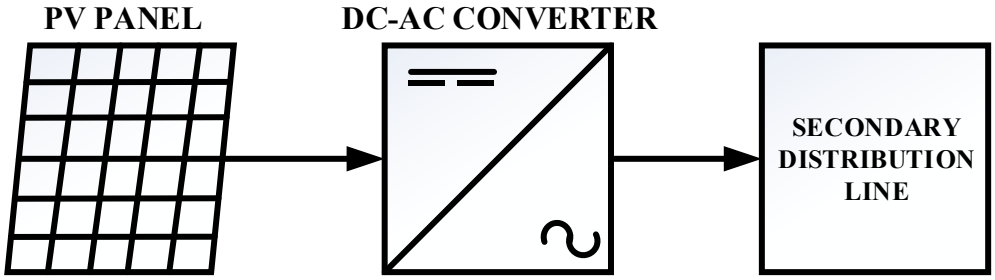

Figure 1.5: General representation of Medium scale PV-DG

1.4.3 Small scale PV-DG

PV systems having capacity less than 10 kW are small-scale PV-DG. These are installed at customer roof tops and connected to secondary distribution lines (230 V). These systems are usually a single-phase or three-phase and produce less power required to consumer and do not need transformer for interconnection as shown in Figure 1.5.

The PV-DG topology shown previously are called as single-stage grid-connected inverter

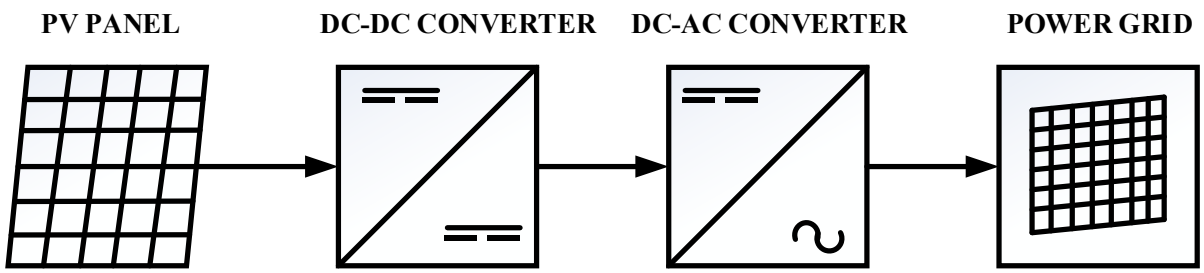

Figure 1. 6: General block diagram representing a Two-stage topology of PV-DG

configuration because there is only inverter in between the PV source and grid. The other topology generally used by PV-DG is two- stage configuration, which have a DC-DC converter and DC-AC converter as shown in Figure 1.6. The disadvantages with the Two-stage topology of PV-DG are the two-stages itself, i.e. with an increase in converter stages leads to increase in losses, low reliability and high cost. In this thesis, a two-stage, three-phase PV system connected to distribution network through distribution transformer is considered.

1.5 Motivation and Thesis Objectives

In the past, typical applications of distribution generation generally included reciprocating engines or small hydro plants, where AC power injection was relatively constant. The PV system has the intermittent resource characteristics that vary the power output throughout the day and requires the conversion of DC-AC power through inverters and having higher power rating with sophisticated control.

The proliferation of PV systems represents a less familiar challenge for distribution utilities and gives rise to various impacts which are different from that of the conventional DGs because of its different characteristics. So there is requirement for in depth investigation of potential dynamic impact of PV system on the distribution network under various load and generating conditions. The major motivation of the thesis, is to identify the oscillations occurring in the

grid-connected PV system. To develop a technique, to achieve damping of these oscillations to provide a stable power system.

Despite the need, there is no standard bench mark model of large scale PV systems for power system simulation studies. Thus, there is a need for developing an accurate model for studying the impact of PV system on distribution network [4]. Moreover, the components (inverter, PV sources etc.) present in PV system are supplied by different manufactures, who may not disclose their product dynamic properties (control structure or methodology, parameters). Therefore, the only option is to build an adequate model, which may not exactly represent the real world PV system but provides a satisfactory tool to analyze the PV system by expert point of view. The main objectives of this thesis are:

- To develop the mathematical model for the grid-connected PV system.
- To build an adequate simulation model in MATLAB/SIMULINK for analysis purpose along with the control architecture..
- To design a power system stabilizer, to achieve better stability and damping of oscillations to the grid-connected PV system.
- To perform stability analysis on the grid-connected PV system with the proposed control technique.

1.6 Thesis Organization

This thesis is organized in six chapters. The current chapter discusses briefly the history of PV generation and various types of PV generations. It describes the basic architectures of different types of PV system and its components. It emphasizes the necessity of studying the impact of PV system on distribution network. It presents the literature survey/state of the art on the controller design and sets the motivation for the present work carried out in this thesis.

In Chapter 2, first a circuit based PV array is modeled. Then mathematical model of the PV system interfaced with stiff grid in dq reference frame is described. Based on the mathematical model, controller for the AC side grid current and PLL are developed. A controller is proposed in order to design the DC-link voltage controller instead of the Active Power Controller. The simulations of the detailed switched model with the proposed control strategy are evaluated at different operating conditions of PV system.

Chapter 3 describes the development of the small signal model, its stability and the eigenvalue analyses of the overall PV system model. In this chapter, the nonlinear equations of the entire PV system are linearized around an equilibrium point. The responses of the linearized model are compared with the responses of the detailed switched model, for verifying the small signal linearized model. An eigenvalue analysis of the linearized model is carried out, so as to observe the various types of interactions in the PV system, help to understand the dynamics of the system, to determine the robustness of the entire PV system, and to identify the control of the system against parameter variations.

Chapter 4 deals with the design and development of the damping controller. The new proposed controller's mathematical model is developed into a Simulink model. A linearized model of the entire PV system with the controller is carried out so as to compare the responses of the two systems thus verifying the linearized model design. The chapter is concluded with the comparison of the PV system with and without damping controller.

Chapter 5 develops a linearized mathematical model for PV system and distribution network. The responses of the new PV system are recorded and analyzed for impacts of PV system on the network and check for parameters which affect the stability of the system.

Chapter 6 concludes the entire thesis and provides scope for future research.

Chapter 2

Structure of the Grid-connected Photovoltaic System

2.1 Introduction

This chapter focuses on the overall design of a PV system interfaced with a grid/stiff grid or utility. In the design, we give a description of each of the components of the PV system, namely the PV module, the boost converter, the inverter, and the grid. This description helps to understand the functionality of each component of the system, leading to its detailed mathematical design, the results of which are shown in the following chapters.

In this part of the thesis, a detailed description of the parts of the two-stage grid connected PV system is provided. The research conducted for each of these major parts of the PV system has helped us understand why each particular component is required in the system. We also mention the type of photovoltaic cell, DC-DC converter, and DC-AC converter model that has been selected as part of this research.

The chapter has been organized as follows: section 2.2 speaks of the overall system architecture, providing a glimpse of the architecture of the two-stage PV system connected to a grid. It is followed with sections describing the PV cell, the MPPT controller, the DC-DC converter, the DC-AC converter, and finally the phase lock loop PLL.

2.2 Overall System Architecture

Figure 2.1 shows the single line diagram of a two-stage PV system that is interfaced with the stiff grid, represented by voltage source V_g. The main components of PV system are the PV array, the DC-DC converter, the VSI or inverter, and the three-phase LC interfacing filter. The PV array is connected to the DC side terminals of the VSI. The DC-link capacitance of the VSI is represented by C. The AC side terminals of the VSI are interfaced with the LC filter.

Each phase of the filter has a series reactor and shunt capacitor. The inductance and resistance of the reactor are represented by L and R respectively.

A parallel RLC load is connected to the system. P and Q represent the active and the reactive power, respectively, that is delivered from the PV system to the grid, at Point of Common Connection (PCC). Figure 2.1 also illustrates different control aspects involved in a PV system. Phase Locked Loop (PLL) is used to extract the phase angle (θ) and frequency (ω) at PCC. The current controller is used to control the AC side inverter currents. A DC-link voltage controller is used to maintain the PV array voltage (V_{dc} or V_{pv}) at the reference value V_{dcref} which is given by the MPPT controller. Thus, the Figure 2.1 represents the complete PV generation, conversion and connection to the grid with a load. This model can be assumed for

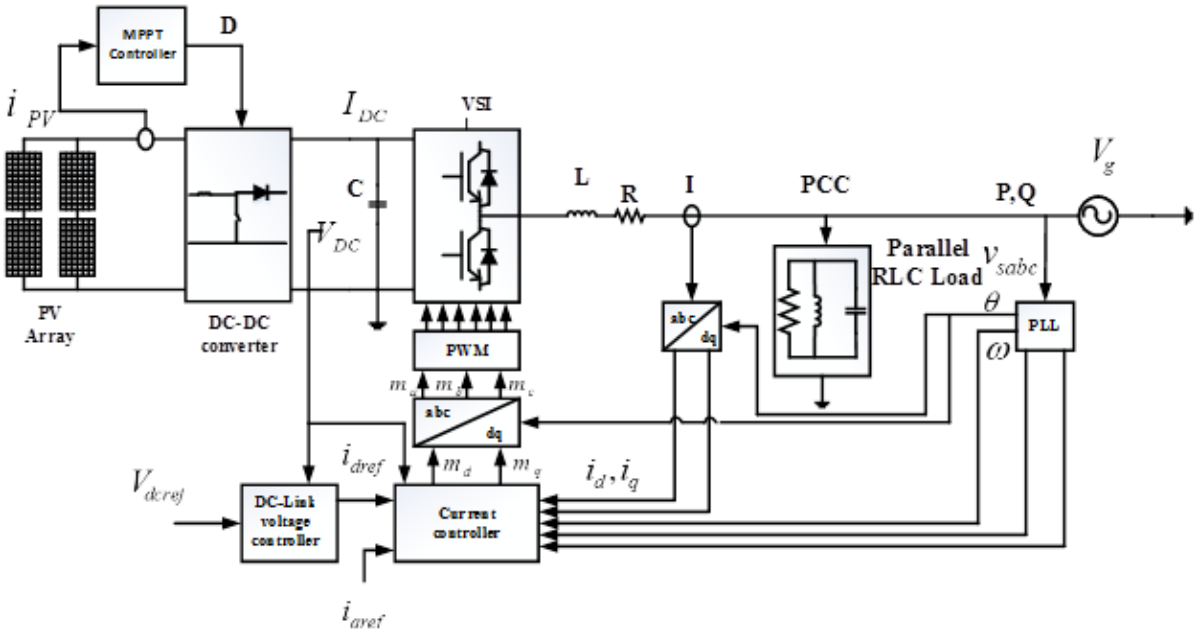

Figure 2. 1: Overall System Architecture

performing stability analysis. It covers the basic architecture of a PV-DG, the mathematical model of this system shall help us identify oscillations occurring in the system. The main motivation, is to deliver maximum and stable supply of power from the PV.

2.3 Photovoltaic (PV) Module

A material or gadget that is equipped to change the energy contained in photons of light into an electrical voltage and current is said to be photovoltaic. The history of photovoltaics can be traced as far back as 1839, to Edmund Becquerel, who caused a voltage to appear by illuminating a metal electrode in a weak electrolyte solution. Since then, the development of photovoltaics has continued rising, from the development of Selenium photovoltaic cells with an efficiency of 1% to 2% [4], to the latest silicon based cells (efficiency of 24%). A photovoltaic (PV) system directly converts solar radiation (sunlight) into electricity. The PV system's basic device is the PV cell. A generic photovoltaic cell (Figure 2.2) can be described as a diode whose p-n junction is exposed to sunlight. When sunlight strikes the junction, photons (i.e. energy transported by electromagnetic waves) are absorbed, resulting in the formation of electron-hole pairs.

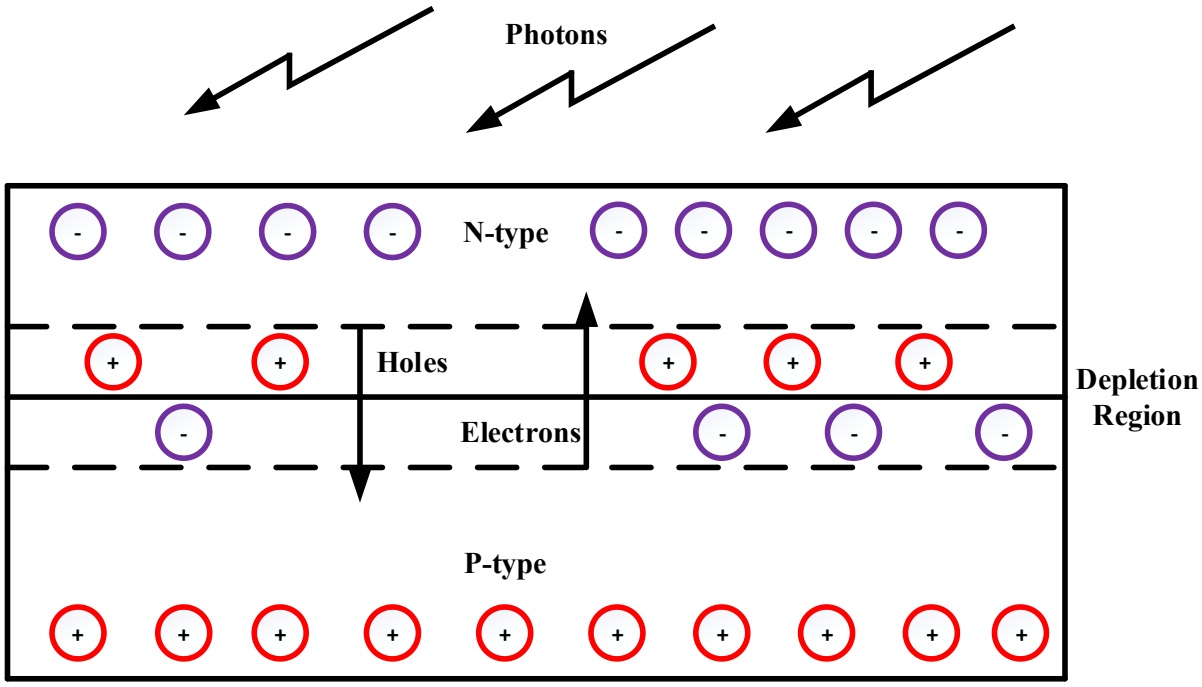

Figure 2. 2: Structure of PV cell

The photons are small packets of energy which carry electromagnetic radiation who, on

reaching the depletion region, cause the holes to move to the p-side of the junction and the electrons to move to the n-side, thus resulting in the generation of an electric voltage which can be tapped by placing electrical contacts, and delivering the voltage to the load. The workings of the whole PV cell can be described as the absorption of sunlight causing the generation of free carriers at the p-n junction, resulting in an electric current being generated and collected at the terminals of the PV cell. The photovoltaic cell described above can produce a voltage of approximately of 0.5 V, but very few applications make use of a single cell. Usually, the basic building block of a PV application is a *module*. A module is a number of PV cells connected in series and properly packaged. Typically, a module contains 36 cells in series and is often designated as a "12-V module" [1]; it is capable of delivering voltages higher than the specified value. At times, there are 12 V modules that only have 33 cells connected in series. In turn, a number of such modules can be connected in either series combinations to increase voltage, or in parallel combinations to increase current, the end result always being power.

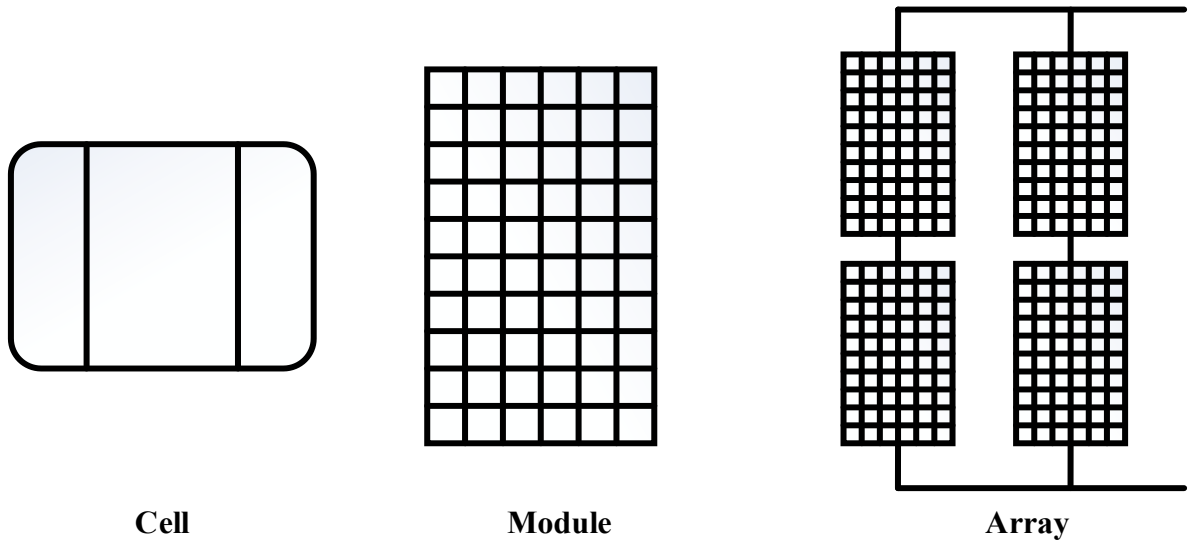

Figure 2. 3: Cells, Modules and Arrays

These different combinations of modules can be referred to as *arrays*. Figure 2.3 shows us the

distinction between cells, modules, and arrays. When a module is in series, the total voltage of the array is calculated as the sum of the individual module voltages. The current flowing through all the modules remains the same. In a parallel connection of the modules, the total current of the array is calculated as the sum of the individual module currents. The voltage through all modules remains the same. Thus, to achieve a large power from the PV system, various combinations of series and parallel modules are constructed. Before connecting a load to a PV module, we need to identify certain important electrical characteristics such as short-circuit current I_{SC} and open-circuit voltage V_{OC}. The current and the voltage, i.e., the power of the PV system, depend on the temperature and the amount of solar irradiation. These two parameters keep varying throughout the day, which is why standard test conditions are established to help compare different modules. These conditions are an irradiance of 1 kW/m^2, a cell temperature of 25 ^{o}C, and an air mass ratio of AM 1.5.

The PV cell described in this section can be represented as an equivalent circuit containing a single diode used to calculate the current and the voltage at the key operating points (i.e. maximum power point MPP).

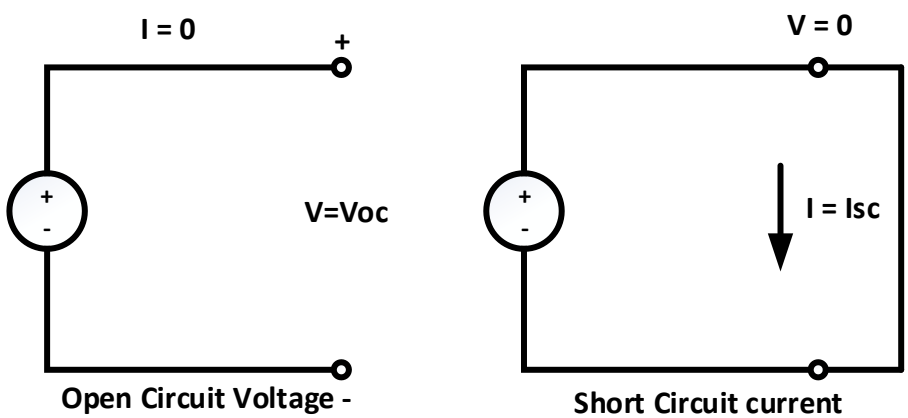

Figure 2.4: Circuits representing Open circuit voltage & Short circuit current

The equations are a function of the cell temperature, irradiation and other data given by the

manufacturer. A few of the other important parameters are the open-circuit voltage (V_{OC}), the short-circuit current (I_{SC}), the number of cells, the voltage, and the current at maximum power. The open-circuit voltage and the short-circuit current are calculated for the panel as they are zero power conditions, as explained below:

- Open-circuit Voltage (V_{OC})

  The condition can be represented as a circuit shown in Figure 2.4. When the PV module is kept in the sun but no load is connected to it, the panel produces an open-circuit voltage. No current is flowing through the panels at this time.

- Short-circuit Current (ISC)

  This condition is represented in circuit form in Figure 2.4. The parameter is calculated by shorting the terminals of the PV panel, thus producing a short-circuit current. The voltage is zero at the output terminal of the panel.

As power is a product of both voltage and current, we see that for the two conditions mentioned above, power is zero. This is true since the current and the voltage are zero for an open-circuit voltage and a short-circuit current respectively; they are known as zero power conditions. With the connection of a load, a power is generated and its value can be determined with the help of the I-V characteristic curve (Figure 1.1).

The effects of temperature and irradiance on the cell are further investigated with the help of some simulation results. We take a PV panel in which 5 series modules and 66 parallel strings are connected to the grid. We then observe the I-V and P-V curves of the module and the array. The I-V and P-V curves of the module are shown in Figure 2.5. The temperature has been kept constant at 25 ^{o}C, but the irradiation values change. The different curves for the irradiation values from 250 W/m^2 to 1000 W/m^2 in steps of 250 W/m^2 are measured. We can observe that

the power vs voltage curve in the Figure 2.5 shows the points of maximum power (pink circles). The I-V and P-V curves of the array is shown in Figure 2.6. The major differences that can be observed are that the

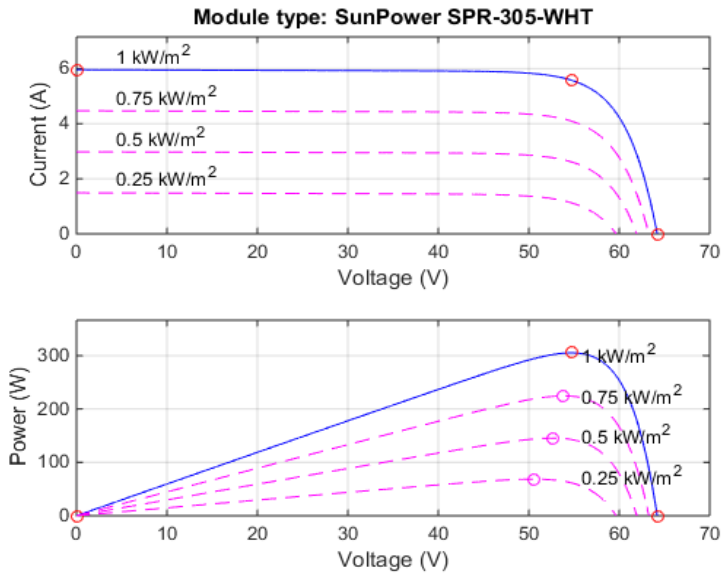

Figure 2. 5: The I-V & P-V characteristic curves for a PV module

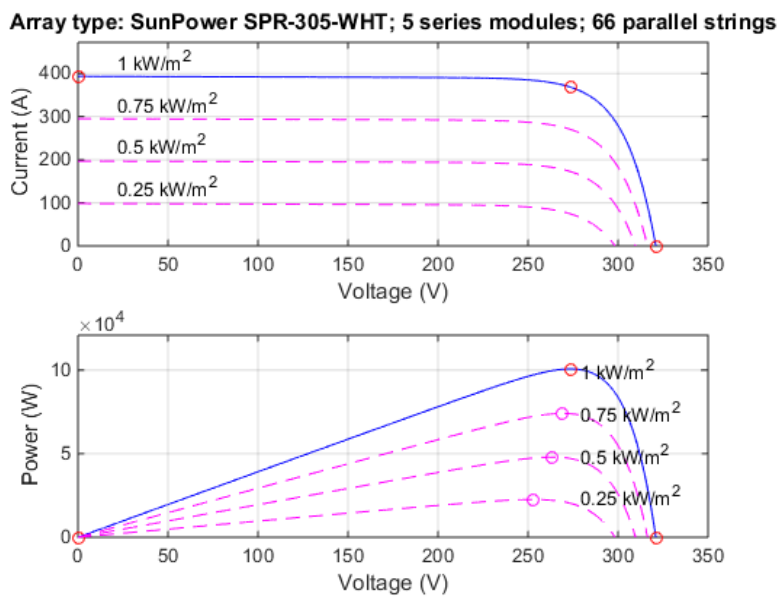

Figure 2. 6: The I-V & P-V characteristic curves for a PV array

values of the current, power, and voltage have all increased, which was expected since the

array contains multiple modules in series and parallel combinations. The conditions for temperature and the irradiation values are the same. Through this we have investigated the effects of irradiance on PV cells. The PV panel used in this thesis is of mono-crystalline Silicon with multi-contact output terminals. The PV characteristics are mentioned in Chapter 3.

2.4 Maximum Power Point Tracking (MPPT)

Maximum power point tracking is the relationship between the behavior of the current-voltage of solar panels and the solar irradiance and temperature. As seen in Figure 2.6, an increase in solar irradiance leads to a higher current and voltage output. The variations in environmental conditions affect the maximum output power of PV panels.

As mentioned in the overall system architecture, the power produced by PV panels is given to the DC-DC converter for boosting before being supplied to the DC-AC converter. To ensure that the maximum power is being delivered to the DC-DC converter, an interface is being used between the panels and the boost converter; this interface is known as maximum power point tracking (MPPT).

Various MPPT algorithms have been developed based on different implementation topologies. In respect to analog implementations, the options for MPPT techniques are short-circuit current, open-circuit voltage, and temperature. Similarly, for the digital circuit implementation, the various algorithms are perturb and observe (P&O) and incremental conductance (IC) [45]. Currently, the most popular MPPT algorithm is the perturb and observe algorithm (P&O). It has very few mathematical calculations, making its implementation fairly easy. Its principal disadvantage occurs during steady state operation, where there is an oscillation of power at the maximum power point [19].

For the purpose of this research, we use an MPPT control already available in the Simulink

environment. The design and mathematical modeling of the MPPT is out of the scope of this thesis.

2.5 DC/DC (Boost) Converter

The need for converters can be explained with the help of a practical example. The voltage ratings and frequency are different for various countries. To use an electronic device with electrical specifications that are from a different location (country), we need to match the electrical specifications of the electronic device to that of the local utility in that location. Therefore, we use a converter to help achieve the voltage match, making it easy to use our electronic device (e.g. a phone bought in North America needs a converter in order to be charged in Europe). Similarly, we make use of these various converters depending on its functionality in the power system. A converter provides various functionalities on the signals being fed to it; this also depends on the type of converter being used in the process.

The various types of converters are:

- Switching converter
- DC-DC converter
- AC-DC rectifier
- DC-AC inversion
- AC-AC cyclo-conversion

These converters provide a number of functions such as step-up of voltage, step-down, polarity inversion, and conversion of AC to DC, and vice-versa. This thesis makes use of the DC-AC converter and the DC-DC converter. In this section we elaborate on the design and mathematical modeling of the DC-DC converter. The major functions of the DC-DC converter are:

- As a basic function, as the name suggests, it converts an input DC voltage of some magnitude to an output DC voltage of a different magnitude (step-up or step-down).
- Regulates the output DC voltage against load and line variations;
- Reduces the AC ripple voltage on the DC output voltage below required levels;
- Provides the isolation between the input source and the load;
- Provides protection from electromagnetic interferences to the supply and input systems;
- Also satisfies various international and national safety standards.

DC-DC converters can be classified into two types: hard-switching pulse width modulated (PWM) converters and resonant or soft-switching converters. In this thesis, we use a hard switching pulse width modulated converter. The advantages of using a PWM converter are high efficiency, constant frequency operation, and simple control. The PWM converter helps to control the switch used in the boost converter, and this control of the switch of a DC-DC converter also helps to achieve the step-up application of the converter. The two operation modes for the DC-DC converter are:

- Continuous conduction mode (CCM) &
- Discontinuous conduction mode (DCM).

These operating modes are with respect to the value of the current flowing through the inductor (refer Figure 2.9). In CCM mode, the value of the inductor current is always greater than zero. When the value of input current is low, or the switching frequency is low, the converter enters DCM mode. The inductor current is zero for a certain time when it is in DCM mode. In this research we considered the DC-DC converter to be operating in CCM mode, as it has better efficiency and utilizes the semiconductor switches in a good manner. As the power generated

from the module is very low, we make use of a boost converter that takes the low input DC-voltage and provides a high output DC-voltage. Figure 2.7 shows a general connection between the PV array and the boost converter. The output voltage and current of the PV module is fed to the DC-DC converter. The input and output voltage relationship is controlled by the duty cycle (D).

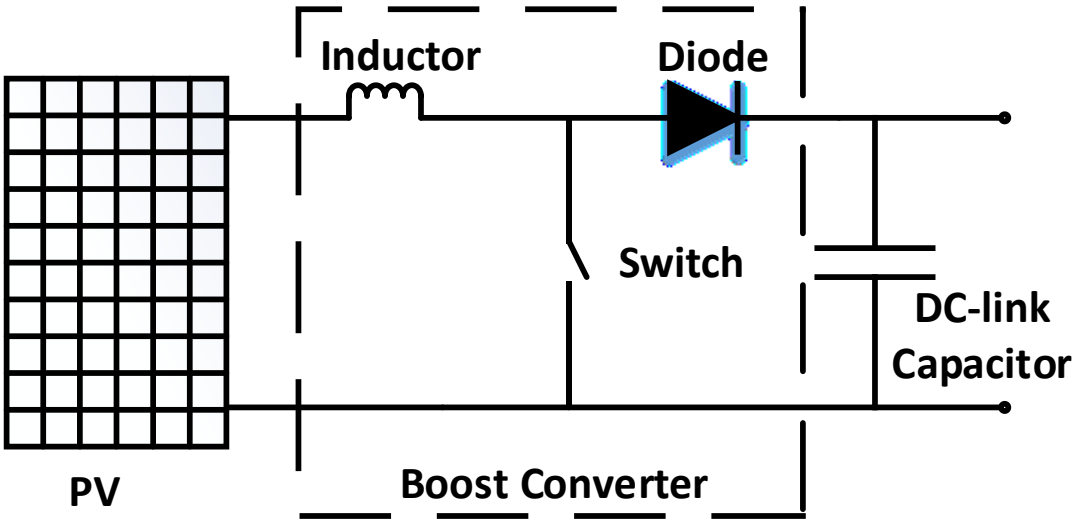

Figure 2. 7: Circuit diagram for a PV module in connection with a DC-DC converter

2.6 Grid Connected Inverter

This section describes the inverter and its design and modeling. The inverter, also known as the DC-AC converter, is a crucial part of a grid connected PV system. As we have seen, the output of the PV panel is DC voltage, but the local utility or grid supplies AC voltage and current. The conversion of the PV system DC voltage and current to the AC voltage and current is necessary for the PV system to be connected to the grid. If the AC power generated by the PV system is greater than the need of the owner, the inverter shall supply this surplus power to the utility grid. At night, the utility provides AC power to satisfy the requirements of the owners that have exceeded the capability of the PV system [32].

The design of the grid-connection inverter must take into consideration the peak power of the system and deal with issues such as power quality, islanding detection, grounding, and maximum power point tracking [33]. The inverter peak power is the net power of the PV generator that is installed. The two types of inverters considered for such DG applications are the voltage source inverter (VSI) and the current source inverter (CSI). The difference is in their design, as the CSI makes use of silicon controlled rectifiers (SCR's) or gate commutated thyristors (GCT's) for the switching devices, whereas the VSI uses the insulated gate bipolar transistors (IGBT's). Generally, the VSI is used in DG applications as it is easy to control and also better satisfies the requirements for DG interconnection to the grid. Another drawback of CSI is that it requires filters at the input and output, due to high harmonic content [34]. This thesis also considers the design of the voltage source inverter to convert the DC voltage to AC voltage. Once the type of inverter is selected, the topology of the inverter is chosen based on the system configuration. The system can be configured depending on the number of stages:

- Single stage configuration: In this configuration, the PV array is directly connected to the DC-AC inverter, and then a transformer is used to change the voltage levels to suit that of the utility grid. The configuration is shown in Figure 2.8.

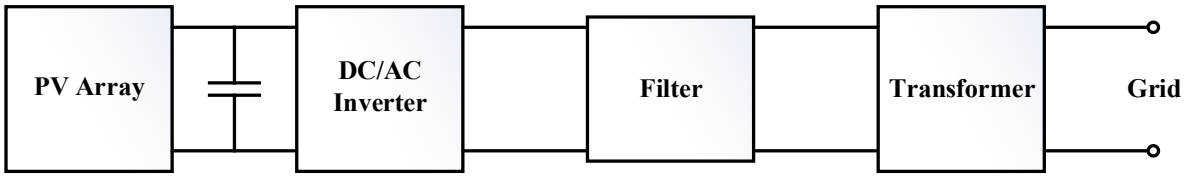

Figure 2. 8: Single-stage configuration of a grid-connected PV system

Two-stage configuration: Here, the system initially uses a DC-DC converter to step-up the PV generated voltage, then connecting it to the DC-AC inverter for grid interconnection no transformers are used in the design. In this research, the two-stage

configuration is applied, as shown in Figure 2.9.

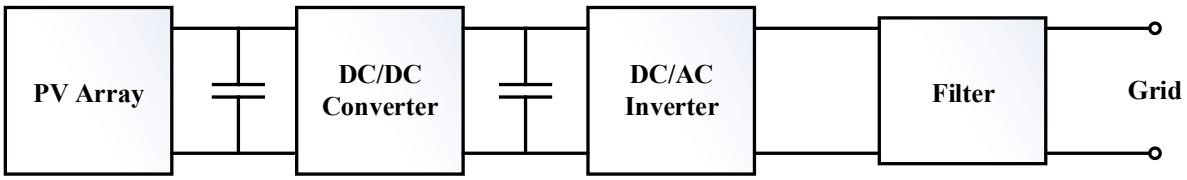

Figure 2. 9: Two-stage configuration of grid-connected PV system

There are various topologies for the grid-connected inverter in the case of a PV system interconnect. The most common types are the centralized inverter, the string inverter, the multi-string inverter, and the AC module concept.

The centralized inverter, as the name suggests, consists of one centralized inverter for all the strings of the PV modules. It produces a high voltage, which is sufficient to avoid the usage of a boost converter or transformer.

The string inverter is a smaller version of the centralized inverter. Each string of PV modules is connected to an inverter. Due to this connection of the inverters, the reliability of the system is improved.

The topology of multi-string inverters is designed so that each PV module is interfaced with a DC-DC converter, which is in turn interfaced to a DC-AC inverter. The advantages of this type of inverter are that the redundancy is reduced and that it provides scalability for grid connection. Lastly, the AC module concept is a bit more complex than the other topologies. Here, modules of the PV panels are interfaced to modules of the DC-DC converter, which in turn is interfaced to modules of DC-AC inverters. The functionality of each of these modules is independent. This provides flexibility from the design aspects, and is mostly suitable for residential applications. We can see from the types of inverters described above that the multi-string inverters and the AC module concept use a two-stage configuration, and we will look at

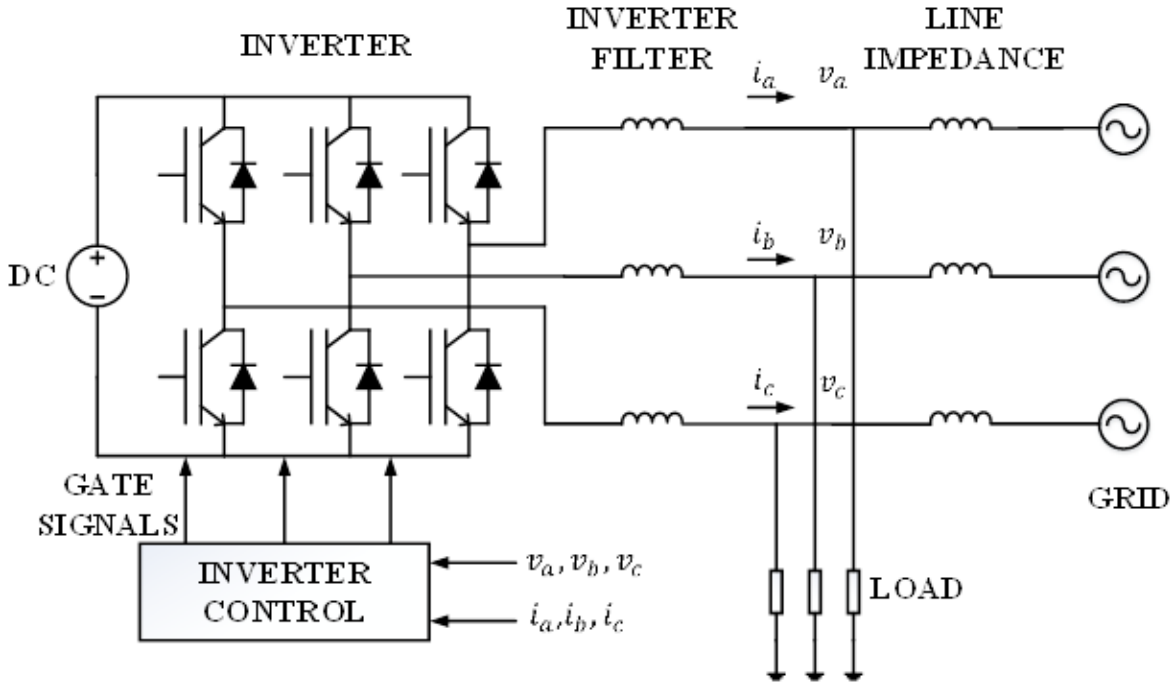

Figure 2. 10: Three-phase grid connected VSI

another topology which similar to these. In this thesis, the VSI is used as an interface with the grid and the DG system, and the research is focused entirely on this type of inverter. The topology for a three-phase grid connected VSI can be seen in Figure 2.10. The switching function inverter is used here.

The three-phase power in a power system, can be explained as three single phase powers that are 120° out of phase with each other. This helps maintain voltage and current sinusoidal waveform peaks close to each other. Thus, providing a constant and smooth power to the system. Whereas, in case of a single-phase the difference in waveform peaks is higher than three-phase.

The other advantages of three-phase over single phase are, it is a time independent function and the power factor and efficiency of the system are greater than a single-phase power system.

2.7 Phase Locked Loop

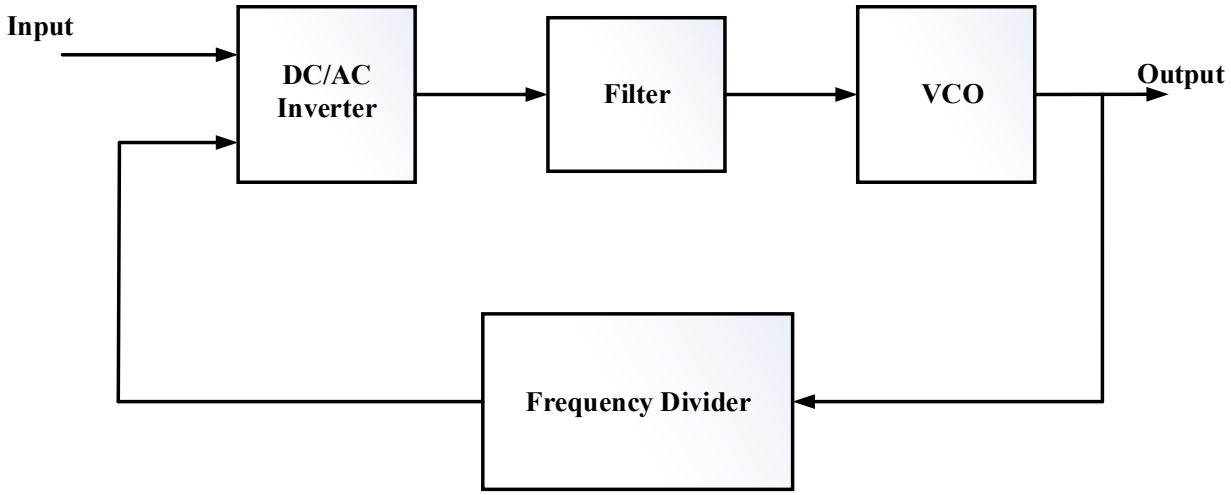

Figure 2.11: Basic structure of a Phase Lock Loop (PLL)

The phase lock loop (PLL) is one of the grid synchronization techniques. It is defined as a device that causes a signal to track another signal. It synchronizes an output signal with a reference input signal, with respect to frequency and phase. A basic PLL circuit consists of the following components: a phase detector, a loop filter, and a voltage controlled oscillator. The PLL minimizes the errors in the phase and the frequency between the output and input signals. The basic PLL schematic is shown in Figure 2.11. This technique has wide practical usages and advantages; additional details regarding the concept of the phase locked loop synchronization technique and its implementation can be found in the following literature [39].

2.7.1 Parks Transformation

Parks transformation is a tool used for the mapping of the three-phase inverter and the load onto a two-axis synchronous rotating reference frame, instead of the fixed two-axis reference frame.

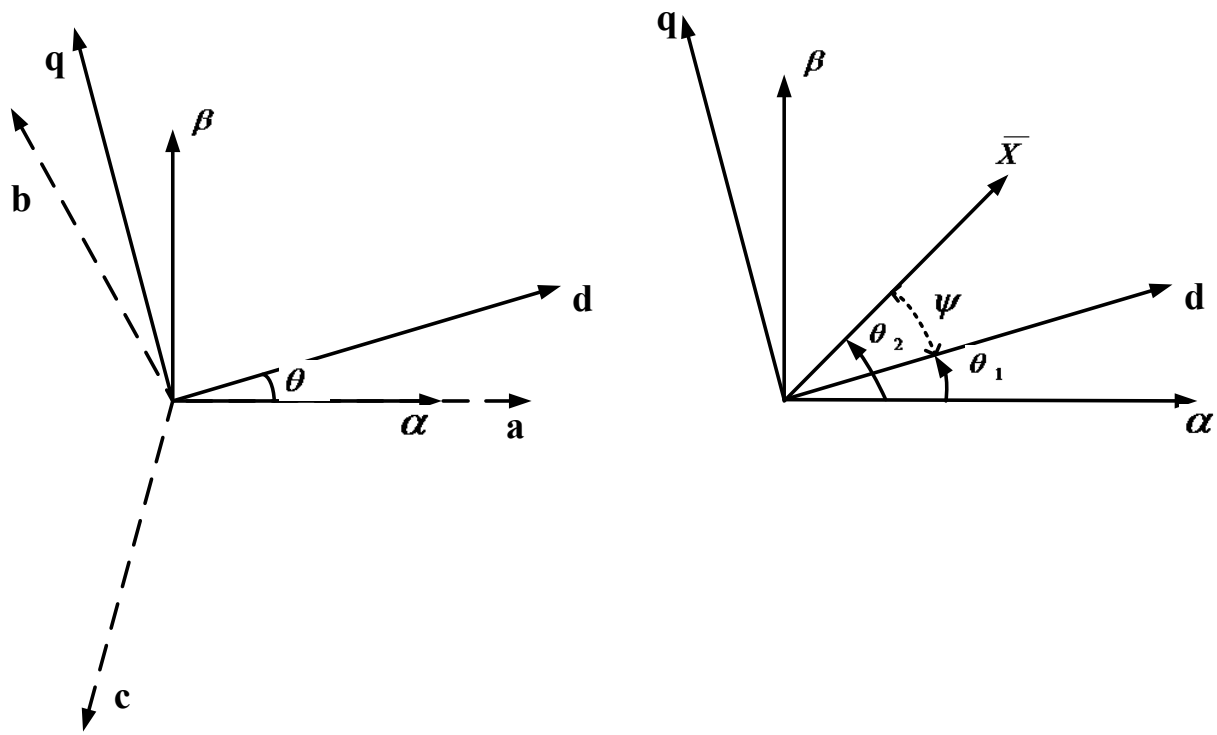

Figure 2. 12: Vector diagrams of Parks Transformation technique

This transformation is from a static coordinate system to a dynamic coordinate system, and a linear transformation with a matrix of time varying coefficients. This new transformation has a set of reference axes, *d* and *q*, that rotate with a fixed angular frequency of ω. When applying the αβ transformation to three sinusoidal signals, the geometrical description is a rotating vector $\overline{X}$. This is seen in Figure 2.12. When the frequency of the sinusoidal signal and the rotating angular speed are equal, this can be considered as the fundamental frequency. If the speed of vector $\overline{X}$ is equal to ω, then in the *dq* reference frame the vector is fixed, i.e., the vector is not moving. The advantage of using this transformation is the three-phase sinusoidal signals when rotating at the angular frequency of ω [39]. These signals shall be considered as constant in the *dq* reference frame. Thus, the implementation of a control technique in the *dq* reference frame is relatively easy.

2.8 PV System Control Strategies

The major tasks related to control in the structure shown in Figure 2.1 are:

- The synchronization of the PWM and control techniques to the voltage at the point of common connection, with the help of a phase locked loop (PLL). This ensures the change of the frame of reference to a *dq*- frame for the three-phase AC signals. Also, the processing of the DC equivalents of the sinusoidal varying signals, by the controllers.
- The connection of a negative feedback damping controller at the input of the inner control loop. It enables the control of the grid frequency.
- The signal i_{dref} is given to the *dq* reference frame, as shown in Figure 2.1. The inner current loop scheme ensures that the signal i_d tracks the signal i_{dref}. The control over the i_d signal helps to achieve control over the voltage V_{dc}. The inner current loop also ensures that the signal i_q tracks the signal i_{qref}. The signal i_q is nothing but the reactive power of the system represented by Q; this is discussed in greater detail in Chapter 3. To ensure that the PV system has a unity power factor, the reference signal i_{qref} is zero, resulting in the reference signal for the reactive power to be zero as well.

Chapter 3

Average Modeling of the Grid-connected Photovoltaic System

3.1 Introduction

This chapter focuses on the detailed design of the PV system interfaced with a grid/stiff grid or utility. The design is a mathematical modeling of the components of the PV system, namely the PV module, the boost converter, the inverter, and the grid. The average large signal equation for each of the components mentioned above are derived, helping in the creation of the average large signal model, which was created in the MATLAB/SIMULINK 2014b environment, and the results of which are shown in the following chapters. In this part of the thesis, an equivalent circuit based PV array is modelled. The system makes use of the Maximum Power Point Tracking (MPPT) controller to obtain the maximum power from the PV module. A DC-link voltage controller is proposed so as to regulate the DC voltage linking to the Voltage Source Inverter (VSI). Controllers for the *d* and *q* components of the AC side currents and the Phase Locked Loop (PLL) are derived.

The chapter is organized as follows, sections 3.1.1 to 3.6 provides the details and mathematical designs of the PV modules, the DC-DC converter, and the DC-AC converter. The mathematical model will include the derivation of equations in *abc* forms to their transformation into the *dq* frame of reference. The simulation results of the entire PV system described in the chapter are also shown. Finally, the chapter concludes with a comparison of the average and detailed large signal models and their results.

3.2 PV Single Diode Model

Figure 3.1 shows the equivalent schematic of an ideal PV single diode model. It's an ideal current source connected in parallel with a diode. The modeling of the PV cell requires data

about four parameters, which can be obtained from the commercially available photovoltaic modules. These parameters are the short-circuit current (I_{SC}), the open-circuit voltage (V_{OC}), the current (I_{mp}), and voltage (V_{mp}) at the maximum power point. The values of the temperature coefficients for the current and voltage are equally important. The equations describing the I-V characteristics of the ideal equivalent model are:

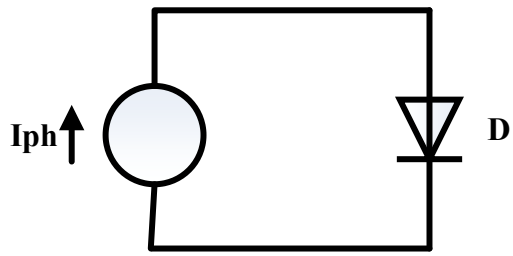

Figure 3. 1: Single diode representation of a PV cell

The current flowing through the ideal PV cell shown above is mathematically represented as:

$$I = I_{ph} - I_D \quad \text{(3.1).}$$

The total current of the ideal equivalent circuit shown in Figure 2.5 is obtained by the difference of the photocurrent and current through diode (I_D). The expression for the diode current is obtained from Shockley's expression.

$$I_D = I_o\left[\exp\left(\frac{qV}{nN_s kT}\right)\right] - 1 \quad \text{(3.2),}$$

where,

Iph = photocurrent (A);

Io = saturation current (A);

q= electrons charge ($-1.602*10^{-19}$C);

n= quality factor of diode;

Ns= number of cells in series;

k= Boltzmann's constant;

T= temperature of the p-n junction (K); [Almost same as the cell temperature]

Thus, substituting (3.2) in (3.1) we get

$$I = I_{ph} - I_o\left[\exp\left(\frac{qV}{nN_s kT}\right) - 1\right] \quad \text{..... (3.3).}$$

The equations for the ideal equivalent circuit are utilized to derive the equations for the more appropriate circuit (Figure 3.2) being considered in this thesis. The circuit has series and parallel resistance.

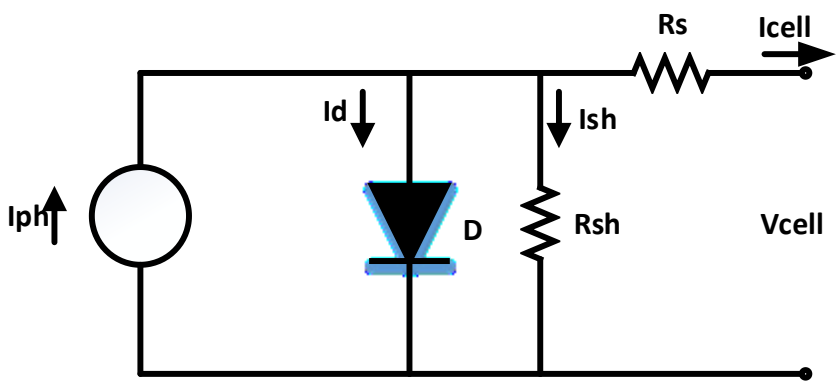

Figure 3. 2: PV cell circuit representation

The circuit shown in Fig 3.2 is the practical PV cell. Series resistance R_S represents the contact resistance associated with the bond between the cell and its wire leads and a resistance of semiconductor, which results in voltage loss of PV cell. Parallel resistance R_{sh} represents a cell leakage current. The effect of the resistances modifies the equation (3.3),

$$I = I_{ph} - I_o\left[\exp\left(\frac{q(V_{cell} + I_{cell}R_s)}{nN_s kT}\right) - 1\right] - \frac{V + IR_s}{R_{sh}} \quad \text{..... (3.4).}$$

After comparing equations (3.4) and (3.3), we see that the series resistance affects the output voltage and the shunt resistance affects the current. The saturation current (I_O) is a result of the charge diffusion and recombination in the space-charge layer. The I-V equation is expressed as shown in (3.5). Where I_{o1}= charge diffusion mechanism saturation current and I_{o2}= re-combi

-nation in space-charge layer mechanism saturation current. The characterization of PV cells as per the following operational points is shown below:

$$I = I_{ph} - \left\{ I_{o1}\left[\exp\left(\frac{q(V_{cell} + I_{cell}R_s)}{N_s kT}\right) - 1\right] - I_{o2}\left[\exp\left(\frac{q(V_{cell} + I_{cell}R_s)}{2N_s kT}\right) - 1\right]\right\} - \frac{V_{cell} + I_{cell}R_s}{R_{sh}}$$

…….. (3.5).

At short-circuit point:

$$V = 0 \text{ and } I = I_{sc} \text{ ……. (3.6).}$$

At open-circuit point:

$$V = V_{oc} \text{ and } I = 0 \text{ ……..…… (3.7).}$$

The maximum power point:

$$V = V_{mp} \text{ and } I = I_{mp} \text{ ……..……..……..…….. (3.8).}$$

From the short-circuit point equation (3.6), it can be approximated that

$$I_{ph} = I_{sc} \text{ …….……. (3.9).}$$

From the open-circuit point equation (3.7) the saturation current may be approximated by assuming that the photon current and the short circuit current (I_{sc}), given by (3.9) are almost equal as the cell voltage tends toward zero, giving the following set of equations:

$$I_{o1} = \frac{1}{2}\frac{I_{ph}}{\left(\exp\left[\frac{qV_{oc}}{kT}\right] - 1\right)} \text{ …….. (3.10),}$$

$$I_{o2} = \frac{1}{2}\frac{I_{ph}}{\left(\exp\left[\frac{qV_{oc}}{2kT}\right] - 1\right)} \text{ ……..…… (3.11).}$$

The peak power point equations:

By substituting the values of saturation currents in equation (3.5) we get value for V_{oc}

$$V_{oc} = \frac{nN_s kT}{q} \ln\left(1 + \frac{I_{sc}}{I_o}\right) \ldots\ldots\ldots\ldots\ldots\ldots\ldots\ldots\ldots\ldots (3.12).$$

Solving the exponent part of (3.3) with V_{oc}

$$\exp\left(\frac{qV_{oc}}{nN_s kT}\right) = \left(1 + \frac{qV_{mp}}{nN_s kT}\right)\exp\left(\frac{qV_{mp}}{nN_s kT}\right) \ldots\ldots\ldots\ldots\ldots (3.13),$$

Then substituting the solved exponent in (3.3) we get,

$$I_{mp} = I_{ph} - I_o\left[\exp\left(\frac{qV_{mp}}{nN_s kT}\right) - 1\right] \ldots\ldots\ldots\ldots\ldots\ldots\ldots\ldots\ldots\ldots (3.14).$$

The PV cell has a hybrid behavior, i.e., of current source at short-circuit point and of voltage source at open-circuit voltage, and we observe that the maximum power point corresponds to trade-off condition between current and voltage, and is found at the point where the current is still high, just before it starts decreasing with the increasing output voltage. We therefore consider a tangent to the I-V curve to evaluate a region of the graph that is similar to the above mentioned behavior, this gives

$$\frac{dI}{dV} = -\frac{qI_o}{nN_s kT}\exp\left(\frac{qV}{nN_s kT}\right) \ldots\ldots\ldots\ldots\ldots\ldots\ldots\ldots\ldots\ldots (3.15).$$

The expression (3.15) is used to calculate the output voltage corresponding to that of Vmp.

$$V_{mp} = \frac{nN_s kT}{q} \ln\left(-\frac{nN_s kT}{qI_o}\left(\frac{dI}{dV}\right)_{V_{mp}}\right) \ldots\ldots\ldots\ldots\ldots\ldots\ldots\ldots\ldots (3.16).$$

We know that the derivative in (3.16) is,

$$\frac{dI}{dV}\Big|_{V_{mp}} \cong -\frac{0 - I_{sc}}{V_{oc} - 0} = -\frac{I_{sc}}{V_{oc}} \ldots\ldots\ldots\ldots\ldots\ldots\ldots\ldots\ldots\ldots (3.17),$$

Using (3.17) in (3.16) we get

$$V_{mp} = \frac{nN_s kT}{q} \ln\left[\frac{nN_s kT}{qI_o} \cdot \frac{I_{sc}}{V_{oc}}\right] \quad \text{..... (3.18).}$$

Similarly we get

$$I_{mp} = I_{ph} + I_o - \frac{nN_s kT}{q}\left(\frac{I_{scr}}{V_{oc}}\right) \quad \text{..... (3.19).}$$

3.2.1 Effect of Temperature and Irradiance on the PV cell

The two major parameters that affect the characteristics of the PV cell or array are the solar irradiance (G) and the cell temperature (T). The relation between the irradiance and short-circuit current I_{SC} are directly proportional to each other. If the irradiance drops, short-circuit current also drops, and vice-versa. The relation between the irradiance and the open-circuit voltage V_{OC} is logarithmic, thus resulting in a small change of the open-circuit voltage for a change in solar irradiance. As the cell temperature increases, the open-circuit voltage descends by a substantial amount, while short-circuit current rises by a small amount. These changes can be placed into a single mathematical equation, as shown in (3.20), for modeling purposes. The equation for the photocurrent I_{ph} is as follows:

$$I_{ph} = \frac{G}{G_{ref}}\left[I_{sc} + \alpha\left(T - T_{ref}\right)\right] \quad \text{..... (3.20),}$$

where the Isc is the value of the short-circuit current calculated at standard temperature conditions (STC), meaning that the operating reference cell temperature (T_{ref}) is 25 ^oC and the solar irradiance reference value (G_{ref}) is 1000 W/m^2. α is the temperature co-efficient for the short-circuit current (0.0005/^{o}C). Equations (3.18), (3.19) and (3.20) get values for V_{mp}, I_{mp} and I_{ph}. These values are for the PV module only, with no connection to the DC-DC converter. Since this connection is made, we shall consider the equation (3.14) from PV module which

is

$$I_{mp} = I_{ph} - I_o\left[\exp\left(\frac{qV_{mp}}{nN_s kT}\right) - 1\right]$$

This equation is solved for the exponent term, linearizing using Taylor series we get,

$$\hat{i}_{mp} = \hat{i}_{ph} - I_o \exp\left(\frac{qV_{mp}}{nN_s kT}\right)\exp\left(\frac{q\hat{v}_{mp}}{nN_s kT}\right) \ldots\ldots\ldots\ldots\ldots\ldots\ldots\ldots (3.21),$$

solving the series

$$\hat{i}_{mp} = \hat{i}_{ph} + qI_o\hat{v}_{mp}\left(\frac{1}{2}\left(\frac{qV_{mp}}{nN_s kT}\right)^2 + \left(\frac{qV_{mp}}{nN_s kT}\right) + 1\right) \ldots\ldots\ldots\ldots\ldots (3.22),$$

from (3.22) we can derive the equation for the current at maximum power. This is dependent on the voltage at the maximum power, the relation of which can be obtained from the design of the DC-DC converter.

3.3 Modeling of DC-DC Converter

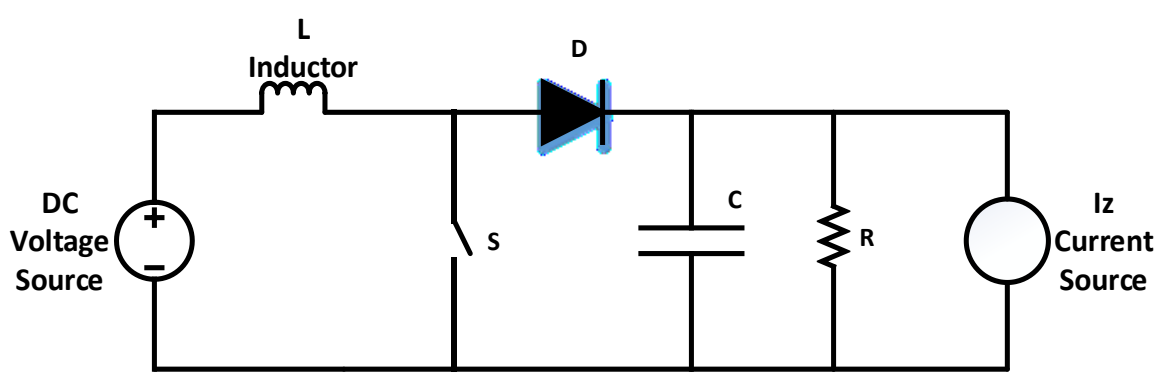

Figure 3. 3: Circuit representation of a DC-DC converter

The next link in the system is the DC-DC converter, and its modeling is explained in this section. The average-model is considered for analysis and a set of equations are derived in

the process. In this thesis, the voltage from the PV panels at maximum power are stepped up to a voltage V_{dc}, which can be later fed into an inverter for grid-interconnection. The DC-DC converter model used to boost the voltage for mathematical modeling in this research is shown in Figure 3.3. The model consists of an input DC voltage source (V_{mp}), which is the voltage at the maximum peak power of the array and is calculated with the help of a maximum power point tracking controller. The boost converter contains the following basic power components, which are also present in the various other converters mentioned previously. It consists of a switch (S), which is usually an IGBT or a thyristor. Iz is a current generator in parallel to a resistance, so that the responses of the converter to the load changes can be examined. The boost converter operation is simple, as the switch controls the inductor; it alternates between charging the inductor by connecting it to the input voltage source, and discharging the stored inductor current into the load.

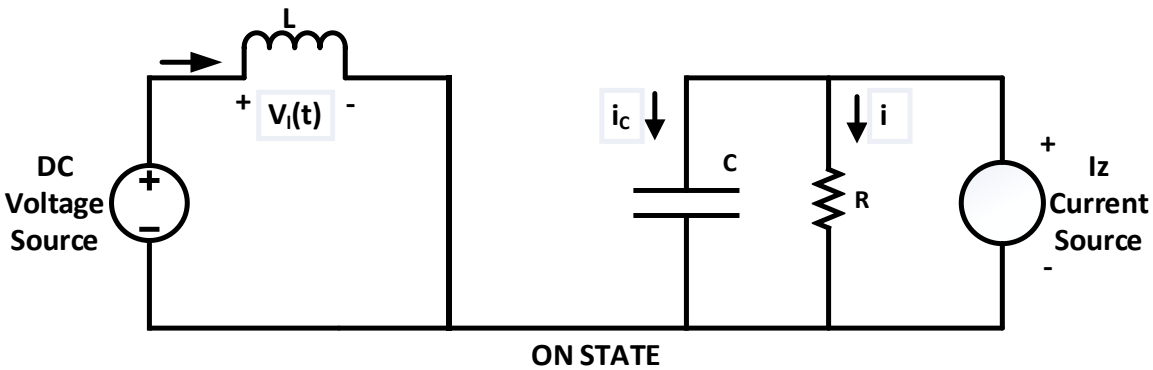

Figure 3. 4: Circuit for ON time of DC-DC converter

The boost converter operations during ON and OFF times are explained as follows:

- <u>ON Time</u>: In this state, the switch (S) is on, and current flows through the inductor. The diode (D) will be off for the same time period. The circuit for the ON time is represented in Figure 3.4.

By applying Kirchhoff's voltage law to the inductor containing loop, we get

$$L\frac{di_l}{dt} = v_{mp} \quad \text{(3.23).}$$

And by applying Kirchhoff's current law on the node of the capacitor branch, we get

$$C\frac{dv_c}{dt} = i_z - i \quad \text{(3.24),}$$

$$C\frac{dv_c}{dt} = i_z - \frac{v_c}{R} \quad \text{(3.25).}$$

The two equations (3.23) and (3.25) mathematically represent the boost converter in ON time.

- <u>OFF State:</u> In this state, the switch is off and the current is flowing through the diode (D) into the capacitor. The circuit is shown in Figure 3.5.

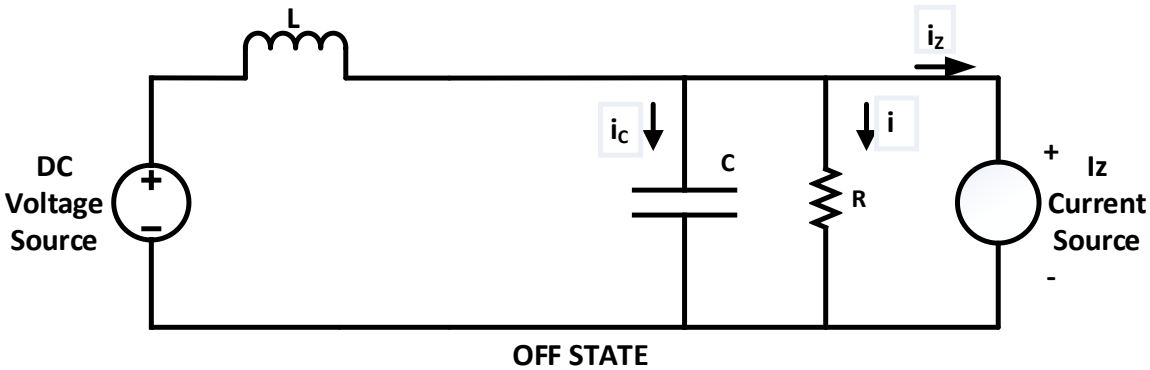

Figure 3. 5: Circuit for OFF time of DC-DC converter

When applying Kirchhoff's voltage law to the loop containing the inductor and the capacitor, we obtain the following equation:

$$L\frac{di_l}{dt} = v_{mp} - v_c \quad \text{(3.26).}$$

Similar, to the procedure followed in ON, when applying Kirchhoff's current law to the node with the capacitor, the following equation is derived:

$$C\frac{dv_c}{dt} = i_l - i_z - \frac{v_c}{R} \quad \text{(3.27).}$$

The two equations (3.26) and (3.27), mathematically represent the boost converter in OFF time. The actual value of the ON & OFF times for the DC-DC converter are not only the switching time taken by the switch. The switching time is expressed with the duty cycle, and the duty cycle (D) presents a relationship between the operating time (ON) of the device and the time it was inactive (OFF). Therefore, the value of the duty cycle is in the range 0 (OFF) to 1 (ON). Based on the description of the duty cycle, we can define the following relationships: If D is the duty cycle during the ON time of the DC-DC converter, then D' is the duty cycle during the OFF time of the DC-DC converter. As we know that the maximum value of the duty cycle is 1, we can correctly say:

$$D + D' = 1 \quad \text{(3.28),}$$

from equation (3.28) it can be easily said that,

$$D' = 1 - D \quad \text{(3.29).}$$

The analysis of the inductor voltage and current waveform helps to determine the relationship between the input and the output voltages, in terms of the duty cycle. During the ON time (DT), the inductor gets charged with energy, and we observe an increase of the signal in the inductor current waveform, as in Figure 3.6. Similarly, during the OFF time (D'T), the inductor discharges all the energy it has stored into the capacitor and load, and we observe a decrease of the signal in the current waveform. Figure 3.6 is the voltage and current waveforms for the boost converter in continuous conduction mode. In this research, and for the purpose of analyzing the system, we consider the average model of the DC-DC converter. To achieve a good result from the analysis, we consider the equivalent average models for ON and OFF times. The circuit representations for the equivalent model shall use the voltage and current

sources. It is also important to understand the volt-seconds being applied to the inductor for a switching period, either ON or OFF.

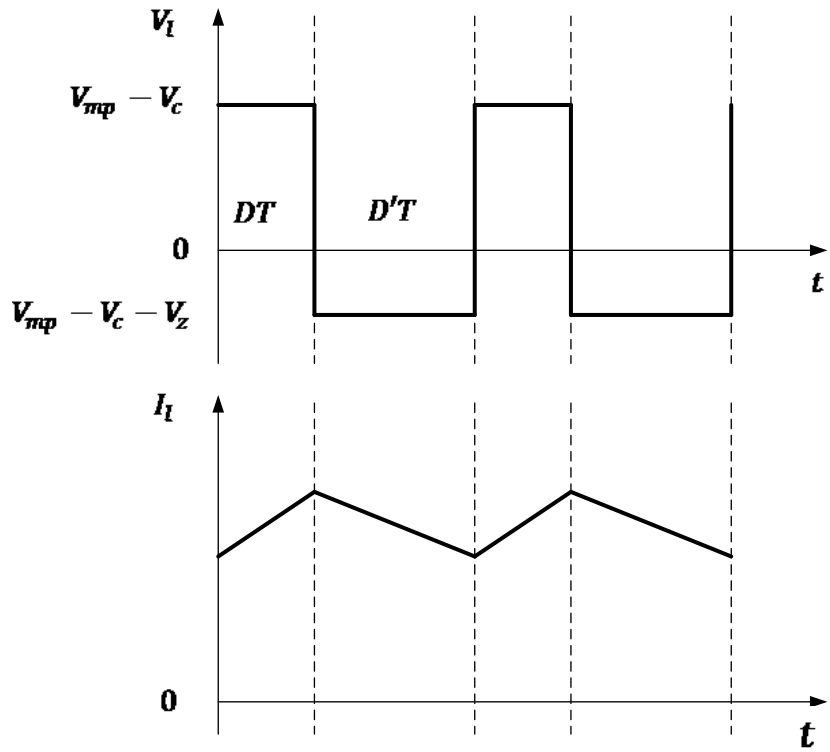

Figure 3. 6: Waveforms for the DC-DC converter inductor voltage and current

This understanding is easy to obtain by observing the inductor voltage and current waveforms. Figure 3.7 represents the circuit for the equivalent model during ON time. As mentioned in the previous paragraph about the inductor volt-second balance, we can arrive at the following mathematical equation:

The inductor net volt-seconds applied over one full switching period:

$$v_l(t) = \frac{1}{T_s}\int_0^{T_s} v_l(t)dt = D\left(v_{mp} - i_l R_l\right) + D'\left(v_{mp} - i_l R_l - v_c\right) \ldots\ldots \quad (3.30).$$

Integrating both sides, and as the area under the inductor voltage curve for a steady state is zero.

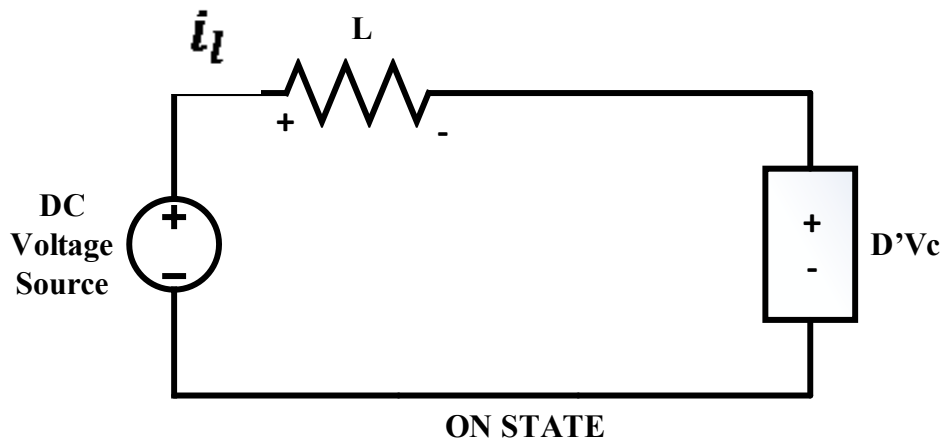

Figure 3. 7: Equivalent circuit for ON state of DC-DC converter

Equating (3.30) to zero,

$$0 = v_{mp}(D + D') - i_l R_l (D + D') - D' v_c$$

$$0 = v_{mp} - i_l R_l - D' v_c$$

$$v_l = v_{mp} - i_l R_l - D' v_c \quad \text{.....} \quad (3.31).$$

The principles of inductor volt-second balance state that the average values of the periodic inductor voltage are zero when the converter operates in a steady state.

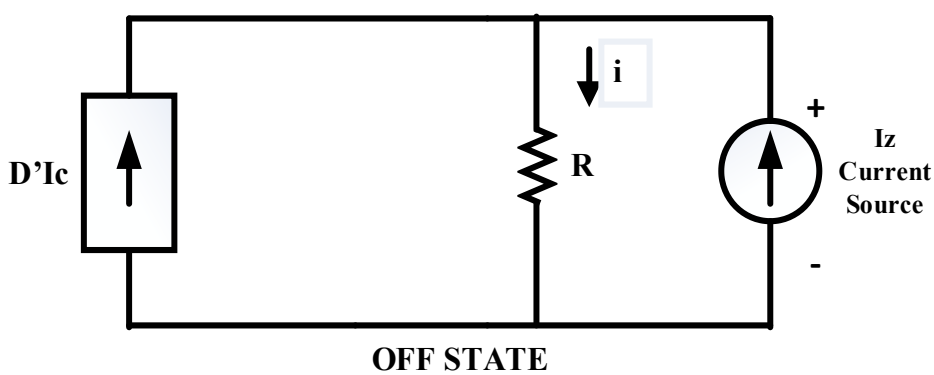

Figure 3. 8: Equivalent circuit for OFF state of DC-DC converter

To determine these steady-state conditions for the DC-DC converter, we equate their average values to zero. We obtain equation (3.31) after equating to zero. Similarly, the OFF time

represented in Figure 3.8 follows the principles of the capacitor charge balance technique, which is the same procedure as for the ON time.

Similarly, the capacitor charge balance over a full switching period:

$$i_c(t) = \frac{1}{T_s}\int_0^{T_s} i_c(t)dt = D\left(-\frac{v_c}{R}\right) + D'\left(i_z - \frac{v_c}{R}\right) \quad \text{..... (3.32).}$$

Integrating both sides, as the area under the capacitor current waveform is zero.

Equate (3.32) to zero,

$$0 = -\frac{v_c}{R}\ (D + D') + D' i_z$$

$$0 = -\frac{v_c}{R} + D' i_z$$

$$i_c = -\frac{v_c}{R} + D' i_z \quad \text{..... (3.33).}$$

Equation ((3.33) helps to determine the DC component of the inductor current. A complete equivalent circuit, a combination of the ON and OFF states, is shown in Figure 3.9. The mathematical equations (3.31) and (3.33) represent the DC-DC converter as a boost converter. The power generated at the DC-DC converter is DC power, which when generated in excess cannot be supplied to the utility/grid, as the grid supplies only AC power. We therefore need an inverter to convert the generated DC power to AC power. Before connecting the inverter, we connect a capacitor to achieve the power balance on the DC-DC converter side as well as on the DC-AC inverter side.

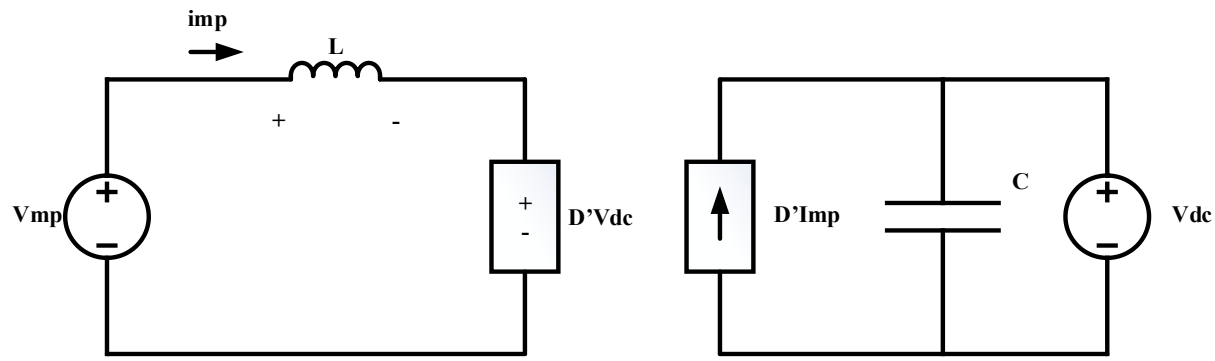

Figure 3. 9: Equivalent circuit for DC-DC converter

3.4 Modeling of PV System Dynamics

The most crucial link in the modeling of the whole system is the DC-link capacitor, which follows the principle of power balance. The equation (34) shows the power balance equation

$$\frac{C}{2}\frac{dv_{dc}^2}{dt} = P_{pv} - P_{dc} \quad \text{(3.34)},$$

here, P_{pv} is the power being drawn by the capacitor from the PV array, and P_{dc} is the power drawn by the DC-side of the inverter. By assuming that the power losses in the inverter and the filter are negligible, we can conclude that the power being delivered to the input will be equal to the power at the output terminals of the inverter at the point of common connection. This gives the following equation (3.35).

$$P_{dc} = P_{ac} \quad \text{(3.35)},$$

where P_{ac} is the power being delivered to the grid at point of common connection.

$$P_{dc} = P_{ac} = real\left(\overline{V}_s \overline{I}^*\right) \quad \text{(3.36)},$$

when substituting the values of (3.36) in (3.34) we get,

$$\frac{C}{2}\frac{dv_{dc}^2}{dt} = P_{pv} - real\left(\overline{V}_s \overline{I}^*\right) \ldots\ldots\ldots\ldots\ldots\ldots\ldots\ldots\ldots (3.37).$$

The equation (3.37) represents the dynamics of the DC-link capacitor. This equation depends on the dynamics of the inverter current as well.

3.5 Modeling of Grid Connected Inverter

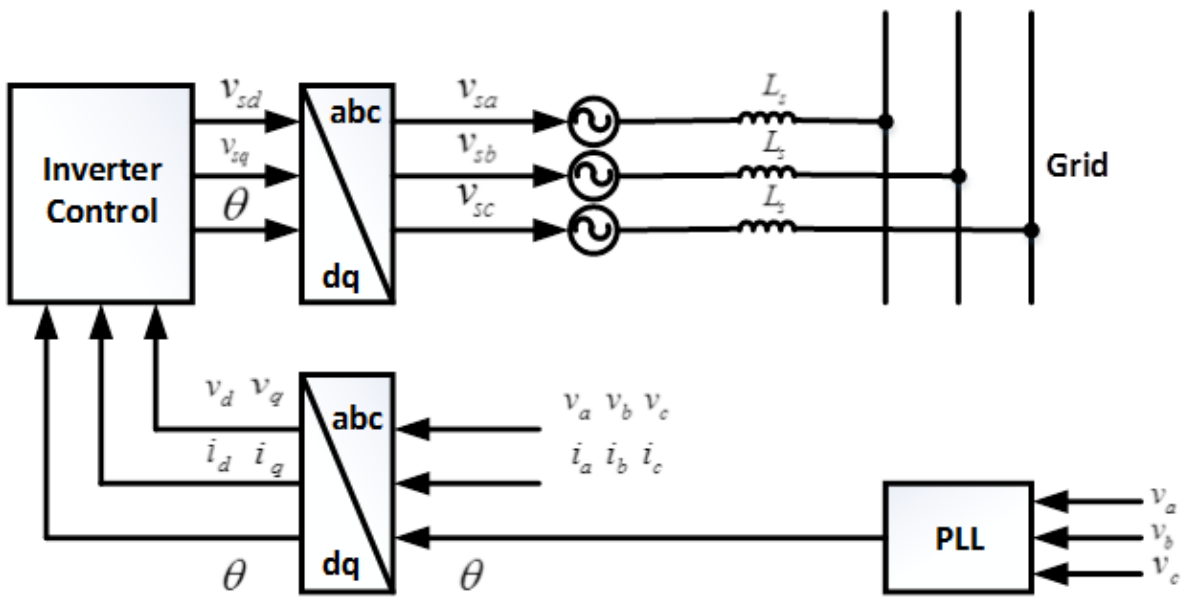

Figure 3.10: Averaged inverter control and PLL

In the previous chapter, we read about the different configurations and topologies of the inverters available to use for grid interconnection. The inverter may also decide on the voltage level at which the PV panel operates, or use the maximum power point tracking function to identify the operating voltage point. The inverter is designed to operate in sync with the utility or grid (i.e. unity power factor), and it generally delivers the maximum power to the electric utility/grid, depending on the environmental conditions for PV power generation.

For analyzing purposes, we will use the average inverter model. Figure 3.10 shows the average model of the three phase VSI inverter. The inverter's current dynamics can be represented by equations (3.38) and onwards. The inverter is the start of the connection with the grid. The inverter uses the DC voltage provided by the DC-DC converter (boost) and converts it to AC voltage. It has an in series inductor that acts as a filter. The average model is used in this thesis, as it is suitable for analytical purposes. In the average model, we replace the PWM generator, DC sources, and switches (i.e. insulated gate bipolar transistors IGBT's) by ideal voltage sources. These are controlled by the inverter control block. The generator terminal voltage is the sum of the voltage drop across the inductive filter and the inverter terminal voltages. v_a, v_b and v_c are inverter terminal voltages, and v_{sa}, v_{sb} and v_{sc} are the generator terminal voltages.

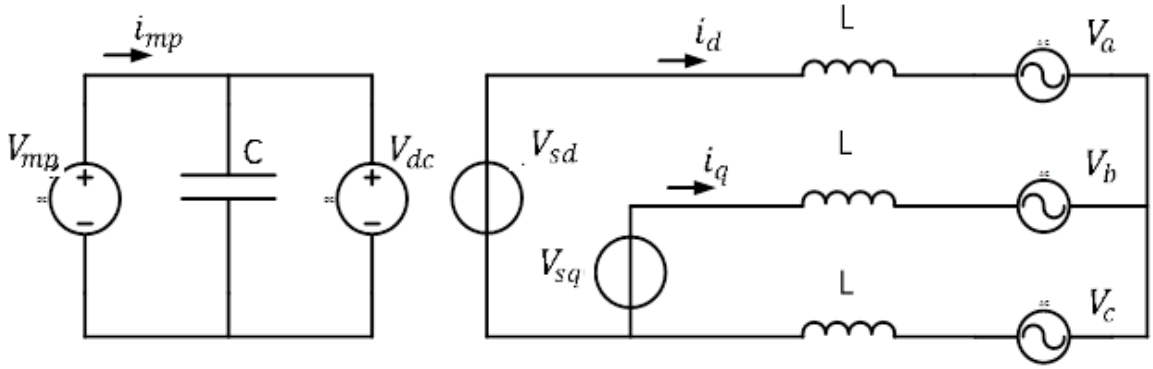

Figure 3.11: Equivalent circuit for grid connected DC-AC converter

The equations for the analysis are given in the synchronous reference frame *dq*, as seen in Figure 3.10. We will be using the grid synchronization technique of Park's Transformation, as mentioned in Chapter 2. The mathematical equations describing the change of reference frames from *abc* to *dq,* and *dq* to *abc*, are expressed by equations (3.38) and (3.39) respectively. The equivalent circuit for the PV system connected to the inverter is shown in Figure 3.11. The left half of the Figure 3.11 is the equivalent circuit of the PV panel and the DC-DC converter with the DC-link capacitor. The right half of Figure 2.11 depicts the equivalent

circuit of the inverter,

The basic equation for a change of reference frame from *abc* to *dq*

$$\begin{bmatrix} v_d \\ v_q \end{bmatrix} = \frac{2}{3}\begin{bmatrix} \cos\theta & \cos(\theta-\gamma) & \cos(\theta+\gamma) \\ -\sin\theta & -\sin(\theta-\gamma) & -\sin(\theta+\gamma) \end{bmatrix}\begin{bmatrix} v_a \\ v_b \\ v_c \end{bmatrix} \quad \text{..... (3.38).}$$

The equation for a change of reference frame from *dq* to *abc*.

$$\begin{bmatrix} v_a \\ v_b \\ v_c \end{bmatrix} = \begin{bmatrix} \cos\theta & -\sin\theta \\ \cos(\theta-\gamma) & -\sin(\theta-\gamma) \\ \cos(\theta+\gamma) & -\sin(\theta+\gamma) \end{bmatrix}\begin{bmatrix} v_d \\ v_q \end{bmatrix} \quad \text{..... (3.39).}$$

The angle θ used in the change of reference frames is obtained from the phase locked loop.

The value of $\gamma = 2\pi/3$.

The DC-AC converter filter is an inductor, whose voltage is calculated as the difference of the generator terminal voltage and the inverter terminal voltage for a single phase. Similarly, for the other two phases combined with the inductor voltage, we arrive at the following equations:

$$L_s \frac{di_a}{dt} = v_{sa} - v_a \quad \text{..... (3.40),}$$

$$L_s \frac{di_b}{dt} = v_{sb} - v_b \quad \text{..... (3.41),}$$

$$L_s \frac{di_c}{dt} = v_{sc} - v_c \quad \text{..... (3.42).}$$

Representing the above equations in matrix form for conversion to *dq* reference frame,

$$L_s\begin{bmatrix} i_a \\ i_b \\ i_c \end{bmatrix} = \begin{bmatrix} v_{sa} \\ v_{sb} \\ v_{sc} \end{bmatrix} - \begin{bmatrix} v_a \\ v_b \\ v_c \end{bmatrix} \quad \text{..... (3.43).}$$

Applying transformation matrix

$$L_s.T\begin{bmatrix}\dot{i}_a\\ \dot{i}_b\\ \dot{i}_c\end{bmatrix}=T\begin{bmatrix}v_{sa}\\ v_{sb}\\ v_{sc}\end{bmatrix}-T\begin{bmatrix}v_a\\ v_b\\ v_c\end{bmatrix} \quad \text{……...……. (3.44).}$$

Here, T is the transformation matrix shown in (3.45)

$$T=\begin{bmatrix}\cos\theta & \cos(\theta-\gamma) & \cos(\theta+\gamma)\\ -\sin\theta & -\sin(\theta-\gamma) & -\sin(\theta+\gamma)\end{bmatrix} \quad \text{……...……. (3.45).}$$

The terms in (3.44) will become

$$T\begin{bmatrix}v_a\\ v_b\\ v_c\end{bmatrix}=\begin{bmatrix}v_d\\ v_q\end{bmatrix} \quad \text{……. (3.46a),}$$

$$T\begin{bmatrix}v_{sa}\\ v_{sb}\\ v_{sc}\end{bmatrix}=\begin{bmatrix}v_{sd}\\ v_{sq}\end{bmatrix} \quad \text{…… (3.46b),}$$

$$T\begin{bmatrix}\dot{i}_a\\ \dot{i}_b\\ \dot{i}_c\end{bmatrix}=\begin{bmatrix}\hat{i}_d\\ \hat{i}_q\end{bmatrix}-\omega AT^{-1}\begin{bmatrix}i_d\\ i_q\end{bmatrix} \quad \text{…….…….. (3.46c).}$$

ω is the measured voltage frequency ω_{PLL}, which can be calculated at the PLL. After applying the transformations we get,

$$v_{sd}=v_d-\omega\, L_s i_q+L_s\dot{i}_d \quad \text{…….…….. (3.47),}$$

$$v_{sq}=v_q+\omega\, L_s i_d+L_s\dot{i}_q \quad \text{……..…….. (3.48).}$$

Equations (3.47) and (3.48) are the main equations for the inverter and filter.

The capacitor in Figure 3.11 is nothing but the DC link which shows us the conversion of DC power to AC power, and its connection. We already know that one of equations used to ensure the equality of the power, for transmission is:

$$P_{dc} = P_{ac} \quad \text{..... (3.49a),}$$

this is,

$$v_{dc}.i_{dc} = v_d i_d + v_q i_q \quad \text{..... (3.49b).}$$

The power relation shown above in (3.49a) is the instantaneous power. Thus, the values of the current and voltage in equation (3.49b) are all instantaneous values. From Figure 3.11 we can deduce that the instantaneous value for DC current is.

$$C\frac{dv_{dc}}{dt} = i_{mp} - i_{dc} \quad \text{..... (3.50),}$$

re-arranging the equation, taking into account overall equivalent model, we get the duty cycle factor in it as well:

$$C\frac{dv_{dc}}{dt} = D' i_{mp} - i_{dc} \quad \text{..... (3.51).}$$

A grid connected inverter is used to generate electrical quantities at a fixed frequency. The grid is modeled as a simple AC source with line impedance. The equations for the voltage at the grid connection point are expressed in *abc* form, as follows:

$$v_a = R_g i_a + L_g \frac{di_a}{dt} + e_a \quad \text{..... (3.52a),}$$

$$v_b = R_g i_b + L_g \frac{di_b}{dt} + e_b \quad \text{..... (3.52b),}$$

$$v_c = R_g i_c + L_g \frac{di_c}{dt} + e_c \quad \text{..... (3.52c).}$$

The Rg and Lg are the line impedance in the grid side. We can express the equations (3.52) in matrix form as follows:

$$\begin{bmatrix} v_a \\ v_b \\ v_c \end{bmatrix} = R_g \begin{bmatrix} i_a \\ i_b \\ i_c \end{bmatrix} + L_g \begin{bmatrix} \dot{i}_a \\ \dot{i}_b \\ \dot{i}_c \end{bmatrix} + \begin{bmatrix} e_a \\ e_b \\ e_c \end{bmatrix} \quad \text{..... (3.53),}$$

converting to the *dq* transform:

$$T\begin{bmatrix} v_a \\ v_b \\ v_c \end{bmatrix} = R_g T\begin{bmatrix} i_a \\ i_b \\ i_c \end{bmatrix} + L_g T\begin{bmatrix} \dot{i}_a \\ \dot{i}_b \\ \dot{i}_c \end{bmatrix} + T\begin{bmatrix} e_a \\ e_b \\ e_c \end{bmatrix} \quad \text{…….. (3.54).}$$

The values for the transforms of equation (3.54) are shown below:

$$T\begin{bmatrix} v_a \\ v_b \\ v_c \end{bmatrix} = \begin{bmatrix} v_d \\ v_q \end{bmatrix} \quad \text{……. (3.55a),}$$

$$T\begin{bmatrix} i_a \\ i_b \\ i_c \end{bmatrix} = \begin{bmatrix} i_d \\ i_q \end{bmatrix} \quad \text{……. (3.55b),}$$

$$T\begin{bmatrix} \dot{i}_a \\ \dot{i}_b \\ \dot{i}_c \end{bmatrix} = \begin{bmatrix} \dot{i}_d \\ \dot{i}_q \end{bmatrix} + \omega A T^{-1}\begin{bmatrix} i_d \\ i_q \end{bmatrix} \quad \text{…… (3.55c),}$$

$$T\begin{bmatrix} e_a \\ e_b \\ e_c \end{bmatrix} = \begin{bmatrix} e_d \\ e_q \end{bmatrix} \quad \text{…… (3.55d).}$$

When the equations of (3.55) are substituted in (3.54) we get the following:

$$\begin{bmatrix} v_d \\ v_q \end{bmatrix} = R_g\begin{bmatrix} i_d \\ i_q \end{bmatrix} + L_g\begin{bmatrix} \dot{i}_d \\ \dot{i}_q \end{bmatrix} + \omega A T^{-1}\begin{bmatrix} i_d \\ i_q \end{bmatrix} + \begin{bmatrix} e_d \\ e_q \end{bmatrix} \quad \text{…….. (3.56).}$$

When we open the term in equation (3.56), we get

$$\begin{bmatrix} v_d \\ v_q \end{bmatrix} = \begin{bmatrix} R & -\omega L \\ \omega L & R \end{bmatrix}\begin{bmatrix} i_d \\ i_q \end{bmatrix} + L_g\begin{bmatrix} \dot{i}_d \\ \dot{i}_q \end{bmatrix} + \begin{bmatrix} E\cos\delta \\ -E\sin\delta \end{bmatrix} \quad \text{……. (3.57).}$$

From (3.57) we deduce the values for ed and eq as

$$e_d = E\cos(\delta_{PLL}) \quad \text{……..…… (3.58),}$$

$$e_q = -E\sin(\delta_{PLL}) \quad \text{(3.59)}.$$

The equations (3.58) and (3.59) are the final grid equations in the *dq* form.

3.6 Phase Locked Loop (PLL) Design

A three-phase PLL helps to find the angle and frequency information of the grid voltage coming to the inverter. The angle obtained will be used for the conversion of the reference frames from *abc* to *dq*. We consider the inverter terminal voltages in three-phases, as follows:

$$v_a = V\cos(\omega \cdot t + \delta_0) \quad \text{(3.60a)},$$

$$v_b = V\cos\left(\omega \cdot t - \frac{2\pi}{3} + \delta_0\right) \quad \text{(3.60b)},$$

$$v_c = V\cos\left(\omega \cdot t + \frac{2\pi}{3} + \delta_0\right) \quad \text{(3.60c)}.$$

Where V is the voltage magnitude and ω is the voltage frequency. At a steady state of operation, the system will have an initial phase angle δ_o.

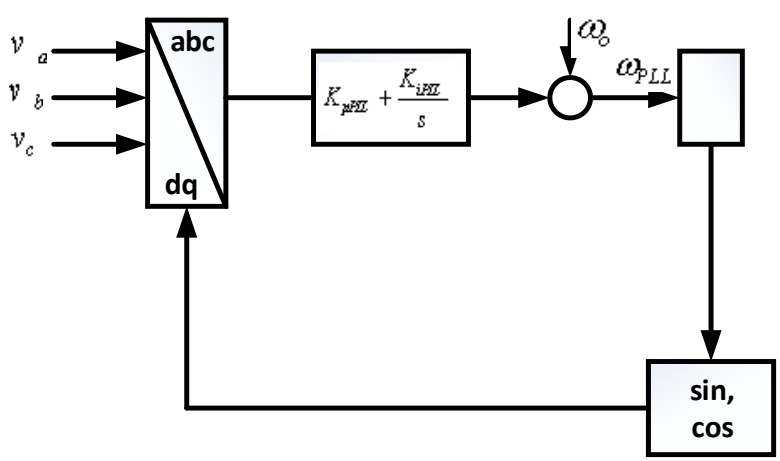

Figure 3.12: PLL control

Figure 3.12 represents the PLL control structure used in the research.

We assume that a change in the phase reflects a change in the voltage frequency, so we have

$$\theta = \omega t + \delta \quad \text{..... (3.61),}$$

where δ is the unknown angle, the change shall be shown by considering the derivative of the angle, thus representing a change in the voltage frequency. This is mathematically represented in equation (3.62).

$$\dot{\delta} = \omega - \omega_o \quad \text{..... (3.62).}$$

The angle in which we are interested is θ; it is being tracked by the phase locked loop measured angle θ_{PLL}. From the grid equations mentioned previously, we know that:

$$\begin{bmatrix} v_d \\ v_q \end{bmatrix} = \begin{bmatrix} V\cos\delta \\ -V\sin\delta \end{bmatrix}$$

$$v_q = V\sin\delta \approx \delta \quad \text{..... (3.63).}$$

The measured inverter terminal voltage angle from PLL is θ_{PLL}. This value tracks the actual voltage angle θ. The difference between them is seen when a transition occurs. The value of the measured voltage phase angle is defined as:

$$\delta_{PLL} = \theta_{PLL} - \omega_o t \quad \text{..... (3.64).}$$

We make use of a simple PI controller to the find the correct difference in the frequency. This difference is then added to the system as ω_o, as seen in Figure 3.12. To obtain the exact frequency, we add the initial voltage frequency to the difference, as follows:

$$\omega_{PLL} = \left(k_{pPLL} + \frac{k_{iPLL}}{s} \right) v_q + \omega_o \quad \text{..... (3.65).}$$

So equation (62) can be re-written as

$$\dot{\delta}_{PLL} = \omega_{PLL} - \omega_o \quad \text{(3.66).}$$

The actual voltage angle θ_{PLL} can be calculated by considering the integral of equation (3.66).

3.7 Design of Current Control

As mentioned in Chapter 2 when discussing the various controls used in this thesis, we shall explain the inverter's role in the current and voltage control. To control the quality of the output power being delivered to the grid, we use a current control and a voltage control as the DC-AC converter control. The inverter control block consists of a voltage regulator (voltage controller) and a current regulator (current controller). Fig 3.13 shows the voltage and current controllers.

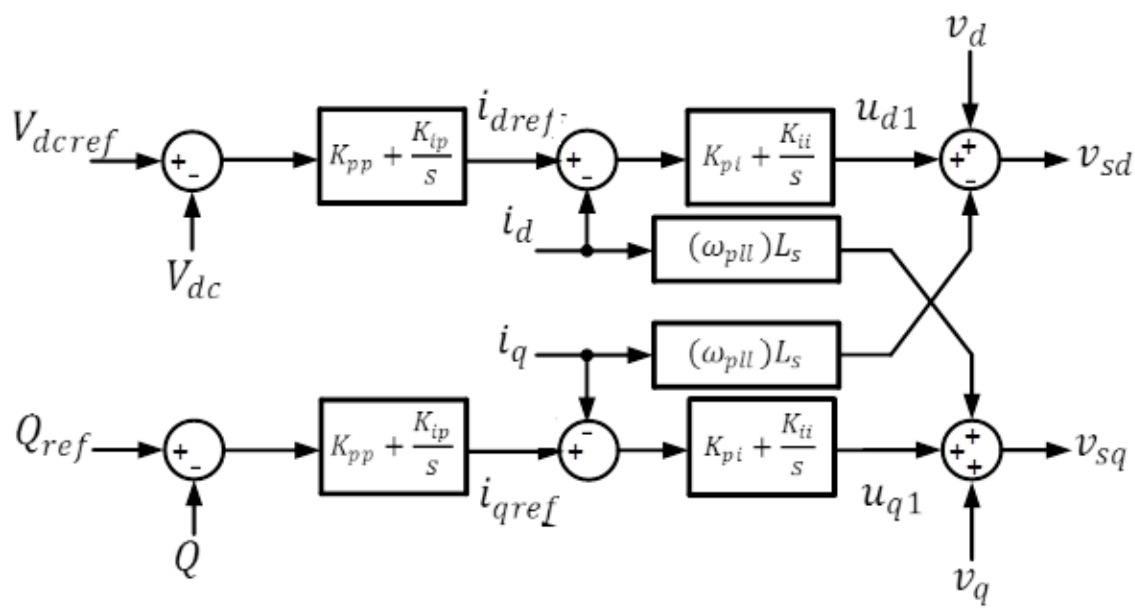

Figure 3.13: The voltage and current controllers

From Figure 3.13 we can observe that the proportional-integral (PI) controllers are used with $\omega_{PLL} L_s i_q$ and $\omega_{PLL} L_s i_d$ as the decoupling components. This thesis uses a technique to control the DC voltage, which in turn controls the power, as power is the product of voltage and current. The constant current control acts as an inner current loop. The active current reference

i_{dref} comes from the voltage controller. The following equations can be derived from the controller structures:

$$i_{dref} = \left(v_{dcref} - v_{dc}\right)\left(k_{pp} + \frac{k_{ip}}{s}\right) \quad \text{(3.67a)},$$

$$i_{qref} = \left(Q_{ref} - Q\right)\left(k_{pp} + \frac{k_{ip}}{s}\right) \quad \text{(3.67b)},$$

$$v_{sd} = \left(i_{dref} - i_d\right)\left(k_{pi} + \frac{k_{ii}}{s}\right) + v_d - \omega_{PLL} L_s i_q \quad \text{(3.68)},$$

$$v_{sq} = \left(i_{qref} - i_q\right)\left(k_{pi} + \frac{k_{ii}}{s}\right) + v_q - \omega_{PLL} L_s i_d \quad \text{(3.69)}.$$

The output voltage of the filter in connection with the grid controller is given by:

$$v_{sd} = v_d - \omega_{PLL} L_s i_q + L_s \dot{i}_d \quad \text{(3.70a)},$$

$$v_{sq} = v_q + \omega_{PLL} L_s i_d + L_s \dot{i}_q \quad \text{(3.70b)}.$$

The output of current control is the compensation for the drop in voltage across the filter.

The equation is given by

$$u_{d1} = \left(k_{pi} + \frac{k_{ii}}{s}\right)\left(i_{dref} - i_d\right) \quad \text{(3.71a)},$$

$$u_{q1} = \left(k_{pi} + \frac{k_{ii}}{s}\right)\left(i_{qref} - i_q\right) \quad \text{(3.71b)}.$$

The active and the reactive powers at the inverter terminal can be measured as follows

$$P = v_d i_d + v_q i_q \quad \text{(3.72a)},$$

$$Q = v_d i_q - v_q i_d \quad \text{(3.72b)}.$$

The inverter controller equations above are all expressed in the per unit system. The three-phase per unit system adopted in the thesis is as follows:

$$Z_{base} = \frac{V_{base}}{I_{base}} \quad \text{..... (3.73),}$$

$$I_{base} = \frac{2}{3}\frac{S_{base}}{V_{base}} \quad \text{..... (3.74).}$$

The V_{base} is the system rated voltage at a peak value, and the S_{base} is the three-phase system base power. The angle and frequency information is obtained from the PLL, as seen in the previous section.

Thus, with the inverter control design, we complete the entire PV system connected to the grid. This chapter provided a detailed description of the mathematical modeling of all the components of the PV system, from the PV cell to the grid side. Thus, able to successfully derive the mathematical equations for the PV cell, the DC-DC converter, the link capacitor, the DC-AC converter, and the grid. These equations help to design the system in an environment where various parameters can be tested for its stability.

Chapter 4

Small Signal Modeling of the Grid-connected Photovoltaic System

4.1 Introduction

This chapter shall present large signal analysis and small signal analysis conducted within this thesis.

We saw in Chapter 3 that the mathematical equations for the PV system connected to a grid were designed. These equations will be used to create a model on which the above mentioned two analyses will be performed.

The large signal analysis shall be done by creating an average model of the PV system in the MATLAB/Simulink environment, with the help of the equations. This model will help us to understand how the system works, and thus also validate our model.

The small signal analysis is conducted on the same model but by following a different procedure. This procedure is explained in this chapter and the results of this analysis will help to understand the various parameters that affect the PV system. Finally, the chapter concludes with a comparison of the average and detailed large signal models and their results.

4.2 Small Signal Analysis

Small signal stability, as defined in [12], is a system's ability to be stable or maintain synchronism when subjected to small disturbances. The disturbances mentioned in the definition depend on the equation description of the system response, which, for the purpose of analysis, can be linearized. In the power systems available today, the problem of small-signal stability arises due to insufficient damping. This need for damping is the result of either the increasing amplitude of the rotor oscillations or the steady increase in the rotor angle of the generator, the latter being caused by a lack of synchronizing torque [41]. The small signal

model of the PV system is derived from the equations of the large signal model. For the purpose of analysis, these equation shall be linearized, which will help to understand the aspect of stability in dynamic systems. The analysis will also help to identify the various parameters or factors that affect the stability of a given power system.

The linearization technique used in this thesis has been adopted from the method used in [12]. It is called the state-space representation technique, and is explained below.

4.2.1 Linearization methodology

State-space representation is a dynamic power system, which can be expressed as a set of *n* first order differential equations, in the following manner:

$$\dot{x}_i = f_i(x_1, x_2 .x_3, \ldots .x_n; u_1, u_2, u_3, \ldots .u_n; t) \quad \ldots\ldots (4.1)$$

Where t = 1, 2, 3… *n*. The order of the system is denoted by *n* and *r* is the number of inputs. The above equation (4.1) can be re-written in the vector matrix form as follows:

$$\dot{x} = f(x, u, t) \quad \ldots\ldots (4.2)$$

Where, *x, u, f* are expressed as column vectors. The column vector *x* is referred as the state vector, and the elements of that vector as state variables. The column vector *u* contains the vector of the system inputs. The $\dot{x}$ is the derivative of *x* with respect to time *t*. The column vectors are shown below:

$$x = [x_1 \quad x_2 \quad x_3 \quad \ldots\ldots \quad x_n]^T \quad u = [u_1 \quad u_2 \quad u_3 \quad \ldots\ldots \quad u_n]^T \quad f = [f_1 \quad f_2 \quad f_3 \quad \ldots\ldots \quad f_n]^T$$

In case the system is autonomous, that is a state variable derivative is not a function of time, In case then (4.2) can be expressed as:

$$\dot{x} = f(x, u) \quad \ldots\ldots (4.3)$$

We are interested in the output variables which are expressed in terms of the state and input

Variables are:

$$y = g(x,u) \quad \text{.....} \quad (4.4)$$

Where y and g are column vectors representing the output variables and the nonlinear function of input variables and state variables. These column vectors are shown below:

$$y = [y_1 \quad y_2 \quad y_3 \quad \ldots\ldots \quad y_m]^T \qquad g = [g_1 \quad g_2 \quad g_3 \quad \ldots\ldots \quad g_m]^T$$

A set of n linearly dependent variables in a system can be used to describe the state of the system. These variables are referred to as state variables. These variables, along with the system inputs, can provide a complete description of the behavior of the system. A mathematical variable, or a physical quantity such as voltage, speed, etc., can qualify as a state variable, which in turn can describe the system dynamics. Any set of chosen state variables will provide the same information about the system dynamics. Defining too many state variables may lead to a redundancy in the variables, and they will become dependent on some of the other variables. The state of the system can be represented in an n dimension Euclidean space called the state space [12]. The next step is the identification of the equilibrium points or the steady state points. This is achieved by equating the derivatives in the system to zero.

$$f(x_0) = 0 \quad \text{.....} \quad (4.5)$$

Here, xo is the state vector, and x is the equilibrium point. While testing local stability, or stability in the small or the small signal analysis, we consider the system to be stable around an equilibrium point or a steady state point, and then subject the system to small perturbations. Consider the equation (4.3), in which x_o is the initial state vector and u_o is the input variable at a steady state point. We introduce a small perturbation into the system, which leads to the following new variables:

$$x = x_0 + \Delta x \qquad\qquad u = u_0 + \Delta u$$

Where Δ denotes the small deviation, all perturbations are assumed to be small, and the terms are expressed with the help of Taylor's series expansion. The higher order terms are neglected for the purpose of analysis.

The linearized set of equations are finally expressed in the following way:

$$E\dot{\hat{x}} = A\hat{x} \quad \text{..... (4.6)}$$

Where term E represents a matrix with the coefficients of the derivative part of size n*n.

The term A represents a state matrix of size n*n. After the calculation of the state-space matrix for a steady state point of the entire power system, we can check for the Eigen properties of the matrix. The eigenvalues can be real or complex values, and always occur in conjugate pairs [12]. The significance of eigenvalues is explained as follows: *The real component of the eigenvalues gives the damping, and the imaginary component gives the oscillation. A negative real part represents a damped oscillation whereas a positive real part represents an oscillation of increasing amplitude* [12].

We can calculate the frequency of oscillation and the damping ratio from a pair of eigenvalues. A complex pair of eigenvalue is represented generally as:

$$\lambda = \sigma \pm j\omega \quad \text{..... (4.7).}$$

The frequency of the oscillations is calculated in Hz as:

$$f_{OSC} = \omega / 2\pi \quad \text{..... (4.8).}$$

The damping ratio is calculated as:

$$\xi = -\left(\frac{\sigma}{\sqrt{\sigma^2 + \omega^2}} \right) \quad \text{..... (4.9).}$$

As mentioned previously, in this thesis the methodology was developed and the small signal stability test were conducted on the PV system. Some of the small signal linearized equations are shown in the next section. A complete list of the small signal linearized equations is available in Appendix B.

4.3 Small Signal of the PV System Connected to a Parallel RLC Load

Figure 4.1 shows a three-phase PV system with a parallel RLC load connected to the grid. The PV system shown above is considered for the small signal stability analysis. R and L are the distribution line impedance. A circuit breaker is placed between the grid and the distributed generation system. The power being delivered by the PV-DG system is P_{DG},Q_{DG}. The power flowing to the parallel RLC load is P_L,Q_L. The difference of the power consumed by the load and the PV-DG supplied power is then fed to the distribution system or grid, i.e. P_G,Q_G. The direction of the power flow is defined from the DG side to the grid side. The current of the DG are i_a, i_b, i_c. The parallel RLC branch currents are as follows for the R_L branch is i_{Ra}, i_{Rb}, i_{Rc} for the L_L branch is i_{La}, i_{Lb}, i_{Lc} and for the C_L branch is i_{Ca}, i_{Cb}, i_{Cc}. The current flowing through the distribution line is i_{Ga}, i_{Gb}, i_{Gc} and the and the terminal voltages of the PV-DG system are v_a, v_b, v_c.

The equations for the system shown in Figure 4.1 are expressed as follows:

$$v_a = Ri_{Ga} + L\frac{di_{Ga}}{dt} + e_a \quad \text{(4.10a)}$$

$$v_b = Ri_{Gb} + L\frac{di_{Gb}}{dt} + e_b \quad \text{(4.10b)}$$

$$v_c = Ri_{Gc} + L\frac{di_{Gc}}{dt} + e_c \quad \text{(4.10c)}$$

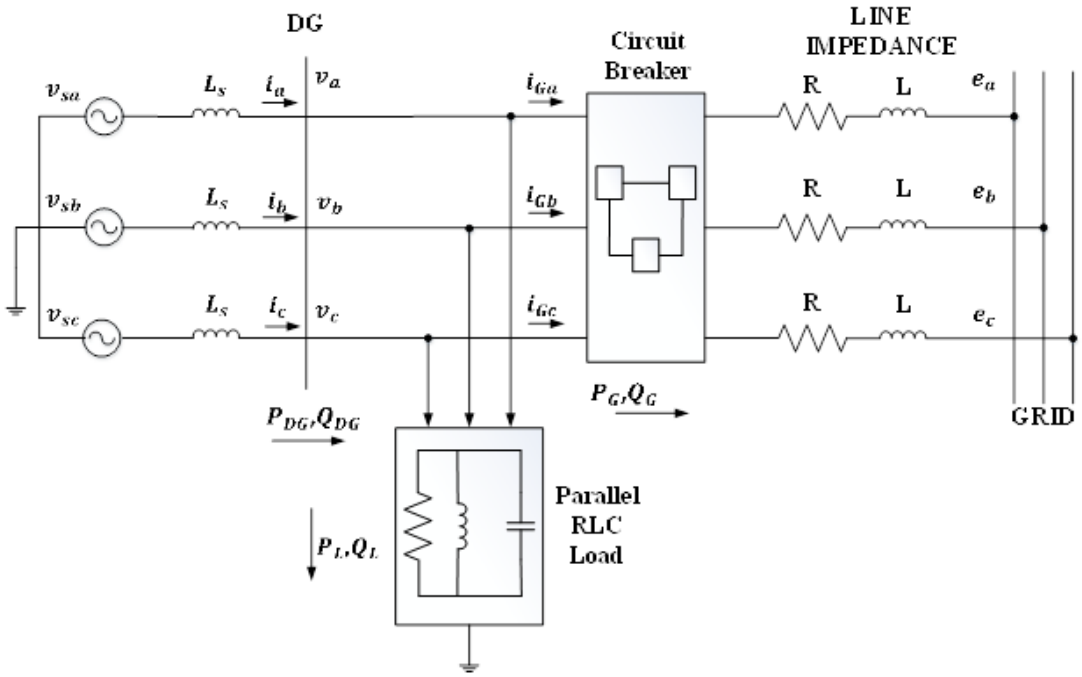

Figure 4.1: PV system connected to a parallel RLC load

The equation for the PV-DG current is the sum of the currents through the load and the current flowing to the grid. This is expressed as follows:

$$i_a = i_{Ra} + i_{La} + i_{Ca} + i_{Ga} \quad \text{(4.11a)}$$

$$i_b = i_{Rb} + i_{Lb} + i_{Cb} + i_{Gb} \quad \text{(4.11b)}$$

$$i_c = i_{Rc} + i_{Lc} + i_{Cc} + i_{Gc} \quad \text{(4.11c)}$$

The value for the current flowing through the load resistance can be calculated by using the Ohms law; it is found by dividing the DG terminal voltage with the load resistance.

$$i_{Ra} = \frac{v_a}{R_L} \quad \text{(4.12a)}$$

$$i_{Rb} = \frac{v_b}{R_L} \quad \text{(4.12b)}$$

$$i_{Rc} = \frac{v_c}{R_L} \quad \text{(4.12c)}$$

The relation between the load inductance, the capacitance to the terminal voltages, and the current are shown below

$$v_a = L_L \frac{d}{dt} i_{La} \quad \text{(4.13a)}$$

$$v_b = L_L \frac{d}{dt} i_{Lb} \quad \text{(4.13b)}$$

$$v_c = L_L \frac{d}{dt} i_{Lc} \quad \text{(4.13c)}$$

The load capacitance equations:

$$i_{Ca} = C_L \frac{d}{dt} v_a \quad \text{(4.14a)}$$

$$i_{Cb} = C_L \frac{d}{dt} v_b \quad \text{(4.14b)}$$

$$i_{Cc} = C_L \frac{d}{dt} v_c \quad \text{(4.14c)}$$

These equations are also represented in the *dq* frame

$$v_d = Ri_{Gd} + L\frac{di_{Gd}}{dt} - \omega_{PLL} Li_{Gq} + e_d \quad \text{(4.15a)}$$

$$v_q = Ri_{Gq} + L\frac{di_{Gq}}{dt} + \omega_{PLL} Li_{Gd} + e_q \quad \text{(4.15b)}$$

Similarly, the *dq* reference frame equations for the DG current, the load resistance, and the inductance and capacitance are shown below:

$$i_d = i_{Rd} + i_{Ld} + i_{Cd} + i_{Gd} \quad \text{(4.16a)}$$

$$i_q = i_{Rq} + i_{Lq} + i_{Cq} + i_{Gq} \quad \text{(4.16b)}$$

$$i_{Rd} = \frac{v_d}{R_L} \quad \text{(4.17a)}$$

$$i_{Rq} = \frac{v_q}{R_L} \quad \text{(4.17b)}$$

$$v_d = L_L \frac{di_{Ld}}{dt} - \omega_{PLL} L_L i_{Lq} \quad \text{(4.18a)}$$

$$v_q = L_L \frac{di_{Lq}}{dt} + \omega_{PLL} L_L i_{Ld} \quad \text{(4.18b)}$$

$$i_{Cd} = C_L \frac{d}{dt} v_d - \omega_{PLL} C_L v_q \quad \text{(4.19a)}$$

$$i_{Cq} = C_L \frac{d}{dt} v_q + \omega_{PLL} C_L v_d \quad \text{(4.19b)}$$

As mentioned in Chapter 3, the angle of the transformation is obtained from the PLL, as it is in the case of the transformations conducted above for the PV system with a parallel RLC load. The remaining set of equations are the same as modelled before. The detailed set of linearized equations as well as the state-space matrix for the entire system is shown in Appendix B and Appendix C.

4.4 Model Validation

The PV distributed generation system designed in Chapter 3 and Chapter 4 was constructed with the help of MATLAB 2014b and the Simulink Toolbox. The exact parameters are mentioned in Appendix A. In the following sections, we consider two cases for model verification; the case of a small signal stability analysis without PSS, and the case of a large signal model analysis of the average and detailed models.

4.4.1 Small signal stability analysis of PV system without PSS

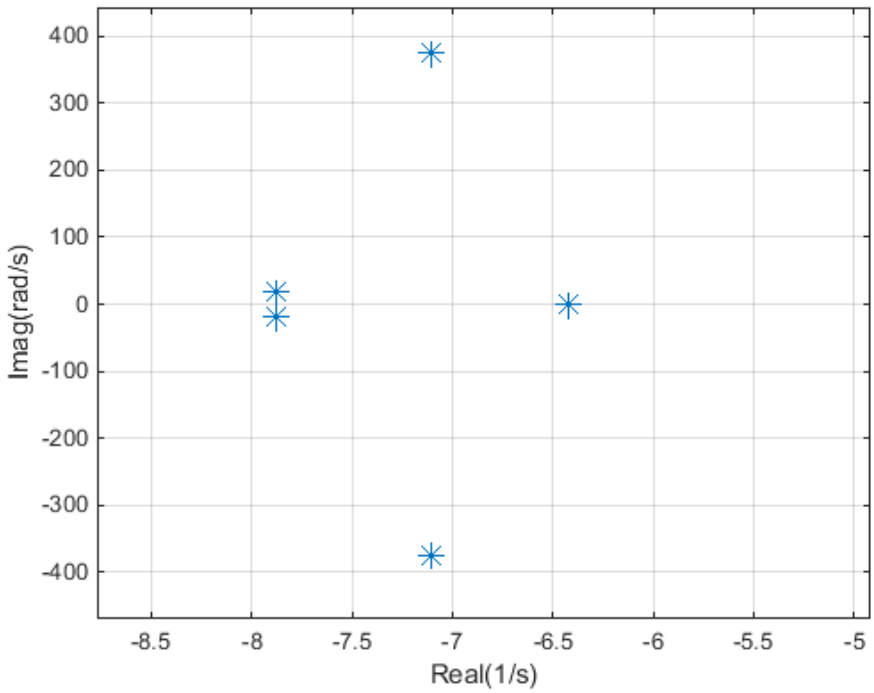

Figure 4.2: Eigenvalue plot for the PV system without PSS controller

The system in Figure 2.1 is linearized and a small signal model is generated from the large signal model by following the procedure explained previously in this chapter. The model considered for the small signal stability analysis is one without the power system stabilizer. The steady state points are calculated and used for the eigenvalue analysis, and the reference command q_{ref} is set to zero. The eigenvalue analysis helps to understand the PV system's control against the variations in the parameters of the system. The operating conditions are G = 1000 W/m^2 and V_{dc} = 550 V. The eigenvalues plotted in Figure 4.2 are all in the left half of the s-plane, therefore the system is said to be stable, as per Lyapunov's first method. Table 4.1 reports the eigenvalues of the overall system with calculations for the damping ratio and their oscillating frequencies. The base values are set and calculated for the per unit system. The steady state values of the PV system, which were obtained in the analysis, can be seen in

Appendix A.

Table 4.1: Eigenvalues for PV system without PSS

	$\lambda = \sigma \pm j\omega$	σ	ω	ξ	f_{osc}
λ_1, λ_2	-165.02±j922.2	-165.0201	922.27509	0.17613	146.78
λ_3, λ_4	-7.10±j375.35	-7.104521	375.35074	0.01892	59.97
λ_5, λ_6	-18.64±j267.54	-18.64304	267.54748	0.06951	42.58
λ_7, λ_8	-206.3±j191.76	-206.3377	191.76182	0.73250	30.52
λ_9, λ_{10}	-7.88±j19.55	-7.881436	19.5548	0.37382	3.11
λ_{11}	-6.419	-6.419737	0	1	0
λ_{12}	-132.644	-132.6444	0	1	0
λ_{13}	-240.412	-240.4123	0	1	0
λ_{14}	-260.351	-260.3511	0	1	0
λ_{15}	-0.02496 E+8	-2496250.3	0	1	0
λ_{16}	-2.26590 E+8	-226590471.5	0	1	0

We use a participation matrix in order to obtain the association of the state variables and the eigenvalues. The element in the matrix in (4.21) is called as the participation factor. The participation factor is the measure of participation of a state variable in a particular mode and vice versa. The participation factors for the system are shown in Table 4.2. The values highlighted in the Table 4.2 show the maximum participation of the state variables. Thus, helping to identify the relation between the eigenvalue and the state variable.

Table 4.2: Participation factor matrix for PV system without PSS controller

	λ_1	λ_2	λ_3	$\lambda_{4,5}$	$\lambda_{6,7}$	$\lambda_{8,9}$	$\lambda_{10,11}$	$\lambda_{12,13}$	λ_{14}	$\lambda_{15,16}$
I_{mp}	0	1	0	0	0	0	0	0	0	0
V_{dc}	0	0	0	0	0	0	0	0.5	0	0
I_{gd}	0	0	0	0.2	0	0	0.3	0	0	0
I_{gq}	0	0	0	0.2	0	0	0.1	0	0	0
I_d	0	0	0	0	0	0	0	0	0	0.4
I_q	0	0	0	0	0	0.4	0	0	0.1	0
I_{ld}	0	0	0	0	0.5	0	0	0	0	0
I_{lq}	0	0	0	0	0.4	0	0	0	0	0
V_d	0	0	0	0.3	0	0	0.2	0	0	0
V_q	0	0	0	0.2	0	0	0.1	0	0	0.5
U_d	0	0	1	0	0	0	0	0	0	0
U_q	0	0	0	0	0	0.4	0	0	0.1	0
I_{dref}	0	0	0	0	0	0	0	0.5	0	0
I_{qref}	0	0	0	0	0	0.2	0	0	0.4	0
ω_{PLL}	0	0	0	0	0	0	0.1	0	0	0.5
δ_{PLL}	0	0	0	0	0	0	0	0	0	0.5

The participation matrix is:

$$p = \begin{bmatrix} p_1 & p_2 & p_3 & \cdots\cdots & p_n \end{bmatrix} \quad \text{(20)}$$

$$p_i = \begin{bmatrix} p_{1i} \\ p_{2i} \\ \cdots \\ p_{ni} \end{bmatrix} = \begin{bmatrix} \varphi_{1i}\rho_{i1} \\ \varphi_{2i}\rho_{i2} \\ \cdots \\ \varphi_{ni}\rho_{in} \end{bmatrix} \quad \text{(21)}$$

φ_{ki} is the kth entry of the right eigen vector φ_i; ρ_{ik} is the kth entry of the left eigen vector ρ_i

From the table 4.2 we can infer which state variables are affected the most.

Table 4.3: Eigenvalues and corresponding state variables

	$\lambda = \sigma \pm j\omega$	ΔX
λ_1, λ_2	-165.02±j922.2	I_{mp}
λ_3, λ_4	-7.10±j375.35	u_d, v_d, I_{Gq}
λ_5, λ_6	-18.64±j267.54	$I_{Ld}, v_d, I_{Lq}, I_{Gq}$
λ_7, λ_8	-206.3±j191.76	I_q, I_{Ld}, I_{Lq}, u_q
λ_9, λ_{10}	-7.88±j19.55	I_{Gd}, i_q, u_q
λ_{11}	-6.419	i_{Gd}
λ_{12}	-132.644	i_{dref}, V_{dc}
λ_{13}	-240.412	i_{dref}, V_{dc}
λ_{14}	-260.351	i_{qref}
λ_{15}	-0.02496 E+8	$i_d, v_q, \omega_{PLL}, \delta_{PLL}$
λ_{16}	-2.26590 E+8	$i_d, v_q, \omega_{PLL}, \delta_{PLL}$

The participation factor table values have been rounded and the thousand place and participation factor values below 0.001 have been considered as zero in the table. From the table 4.2 we can infer which state variables are affected the most. We observe from the matrix, that the eigenvalue λ_2 = -165.02 – j922.2 which belongs to the PV panel in the system, as the state variable which shows dominant participation of the eigenvalue λ_2 is that of the current at maximum power of the panel. In the Table 4.2, the relationship between the eigenvalues and the corresponding state variables is evident. The participation factor matrix helps to derive these results, clearly showing which parameters in the system are affected by the dominant eigenvalues. This analysis helps us to understand the system better and improve its performance by focusing only on the variables with a high value of participation for that mode of operating points.

4.4.2 Large signal model analysis of PV system

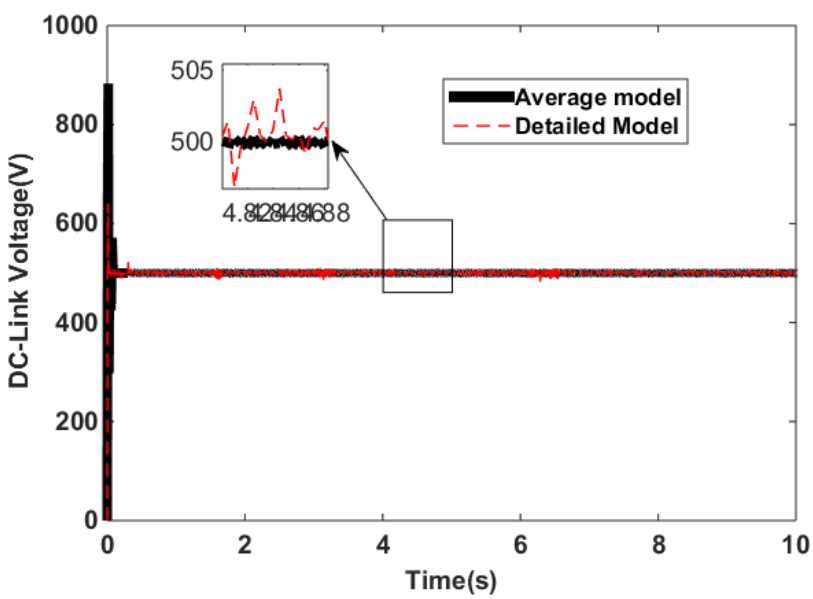

Figure 4.3: DC-voltage for the Average and Detailed large signal model without PSS

The model being validated in this section is the large signal model that was described in Chapters 2 and 3. The system equations designed in the previous chapters are used to build a model in the MATLAB2014b environment by making use of the Simulink toolbox.

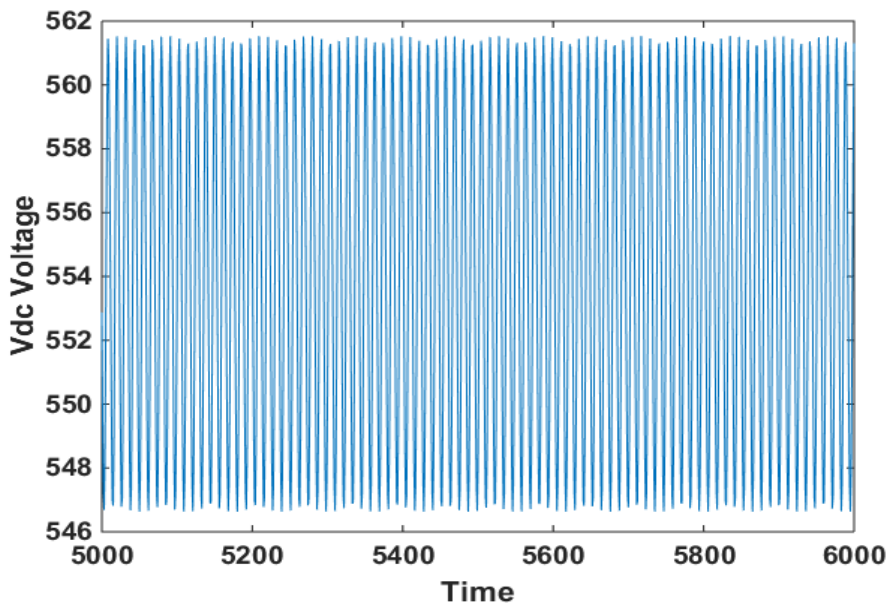

Figure 4.4: DC link voltage for PV system

The system equations developed were the large signal equations, and with the help of these equations a large signal model is developed for analysis. In this thesis we have developed the average model and the switching or detailed model to validate the equations. The two models differ from each other due to their components.

The basic components are the same, i.e., the PV panel, the MPPT controller, DC-DC converter, and the grid connected DC-AC inverter. In the detailed model, the DC-DC converter or boost used consists of IGBT switches, and the pulses for switching are produced by the pulse width modulation. Figure 4.3 is of the dc link voltage, as it is one of the most important parameters being controlled. The system parameters for the average and detailed models are kept same. The other parameters are listed in Appendix A.

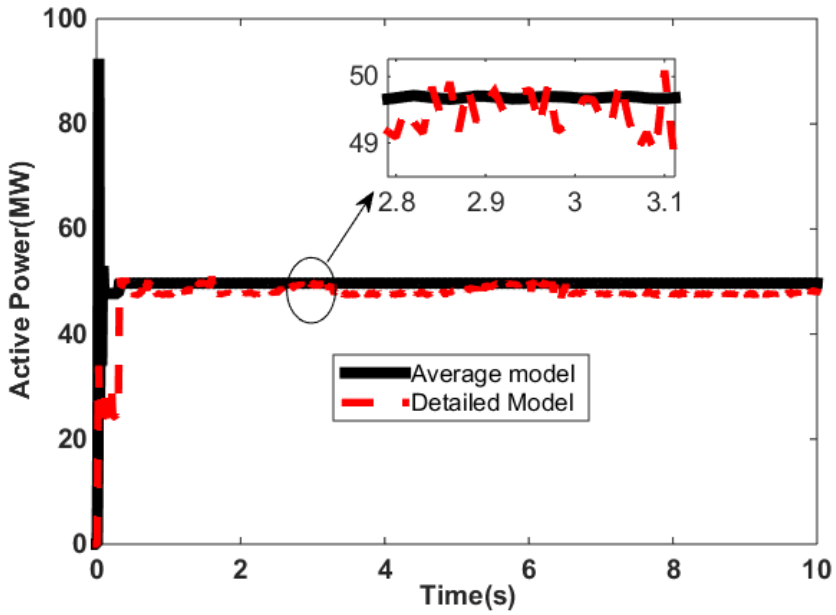

Figure 4.5: Active Power for Average and Detailed model of the system.

We observe that the DC link voltages produced in both the models are very similar, thus proving that both models, as designed, are operating correctly for the mentioned parameters.

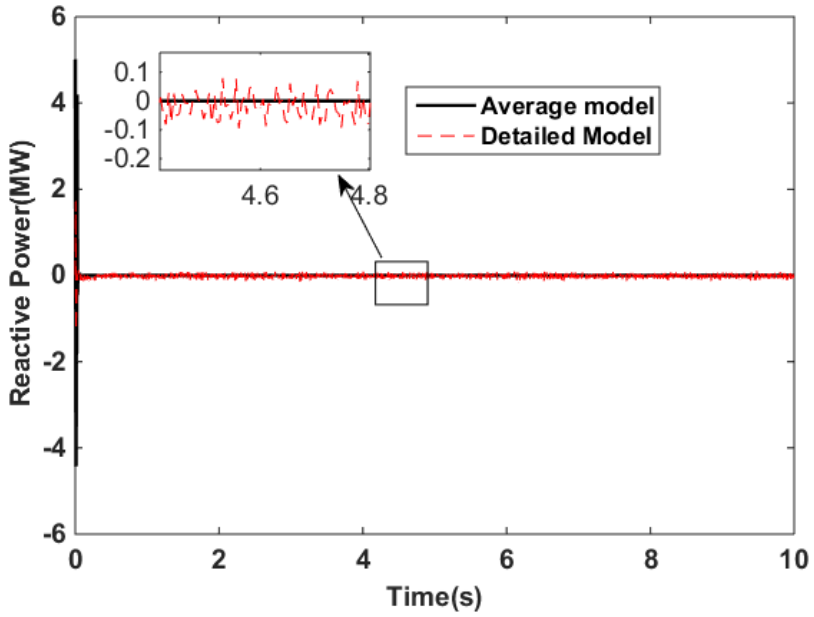

Figure 4.6: Reactive Power for Average and Detailed model of the system.

The detailed model curve (red curve) is not clear, as this model uses the forced commutated devices as switches. The switching action occurs at high rate, resulting in a waveform with lot of switching in it. Whereas, in the average model, we use a set of power electronic converters for the switching. These power electronic converters help attain smoother curves. Since the DC-link voltage is not clearly seen in the Figure 4.3, the proper values can be observed in Figure 4.4. The other important parameters are the active and reactive powers of the system. These two parameters can be observed in Figure 4.5 and Figure 4.6.

4.5 Summary

We understand from the figures that the required active power is being delivered and both the models are in sync with each other as they are producing the same amount of power, thus validating the design of the system. The small signal stability has also shown that the designed system is stable. We shall be observing a similar set of results in the following chapter, where a power system stabilizer is connected. We will try to validate the PSS model designed in the following chapter.

Chapter 5

Power System Stabilizer Design for the Grid-connected Photovoltaic System

5.1 Introduction

This chapter talks about the stability of the power system. It begins with the dynamics of the power system, which helps to understand the stability aspect of a power system. A general overview of the power system dynamics is provided.

The chapter also covers the oscillations in a power system, thus describing the need for damping controllers or power system stabilizers. A general description of the basic structure of a PSS is then described, followed by the design of the PSS adopted in this thesis.

The model of the PSS investigated as part of this research, based on its design, shall be tested for its small signal stability, and the results will validate the PSS design described in the thesis. The results shall also include the calculation of the participation factors for the system with the PSS. Finally, the chapter concludes with the results of a PV system connected to the grid with the PSS controller.

5.2 Overview

In the previous chapter we have read about the stability of the power systems. To gain a better understanding of power system stability, we need to understand the dynamics of it. The term dynamics means the behavior of the system when it encounters a disturbance. The disturbance can be a deliberate one, such as the scheduled switching of generators, or an accidental one, such as the strike of lightning. Power system dynamics are classified on the basis of the time the system takes to respond to these disturbances [42].

The power system dynamics can be categorized into four types:

- Wave dynamics: are more commonly known as surges. They are the fastest

dynamics, mostly occurring in high voltage transmission lines. They can be caused by the switching of operations in the system.

- Electromagnetic dynamics: are slower in comparison to wave dynamics. They usually occur in the windings of the machine, when the system is subjected to a certain disturbance.
- Electromechanical dynamics: When a system is subjected to a disturbance, it not only affects the power system but also affects the components such as the rotating parts of the generator or the motor, which get subjected to oscillations due to the disturbance of the system.
- Thermodynamics: This is the slowest type of response to variations or disturbances. An example is boiler control action in steam power plants.

The growth of new and more complex power systems has led to the birth of various forms of system instability, leading to the proposal of various stability methods, such as voltage stability or frequency stability. However, power system stability is, in itself, a problem with different classes in it.

As mentioned, voltage stability is one of the proposed techniques for system stability. It basically means the ability of a power system to maintain steady voltages when operating under normal conditions or when subjected to disturbances. When instability occurs, it is either caused by a rise or a fall in voltage. One of the main reasons for voltage instability is the loads. The loads on subject to a disturbance usually restores itself, leading to the consumption of reactive power and the voltage keeps falling till it collapses. At this no sufficient power transfer capacity is available nor any generation capability. The problems related to the voltage stability also arise when weak AC systems are connected to HVDC links. It is useful to sub-categorize

the voltage stability as the following:

- Large disturbance voltage stability: As the name suggests, it is the system's ability to overcome the disturbance and control the voltage of the power system. The large disturbance can be due to a generation loss or system faults. To determine the large disturbance stability, we need to analyze the system over a certain period of time to understand its non-linear dynamic performance. Running dynamic simulations for a long time can help in the analysis [24].
- Small disturbance voltage stability: it is the system's ability to maintain the voltage levels when it is subjected to small changes or perturbations. The small changes can be in the form of small load increments. This method is useful as it helps to understand the behavior of a system in response to a change at any given time. The essential part of this analysis is that the entire analysis is conducted for an operating condition or a steady state. The voltage level in the system increases as the reactive power injection is increased for the given operating conditions.

The sub-categorization of the different stability techniques is possible as a linear system is independent of its input. In the case of a non-linear system, it depends on the input and the initial state of the system. The stability of a non-linear system is generally classified into the following:

A. Local stability or small signal stability;
B. Finite stability;
C. Global stability or large signal stability.

Local stability or small signal stability is experienced when a system is subjected to a small perturbation near a steady state point. As time increases, the system will return to its initial or original state. The system remains stable over a small area around the steady state point. To

obtain this stability, we convert the system from non-linear to linear. The technique for linearization has been explained in Chapter 4 and is adopted in this thesis.

5.3 Oscillations in Power Systems

The need for a power system stabilizer (PSS) or a damping controller in power systems has been present since the very beginning, when the damping of oscillations was recognized as an important aspect in the operation of a power system. Over the years, various forms of oscillations in power systems were identified, and although at one point researchers believed they had devised a technique to remove the oscillations, they always re-appeared. There are multiple reasons for these oscillations. To better understand, we shall consider oscillations that are classified based on their interaction characteristics. They are classified as follows:

- Local plant mode oscillations: These oscillations are common at generating stations. They arise when the units at the power generating station oscillate with respect to the rest of the units of the generating station. They are usually caused by the generating units' AVRs working at high output and feeding weak transmission networks. The natural frequency of these oscillations lies in the range of 1-2Hz. Damping can be achieved with the help of PSS, which also helps to understand the characteristics of the oscillation.
- Inter-area mode oscillations: These oscillations occur when machines in one portion of the system oscillate against machines in other parts of the system. They occur when a group of machines are kept in close proximity to one another. The natural frequency of these oscillations lie in the range of 0.1-1 Hz. The characteristics of these oscillations are more tedious and complex.
- Torsional mode oscillations: These are associated with the mechanical aspect of the

turbine-generator's rotational parts. Other instances of these oscillations have been caused by generating unit excitation [42].

- Control mode oscillations: These oscillations are linked to the controls of the generating units. The usual cause of these oscillations is the poorly tuned control of an excitation system, HVDC converters, and other similar equipment.

Based on the above classifications of the nature of the power system oscillations, it is observed that these oscillations in a system are due to its natural mode, and can therefore be damped or eliminated by modification. It is important to note the following: firstly, power systems are evolving with time, leading to the formation of new modes. Secondly, the main reason for negative damping is power system controls, most importantly, excitation systems. Lastly, the inter-area oscillations involve multiple utilities or DG systems, making Power System Stabilizers (PSS) the most commonly used method for damping.

5.4 Design of Power System Stabilizer

As we saw in the previous section, the PSS is commonly used for the damping of the oscillations in a power system.

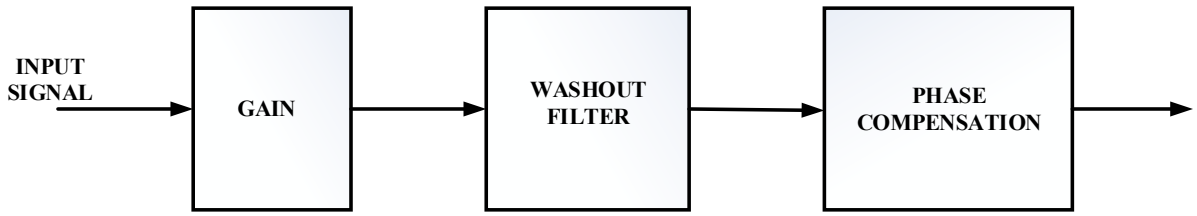

Figure 5.1: General representation of PSS

There are various representations of the PSS, about which literature was reviewed in Chapter 1, with the same motive of providing damping in the power system. The basic design of the PSS on which the controller designed in this thesis is based, is explained below, with the help of Figure 5.1.

The three major components of a PSS are shown above: the phase compensator, the washout filter, and the gain. The phase compensation block is used to compensate for the phase lag between the output of the PSS and the control action being performed. For different conditions of the system, the phase compensation also changes. Usually, an agreed-upon phase compensation is fixed for the different conditions of the power system. The washout filter acts as a high-pass filter by setting a high time constant, enabling the system to allow only the signals associated to the system to pass through. It also allows the PSS to respond in situations when there are changes that are only related to the input signal. The gain decides the amount of damping being achieved by the PSS. It is often fixed at a value where the maximum amount of damping can be achieved, but the value might change depending on the other assumptions made during the design process of the PSS. The addition of the PSS should not decrease the stability of the system but should instead enhance it.

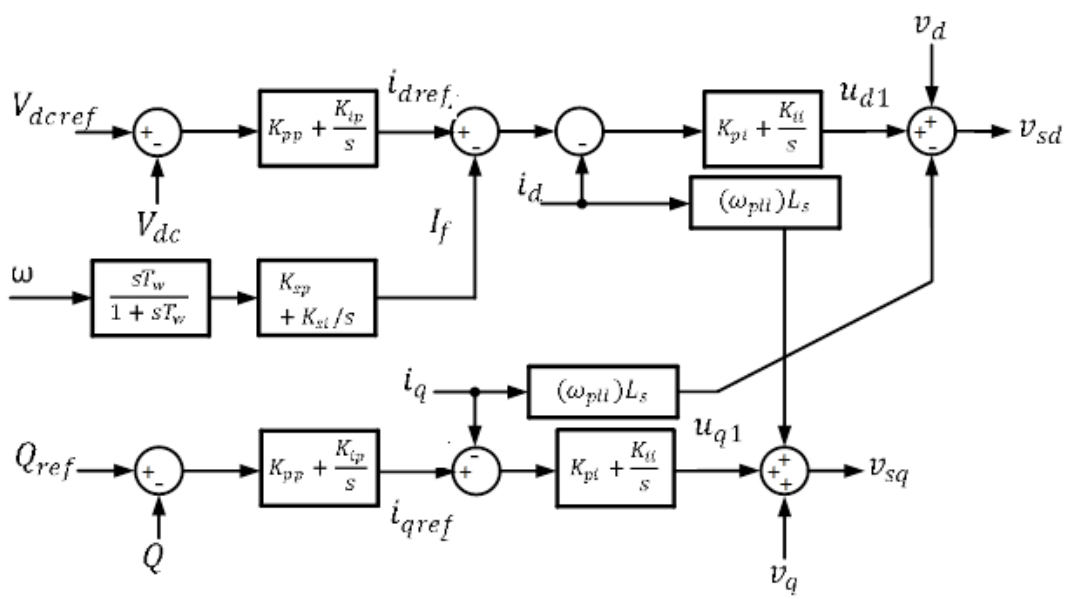

Figure 5.2: PSS controller diagram in the PV system

The power system stabilizer designed and implemented in this thesis is similar to the general representation seen above. The PSS controller design tested in this thesis is shown in Figure 5.2. From Figure 5.2, we observe that the PSS controller is connected to the inner current controller loop. The negative frequency feedback signal detects any change in the V_{dcref} signal, sending a feedback in the form of I_f. The error signal is first obtained at the output of the washout filter block, with a time constant of T_{ω}.

This error signal is then amplified with the help of the negative feedback gain $K_{sp} + K_{si}/s$. When the system is connected to a grid, the frequency of the system is determined by that of the grid. The PSS will destabilize the system when unwanted oscillations affect the system of operation.

$$I_f = (\omega)\left(\frac{sT_w}{1+sT_w}\right)\left(k_{sp} + \frac{k_{si}}{s}\right) \quad \text{(5.1)}$$

$$u_{d1} = \left(k_{pi} + \frac{k_{ii}}{s}\right)\left(i_{dref} - I_f - i_d\right) \quad \text{(5.2)}$$

The mathematical design of the power system stabilizer adopted as part of this thesis is given by equations (5.1) and (5.2). Now, with the addition of these two new equations we shall design the large signal model and implement it in a Simulink environment. The small signal model was developed from this large signal model, to be used in the small signal stability analysis. The procedure followed for the analysis is the same as the one used for the system without PSS, as explained in Chapter 4. In the following sections, the validation of the large signal models with and without PSS is provided, as well as the small signal stability analysis for the PV system with PSS.

5.5 Small Signal Stability Analysis of PV System with PSS

The system is Fig 5.2 is linearized and a small signal model is generated from the large signal model by following the procedure mentioned in Chapter 4. The model considered for the small signal stability analysis is one with a power system stabilizer. The steady state points are calculated and used for the eigenvalue analysis, and the reference command q_{ref} is set to zero. The eigenvalue plot for the grid-connected PV system with PSS, introduces a new state variable and an eigenvalue associated with it (see -1 of Real axis).

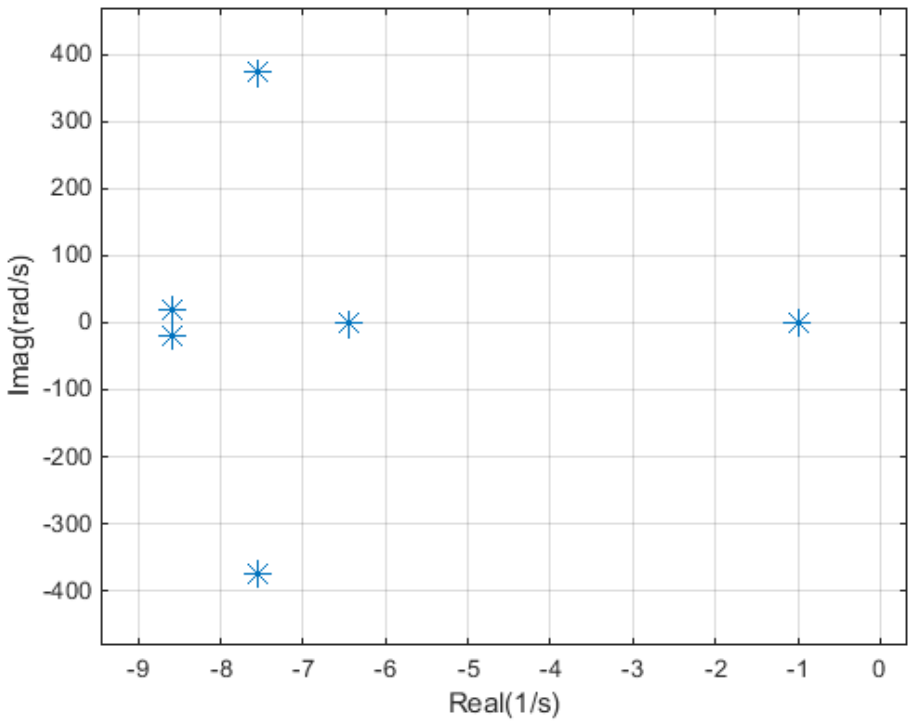

Figure 5.3: Eigenvalue plot for system with PSS.

The other eigenvalues plotted in Figure 5.3 have moved more to the left as compared to the eigenplot for system without PSS. This proves, that the grid-connected PV system is more stable. The operating conditions are G = 1000 W/m^2 and V_{dc} = 550 V. The eigenvalues plotted in Figure 5.3 are all in the left half of the s-plane, and the system is said to be stable as per Lyapunov's first method. Table 5.1 reports the eigenvalues of the overall system, with

calculations for the damping ratio and their oscillating frequencies. The base values are set and calculated as per the per-unit system.

Table 5.1: Eigen values for PV system with PSS

	$\lambda = \sigma \pm j\omega$	σ	ω	ξ	f_{osc}
λ_1, λ_2	-159.6±j935.3	-159.6343939	935.36877	0.1683	1.488
λ_3, λ_4	-699.6±j232.1	-699.6997042	232.16027	0.9491	36.94
λ_5, λ_6	-7.08±j375.2	-7.082289551	375.29944	0.0188	59.74
λ_7, λ_8	-18.55±j268.5	-18.55026186	268.52902	0.0689	42.74
λ_9, λ_{10}	-190.5±j188.6	-190.5013922	188.62327	0.7106	30.02
$\lambda_{11}, \lambda_{12}$	-7.88±j19.53	-7.888265567	19.532015	0.3744	3.10
λ_{13}	-0.99	-0.9999988	0	1	0
λ_{14}	-6.42	-6.420786068	0	1	0
λ_{15}	-133.054	-133.0540964	0	1	0
λ_{16}	-188.40	-188.4089912	0	1	0
λ_{17}	-4.266 E+6	-4.266 E+6	0	1	0

Here $\xi = -(\sigma/\sqrt{\sigma^2 + \omega^2})$ and $f_{osc} = (\omega/2\pi)$

The participation factor matrix help to identify the state variables to the corresponding eigenvalues.

Table 5.2 Participation matrix for PV system with PSS

	λ_1	λ_2	$\lambda_{3,4}$	$\lambda_{5,6}$	$\lambda_{7,8}$	$\lambda_{9,10}$	$\lambda_{11,12}$	λ_{13}	λ_{14}	$\lambda_{15,16}$	λ_{17}
I_{mp}	0	1	0	0	0	0	0	0	0	0	0
V_{dc}	0	0	0	0.9	0	0	0	0.4	0	0	0
I_{gd}	0	0	0.2	0	0	0	0.3	0	0	0	0
I_{gq}	0	0	0.2	0	0	0	0	0	0	0	0
I_d	0	0	0	0	0	0	0	0	0	0.5	0.2
I_q	0	0	0	0	0	0.4	0	0	0.1	0	0
I_{ld}	0	0	0	0	0.5	0	0	0	0	0	0
I_{lq}	0	0	0	0	0.4	0	0	0	0	0	0
V_d	0	0	0.3	0	0	0	0.2	0	0	0	0
V_q	0	0	0.2	0	0	0	0.1	0	0	0.5	0.3
U_d	0	0	0	1.9	0	0	0	0.1	0	0	0
U_q	0	0	0	0	0	0.4	0	0	0.1	0	0
I_{dref}	0	0	0	0.9	0	0	0	0.4	0	0	0
I_{qref}	0	0	0	0	0	0.3	0	0	0.4	0	0
ω_{PLL}	0	0	0	0	0	0	0.2	0	0	0.5	0.1
δ_{PLL}	0	0	0	0	0	0	0	0	0	0.5	0.2
V_{sq}	1	0	0	0	0	0	0	0	0	0	0

This analysis helps in providing information about the parameter which affects the systems stability. The values highlighted in Table 5.2 help identify the relation of the state variable and eigenvalue. The values with highest participation are considered (highlighted). The Table 5.2 provides the relation between the eigenvalues and the variables. This data is collectively presented in Table 5.3.

Table 5.3 Eigenvalue relation with state variables for PSS connected PV system

	$\lambda = \sigma \pm j\omega$	State Variables ΔX
λ_1, λ_2	-159.6±j935.3	I_{mp}, v_{sq}
λ_3, λ_4	-699.6±j232.1	v_d, I_{Gq}
λ_5, λ_6	-7.08±j375.2	V_{dc}, u_d, i_{dref}
λ_7, λ_8	-18.55±j268.5	I_{Ld}, I_{Lq}
λ_9, λ_{10}	-190.5±j188.6	i_q, u_q
$\lambda_{11}, \lambda_{12}$	-7.88±j19.53	I_{Gd}
λ_{14}	-6.42	i_{qref}
λ_{15}	-133.054	$i_d, v_q, \omega_{PLL}, \delta_{PLL}$
λ_{16}	-188.40	$i_d, v_q, \omega_{PLL}, \delta_{PLL}$

The eigenvalue λ_2 from the participation factor matrix Table 5.2 we can observe that, the highest participation is associated with variable I_{mp}. This state variable affects the parameter of the current at maximum point being generated by the panel. The major results obtained as part of this analysis is by comparing the Figure 4.2 and Figure 5.3, we observe that on applying

PSS to the system the eigenvalues have shifted more towards the left half of the s-plane in Figure 5.3. Thus making the system with PSS highly stable as compared to that without PSS in which the eigenvalues are close to the axis (inclining towards instability). This system stability can be achieved by damping the oscillations. The damping effect can be observed in the results of the large signal model.

5.6 Large Signal Model Analysis of PV System with and without PSS

The model being validated here is the large signal model described in Chapters 2 and 3, with the addition of the PSS. The system equations developed were the large signal equations, and with the help of these equations a large signal model is developed for the purpose of analysis. In this thesis, the average model of a system without PSS and the average model of a system with PSS have been developed for validation. The models are exactly the same with respect to

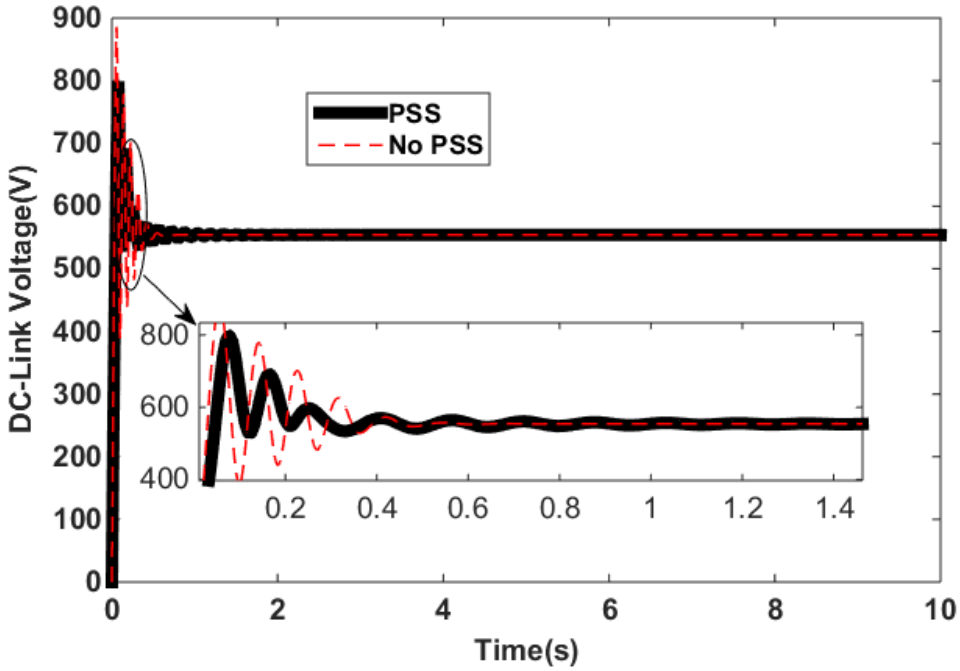

Figure 5.4: DC-Link voltage model with and without PSS

design, but a PSS is added to the inner current control loop, and based on its design equations the model was created and added to the previously designed PV system. Figure 5.4 is of the DC link voltage as it is one of the most important parameters being controlled. The system parameters are kept the same for both models being analyzed. The major parameters are the solar irradiance at G = 1000W/m^2 and the temperature at 25°C.

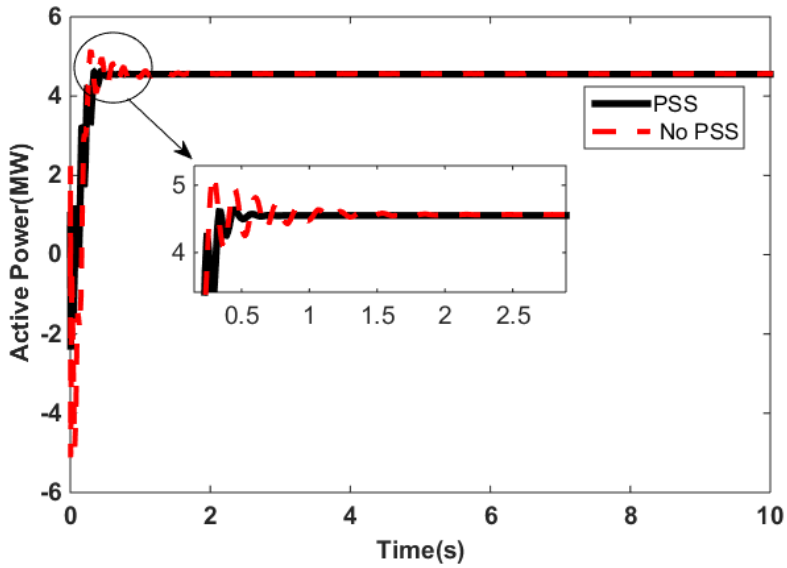

Figure 5.5: Active power curve for model with and without PSS

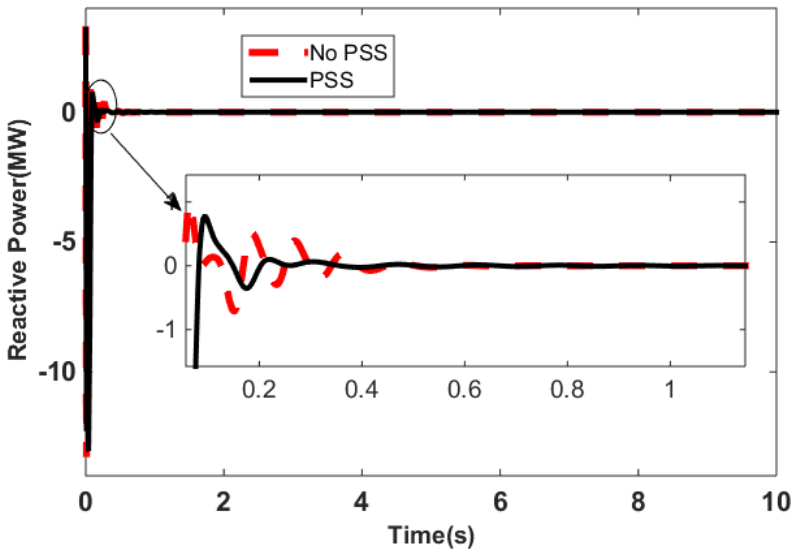

Figure 5.6: Reactive power curve for model with and without PSS

Figure 5.4 clearly shows that by applying a power system stabilizer to the system we can achieve the damping of the oscillations. This damping is also observed in the curves for active and reactive power, as shown in Figure 5.5 and Figure 5.6 respectively.

The damping effect of the power system stabilizer can be seen clearly from the figures, showing the active power and reactive power curves. The curve with PSS shows that the amplitude of the power curve for the oscillations is dampened, thus validating the use of the power system stabilizer in the system. Another aspect to observe is the settling time of the curve, be it voltage or power.

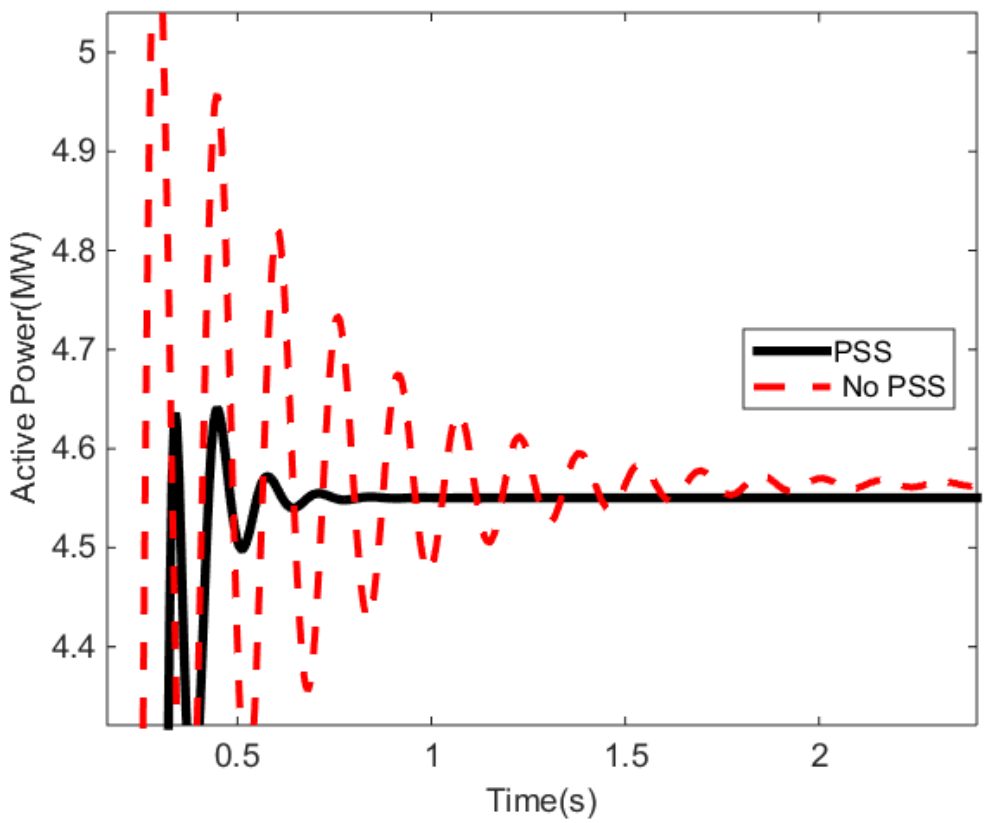

Figure 5.7: Active power curve for model with and without PSS to observe settling time

Fig. 5.7 clearly shows that the settling time for the system without PSS is more than 2 seconds. This means the time taken by the system to achieve a steady state is higher than the time taken by the system with PSS. The black curve indicates that the system has entered a steady state

in less than 1 second. This helps to validate the functionality of the designed power system stabilizer. The damping effect is required more on the Active power curve, as it is the power being delivered by the PV system to the grid. The better damping of oscillations proves a smoother and more stable supply of power from the PV system to the grid. Thus, the active power is the most important parameter to be damped. By control of dc-voltage the smoother power curve is achieved.

5.7 Summary

In this chapter we saw the design of the power system stabilizer using a washout filter and the PI controller, which is being fed to the current controller of the designed PV system. We performed the small signal stability analysis, which led us to the conclusion that the system is not only stable but also more stable than the small signal model of the PV system without a power system stabilizer. The stability was decided based on the comparison of the eigenvalue plot of the system. The damping effect of the PSS was also observed in the large signal model comparisons. The observation of the settling time from the plots were as expected for the PSS. Thus, we can successfully validate the design of the power system stabilizer designed in this thesis.

Chapter 6

Conclusions and Future work

6.1 Summary & Conclusion

The demand for renewable energy is increasing, and solar power generation is one of the fastest growing generation techniques today, with a rise in the number of households using solar power and connecting to the grid/utility. This causes the conversion of the DC voltages produced to AC voltages, with the help of inverters that have different responses, therefore creating an impact when connected to the grid. The study of these dynamic impacts and of system stability for a PV system connected to the grid was the objective of the thesis; the research has proved it to be successful as well.

The major results of the thesis are as follows:

- Chapter 2 mostly discussed the various components or blocks of the PV system used in the thesis. It explained the need for each block in the system and the role that it played.
- Chapter 3 focused on the mathematical modeling of the system described in the previous chapter. This lead to the derivation of the major mathematical equations that will be useful in creating a model in an environment like MATLAB 2014b using the Simulink Toolbox. The models created by these equations help to understand the working of the PV system, and the results can be observed by connecting various scopes at different points in the system.
- In chapter 4, we saw the small-signal technique used in the thesis by linearizing the large signal equations. The model with a parallel RLC load connected to it was designed. The small signal stability analysis of the PV system without a power

system stabilizer is done, and this is validated by the results obtained through the eigenvalue plot, showing that the system is stable with all points in the left-half of the s-plane.

- The participation matrix was successfully calculated, resulting in the identification of the relationship between the eigenvalues and the state variables. A comparison of the average and detailed large signal models is also shown, and the results obtained helped us conclude and validate the system design.
- Chapter 5 discussed the power system stabilizer design implemented in the thesis. The mathematical equations representing the PSS were designed, and the results of the average large signal model with and without PSS were compared. Through this analysis we could clearly validate the observations regarding the damping effect and the settling time comparisons with and without PSS. The small signal stability model for the system with PSS proves to be highly stable as compared to the system without PSS. This conclusion was made when comparing the eigenvalue plots of the two small signal models. The eigenvalues were more to the left of the s-plane in the case of a system with PSS.

When we summarize all the conclusions above, we can see that the objectives of this thesis, which were to create a mathematical model of the PV system connected to a grid, with and without the power system stabilizer, were achieved successfully. The design was validated with the help of the results obtained from the small-signal stability analysis and the large signal analysis of the systems.

6.2 Future Work

A few suggestions on which further investigation could be carried out in the future are:

Firstly, the dynamic effects of the use of an MPPT controller on the system needs to be looked into. The MPPT technique used in the thesis is one that is already available. The major consideration here should be the algorithm chosen for tracking the maximum power point. One, each algorithm has a different implementation method, introducing a new variable in the analysis of the system. Secondly, the research and development of an inverter with good efficiency to provide a better AC output, and an analysis on the chosen inverter so as to maintain the stability of the system. As the inverter plays a crucial role in the connection of the PV system to the grid.

Thirdly, the load considered in the thesis is a constant load or a parallel RLC load. It would be interesting, to find out the performance of the system when catering to a varying load. The stability analysis might help us identify, if the load is the source of instability to the system and the method to curb this instability. Also a fault analysis of the system; would be useful to the utility companies to understand the system's responses when a fault occurs. Lastly, analyzing the islanding behavior of the DG system. This would help to create various anti-islanding schemes.

Appendices

Appendix A

The system parameters are mentioned in the table A.1.

Table A.1: System Parameters

Parameters	**Values**
Reference DC link voltage(V_{dcref})	554 V
Reference Reactive Power (Q_{ref})	0
Washout Filter constant (T_w)	0
Interface inductance (L_s)	1e-5 H
Line Resistance (R)	0.2
Line Inductance (L)	1 mH
Inverter Filter Inductance	1 mH
V_{base}	120*√2
S_{base}	10000

Table A.2: Steady state variables and their values

Parameters	**Values**
w_{PLLo}	2*π*60
I_{qo}	-5.0759
I_{do}	5.1504
D_o	0.5
V_{dco}	548 / V_{base}
I_{dco}	184.14 / I_{base}
I_{mpo}	368.28
V_{mpo}	54.8 / V_{base}
I_{pho}	5.96
del_o	0
V_{sdo}	3.3818
V_{sqo}	0.4495
V_{do}	2.9389
V_{qo}	0

Table A.3: Load Parameters

Parameters	**Values**
Load Resistance	4.32
Load Inductance	6.4 mH
Load Capacitance	1.1 mF

Table A.4: PV Parameters

Parameters	**Values**
Short-circuit current (I_{SC})	5.96 A
Open-circuit voltage (V_{OC})	64.2 V
Irradiance reference value (G_{ref})	1000 W/m^2
Temperature reference value (T_{ref})	298 K
Charge (q)	1.6e-19 C
Diode Quality Factor (n)	1.3
Number of series cells per module (N_s)	96
No. of series connected modules/ string (N_m)	5
Saturation current (I_o)	1.175e-8 A
Boltzmann constant (k)	1.3806503e-23 m^2 kg s^{-2} K^{-1}
Short-circuit current temperature coefficient (mu)	-0.00057 A/K
Open-circuit voltage temperature coefficient (muV)	-0.0027 V/K
Photocurrent reference value (I_{phref})	5.96 A
Actual operating temperature (T)	298 K
Actual operating Irradiance (G)	1000 W/m^2

The controller parameters are mentioned below:

Table A.5: Controller parameter values

Voltage Controller $K_{pp} = 2$	$K_{ip} = 500$
Current Controller $K_{pi} = 3$	$K_{ii} = 500$
PLL Controller $K_{pPLL} = 50$	$K_{iPLL} = 500$
PSS Controller $K_{sp} = 1$	$K_{si} = 1$

The per unit conversions are obtained by the help of the following formulae's:

$$V_{base} = 120 * \sqrt{2}$$

$$S_{base} = 10000$$

$$I_{base} = \left(\frac{2}{3}\right)\left(\frac{S_{base}}{V_{base}}\right)$$

$$Z_{base} = \left(\frac{V_{base}}{I_{base}}\right)$$

$$\omega_{base} = 2 * \pi * 60$$

$$L_{base} = \left(\frac{Z_{base}}{\omega_{base}} \right)$$

$$C_{base} = \left(\frac{1}{\omega_{base} * Z_{base}} \right)$$

Appendix B

The small signal model of system connected to a parallel RLC load is developed with the help of the following linearized equations:

The PV module:

$$\Delta I_{ph} = \left[G_{sun} \cdot I_{phref} + G_{sun} \cdot \alpha \cdot T - G_{sun} \cdot \alpha \cdot T_{ref}\right] \cdot \frac{1}{G_{sunref}} \quad \text{(B.1)}$$

$$\Delta I_{mp} = I_{ph} + q \cdot I_{o}.\Delta V_{mp}\left[\frac{1}{2}\left(\frac{q \cdot V_{mpo}}{nN_s kT}\right)^2 + \left(\frac{q \cdot V_{mpo}}{nN_s kT}\right) + 1\right] \quad \text{(B.2)}$$

The DC-DC converter:

$$L \cdot p(\Delta I_{mp}) = \Delta V_{mp} - \Delta D^{'} \cdot V_{dco} - D_{o}^{'} \cdot \Delta V_{dc} \quad \text{(B.3)}$$

$$C \cdot p(\Delta V_{dc}) = \Delta D^{'} \cdot I_{mpo} + D_{o}^{'} \cdot \Delta I_{mpo} - \Delta I_{dc} \quad \text{(B.4)}$$

The DC-link:

$$V_{dco} \cdot \Delta I_{dc} + \Delta V_{dc} \cdot I_{dco} = V_{do} \cdot \Delta I_{d} + \Delta V_{d} \cdot I_{do} + V_{qo} \cdot \Delta I_{q} + \Delta V_{q} \cdot I_{qo} \quad \text{(B.5)}$$

$$\Delta I_{dc} = D_{o}^{'} \cdot \Delta I_{mp} + I_{mpo} \cdot \Delta D^{'} - C \cdot p\Delta V_{dc} \quad \text{(B.6)}$$

The INVERTER:

$$\Delta V_{d} = L \cdot p(\Delta I_{gd}) + R \cdot \Delta I_{gd} - \omega_{o} \cdot L \cdot \Delta I_{gq} - L \cdot I_{gqo} \cdot \Delta\omega_{PLL} - E \sin\delta_{o}\Delta\delta_{PLL} \quad \text{(B.7)}$$

$$\Delta V_{q} = L \cdot p(\Delta I_{gq}) + R \cdot \Delta I_{gq} + \omega_{o} \cdot L \cdot \Delta I_{gd} + L \cdot I_{gdo} \cdot \Delta\omega_{PLL} - E \cos\delta_{o}\Delta\delta_{PLL} \quad \text{(B.8)}$$

$$\Delta u_d = L_s \cdot p\Delta I_d \quad \text{(B.9)}$$

$$\Delta u_q = L_s \cdot p\Delta I_q \quad \text{(B.10)}$$

$$\Delta I_{gd} = \Delta I_d - \Delta I_{rd} - \Delta I_{ld} - \Delta I_{cd} \quad \text{(B.11)}$$

$$\Delta I_{gq} = \Delta I_q - \Delta I_{rq} - \Delta I_{lq} - \Delta I_{cq} \quad \text{(B.12)}$$

$$\Delta I_{rd} = \frac{\Delta V_d}{R_l} \quad \text{(B.13)}$$

$$\Delta I_{rq} = \frac{\Delta V_q}{R_l} \quad \text{(B.14)}$$

$$\Delta V_d = L_l \cdot p(\Delta I_{ld}) - \omega_o \cdot L_l \cdot \Delta I_{lq} - L_l \cdot I_{lqo} \cdot \Delta\omega_{PLL} \quad \text{(B.15)}$$

$$\Delta V_q = L_l \cdot p(\Delta I_{lq}) + \omega_o \cdot L_l \cdot \Delta I_{ld} + L_l \cdot I_{ldo} \cdot \Delta\omega_{PLL} \quad \text{(B.16)}$$

$$\Delta I_{cd} = C_l \cdot p\Delta V_d - \omega_o \cdot C_l \cdot \Delta V_q - C_l \cdot V_{qo} \cdot \Delta\omega_{PLL} \quad \text{(B.17)}$$

$$\Delta I_{cq} = C_l \cdot p\Delta V_q + \omega_o \cdot C_l \cdot \Delta V_d + C_l \cdot V_{do} \cdot \Delta\omega_{PLL} \quad \text{(B.18)}$$

$$p\Delta u_d = k_{pi} p(\Delta I_{dref} - \Delta I_d) + k_{ii} p(\Delta I_{dref} - \Delta I_d) \quad \text{(B.19)}$$

$$p\Delta u_q = k_{pi} p\left(\Delta I_{qref} - \Delta I_q\right) + k_{ii} p\left(\Delta I_{qref} - \Delta I_q\right) \quad \text{(B.20)}$$

$$p\Delta i_{dref} = -k_{pp} p\Delta V_{dc} - k_{ip}\Delta V_{dc} + k_{ip}\Delta V_{dcref} \quad \text{(B.21)}$$

$$p\Delta i_{qref} = -k_{pp} p\Delta Q - k_{ip}\Delta Q + k_{ip}\Delta Q_{ref} \quad \text{(B.22)}$$

$$p\Delta\delta_{PLL} = \Delta\omega_{PLL} \quad \text{(B.23)}$$

$$p\Delta\omega_{PLL} = k_{pPLL} p\Delta V_q + k_{iPLL}\Delta V_q \quad \text{(B.24)}$$

$$\Delta P = V_{do}\cdot\Delta I_d + I_{do}\cdot\Delta V_d + V_{qo}\cdot\Delta I_q + I_{qo}\cdot\Delta V_q \quad \text{(B.25)}$$

$$\Delta Q = V_{do}\cdot\Delta I_q + I_{qo}\cdot\Delta V_d - V_{qo}\cdot\Delta I_d - I_{do}\cdot\Delta V_q \quad \text{(B.26)}$$

The average model of the grid connected PV system is shown in Fig B.1.

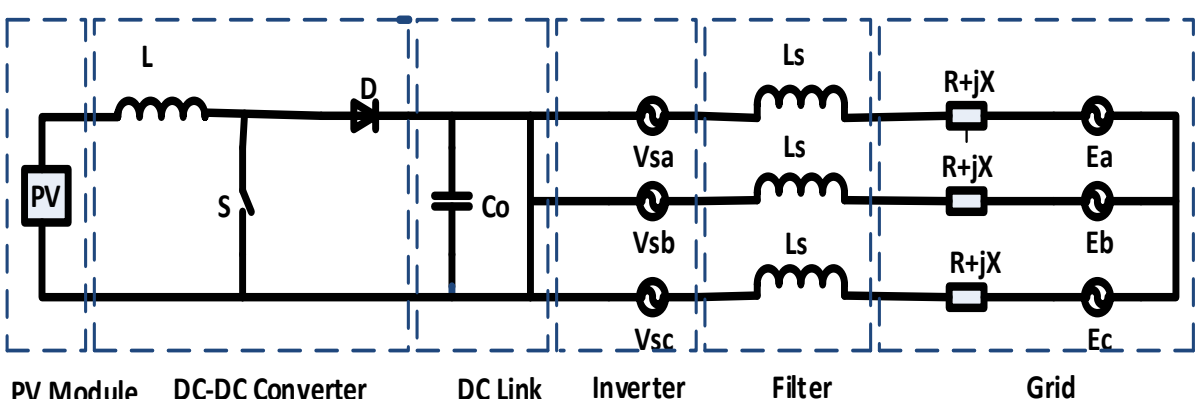

Figure B.1: Average model circuit of PV system connected to grid.

Appendix C

The state space representation of the system with PSS is expressed in the following matrix forms:

$$E\dot{\hat{x}} = A\hat{x}$$

The matrix E is represented as follows:

$$E = \begin{bmatrix} E_1 & E_2 \\ E_3 & E_4 \end{bmatrix}_{26*26}$$

$$E_1 = \begin{bmatrix}
L & 0 & 0 & 0 & 0 & 0 & 0 & 0 & 0 & 0 & 0 & 0 & 0 & 0 \\
0 & C & 0 & 0 & 0 & 0 & 0 & 0 & 0 & 0 & 0 & 0 & 0 & 0 \\
0 & 0 & -X/\omega_o & 0 & 0 & 0 & 0 & 0 & 0 & 0 & 0 & 0 & 0 & 0 \\
0 & 0 & 0 & -X/\omega_o & 0 & 0 & 0 & 0 & 0 & 0 & 0 & 0 & 0 & 0 \\
0 & 0 & 0 & 0 & L_s & 0 & 0 & 0 & 0 & 0 & 0 & 0 & 0 & 0 \\
0 & 0 & 0 & 0 & 0 & L_s & 0 & 0 & 0 & 0 & 0 & 0 & 0 & 0 \\
0 & 0 & 0 & 0 & 0 & 0 & -L_l & 0 & 0 & 0 & 0 & 0 & 0 & 0 \\
0 & 0 & 0 & 0 & 0 & 0 & 0 & -L_l & 0 & 0 & 0 & 0 & 0 & 0 \\
0 & 0 & 0 & 0 & 0 & 0 & 0 & 0 & -C_l & 0 & 0 & 0 & 0 & 0 \\
0 & 0 & 0 & 0 & 0 & 0 & 0 & 0 & 0 & -C_l & 0 & 0 & 0 & 0 \\
0 & 0 & 0 & 0 & k_{pi} & 0 & 0 & 0 & 0 & 0 & 1 & 0 & -k_{pi} & 0 \\
0 & 0 & 0 & 0 & 0 & k_{pi} & 0 & 0 & 0 & 0 & 0 & 1 & 0 & -k_{pi} \\
0 & k_{pp} & 0 & 0 & 0 & 0 & 0 & 0 & 0 & 0 & 0 & 0 & 1 & 0 \\
0 & 0 & 0 & 0 & 0 & 0 & 0 & 0 & 0 & 0 & 0 & 0 & 0 & 1
\end{bmatrix}$$

$$E_2 = \begin{bmatrix} 0 & 0 & 0 & 0 & 0 & 0 & 0 & 0 & 0 & 0 & 0 & 0 \\ 0 & 0 & 0 & 0 & 0 & 0 & 0 & 0 & 0 & 0 & 0 & 0 \\ 0 & 0 & 0 & 0 & 0 & 0 & 0 & 0 & 0 & 0 & 0 & 0 \\ 0 & 0 & 0 & 0 & 0 & 0 & 0 & 0 & 0 & 0 & 0 & 0 \\ 0 & 0 & 0 & 0 & 0 & 0 & 0 & 0 & 0 & 0 & 0 & 0 \\ 0 & 0 & 0 & 0 & 0 & 0 & 0 & 0 & 0 & 0 & 0 & 0 \\ 0 & 0 & 0 & 0 & 0 & 0 & 0 & 0 & 0 & 0 & 0 & 0 \\ 0 & 0 & 0 & 0 & 0 & 0 & 0 & 0 & 0 & 0 & 0 & 0 \\ 0 & 0 & 0 & 0 & 0 & 0 & 0 & 0 & 0 & 0 & 0 & 0 \\ 0 & 0 & 0 & 0 & 0 & 0 & 0 & 0 & 0 & 0 & 0 & 0 \\ 0 & 0 & 0 & 0 & 0 & 0 & 0 & 0 & 0 & 0 & 0 & -k_{pi} \\ 0 & 0 & 0 & 0 & 0 & 0 & 0 & 0 & 0 & 0 & 0 & 0 \\ 0 & 0 & 0 & 0 & 0 & 0 & 0 & 0 & 0 & 0 & 0 & 0 \\ k_{pp} & 0 & 0 & 0 & 0 & 0 & 0 & 0 & 0 & 0 & 0 & 0 \end{bmatrix}$$

$$E_3 = \begin{bmatrix} 0 & 0 & 0 & 0 & 0 & 0 & 0 & 0 & 0 & -k_{pPLL} & 0 & 0 & 0 & 0 \\ 0 & 0 & 0 & 0 & 0 & 0 & 0 & 0 & 0 & 0 & 0 & 0 & 0 & 0 \\ 0 & 0 & 0 & 0 & 0 & 0 & 0 & 0 & 0 & 0 & 0 & 0 & 0 & 0 \\ 0 & 0 & 0 & 0 & 0 & 0 & 0 & 0 & 0 & 0 & 0 & 0 & 0 & 0 \\ 0 & 0 & 0 & 0 & 0 & 0 & 0 & 0 & 0 & 0 & 0 & 0 & 0 & 0 \\ 0 & 0 & 0 & 0 & 0 & 0 & 0 & 0 & 0 & 0 & 0 & 0 & 0 & 0 \\ 0 & 0 & 0 & 0 & 0 & 0 & 0 & 0 & 0 & 0 & 0 & 0 & 0 & 0 \\ 0 & 0 & 0 & 0 & 0 & 0 & 0 & 0 & 0 & 0 & 0 & 0 & 0 & 0 \\ 0 & 0 & 0 & 0 & 0 & 0 & 0 & 0 & 0 & 0 & 0 & 0 & 0 & 0 \\ 0 & 0 & 0 & 0 & 0 & 0 & 0 & 0 & 0 & 0 & 0 & 0 & 0 & 0 \\ 0 & 0 & 0 & 0 & 0 & 0 & 0 & 0 & 0 & 0 & 0 & 0 & 0 & 0 \\ 0 & 0 & 0 & 0 & 0 & 0 & 0 & 0 & 0 & 0 & 0 & 0 & 0 & 0 \end{bmatrix}$$

$$E_4 = \begin{bmatrix} 0 & 1 & 0 & 0 & 0 & 0 & 0 & 0 & 0 & 0 & 0 & 0 \\ 0 & 0 & 1 & 0 & 0 & 0 & 0 & 0 & 0 & 0 & 0 & 0 \\ 0 & 0 & 0 & 0 & 0 & 0 & 0 & 0 & 0 & 0 & 0 & 0 \\ 0 & 0 & 0 & 0 & 0 & 0 & 0 & 0 & 0 & 0 & 0 & 0 \\ 0 & 0 & 0 & 0 & 0 & 0 & 0 & 0 & 0 & 0 & 0 & 0 \\ 0 & 0 & 0 & 0 & 0 & 0 & 0 & 0 & 0 & 0 & 0 & 0 \\ 0 & 0 & 0 & 0 & 0 & 0 & 0 & 0 & 0 & 0 & 0 & 0 \\ 0 & 0 & 0 & 0 & 0 & 0 & 0 & 0 & 0 & 0 & 0 & 0 \\ 0 & 0 & 0 & 0 & 0 & 0 & 0 & 0 & 0 & 0 & 0 & 0 \\ 0 & 0 & 0 & 0 & 0 & 0 & 0 & 0 & 0 & 0 & 0 & 0 \\ 0 & 0 & 0 & 0 & 0 & 0 & 0 & 0 & 0 & 0 & 0 & 0 \\ 0 & -k_{sp} & 0 & 0 & 0 & 0 & 0 & 0 & 0 & 0 & 0 & 1 \end{bmatrix}$$

The Matrix A values are as follows:

$$A = \begin{bmatrix} A_1 & A_2 \\ A_3 & A_4 \end{bmatrix}_{26*26}$$

$$A_1 = \begin{bmatrix} 0 & -D_o & 0 & 0 & 0 & 0 & 0 & 0 & 0 & 0 & 0 & 0 & 0 & 0 \\ D_o & 0 & 0 & 0 & 0 & 0 & 0 & 0 & 0 & 0 & 0 & 0 & 0 & 0 \\ 0 & 0 & R & -\omega_o L & 0 & 0 & 0 & 0 & -1 & 0 & 0 & 0 & 0 & 0 \\ 0 & 0 & \omega_o L & R & 0 & 0 & 0 & 0 & 0 & -1 & 0 & 0 & 0 & 0 \\ 0 & 0 & 0 & 0 & 0 & 0 & 0 & 0 & 0 & 0 & 1 & 0 & 0 & 0 \\ 0 & 0 & 0 & 0 & 0 & 0 & 0 & 0 & 0 & 0 & 0 & 1 & 0 & 0 \\ 0 & 0 & 0 & 0 & 0 & 0 & 0 & -\omega_o L_l & -1 & 0 & 0 & 0 & 0 & 0 \\ 0 & 0 & 0 & 0 & 0 & 0 & \omega_o L_l & 0 & 0 & -1 & 0 & 0 & 0 & 0 \\ 0 & 0 & 0 & 0 & 0 & 0 & 0 & 0 & 0 & -\omega_o C_l & 0 & 0 & 0 & 0 \\ 0 & 0 & 0 & 0 & 0 & 0 & 0 & 0 & \omega_o C_l & 0 & 0 & 0 & 0 & 0 \\ 0 & 0 & 0 & 0 & -k_{ii} & 0 & 0 & 0 & 0 & 0 & 0 & 0 & k_{ii} & 0 \\ 0 & 0 & 0 & 0 & 0 & -k_{ii} & 0 & 0 & 0 & 0 & 0 & 0 & 0 & k_{ii} \\ 0 & k_{ip} & 0 & 0 & 0 & 0 & 0 & 0 & 0 & 0 & 0 & 0 & 0 & 0 \\ 0 & 0 & 0 & 0 & 0 & 0 & 0 & 0 & 0 & 0 & 0 & 0 & 0 & 0 \end{bmatrix}$$

$$A_2 = \begin{bmatrix} 0 & 0 & 0 & 1 & 0 & 0 & 0 & 0 & 0 & 0 & 0 & 0 \\ 0 & 0 & 0 & 0 & -1 & 0 & 0 & 0 & 0 & 0 & 0 & 0 \\ 0 & -L/I_{gqo} & \cos\delta_o & 0 & 0 & 0 & 0 & 0 & 0 & 0 & 0 & 0 \\ 0 & L/I_{gdo} & -\sin\delta_o & 0 & 0 & 0 & 0 & 0 & 0 & 0 & 0 & 0 \\ 0 & 0 & 0 & 0 & 0 & 0 & 0 & 0 & 0 & 0 & 0 & 0 \\ 0 & 0 & 0 & 0 & 0 & 0 & 0 & 0 & 0 & 0 & 0 & 0 \\ 0 & -L_l * I_{lqo} & 0 & 0 & 0 & 0 & 0 & 0 & 0 & 0 & 0 & 0 \\ 0 & L_l * I_{ldo} & 0 & 0 & 0 & 0 & 0 & 0 & 0 & 0 & 0 & 0 \\ 0 & -C_l * V_{qo} & 0 & 0 & 0 & 0 & 0 & 0 & -1 & 0 & 0 & 0 \\ 0 & C_l * V_{do} & 0 & 0 & 0 & 0 & 0 & 0 & 0 & 0 & -1 & 0 \\ 0 & 0 & 0 & 0 & 0 & 0 & 0 & 0 & 0 & 0 & 0 & k_{ii} \\ 0 & 0 & 0 & 0 & 0 & 0 & 0 & 0 & 0 & 0 & 0 & 0 \\ 0 & 0 & 0 & 0 & 0 & 0 & 0 & 0 & 0 & 0 & 0 & 0 \\ -k_{ip} & 0 & 0 & 0 & 0 & 0 & 0 & 0 & 0 & 0 & 0 & 0 \end{bmatrix}$$

$$A_3 = \begin{bmatrix} 0 & 0 & 0 & 0 & 0 & 0 & 0 & 0 & 0 & 0 & 0 & 0 & 0 & 0 \\ 0 & 0 & 0 & 0 & 0 & 0 & 0 & 0 & 0 & 0 & 0 & 0 & 0 & 0 \\ 0 & 0 & 0 & 0 & 0 & -\omega_o * L_s & 0 & 0 & 1 & 0 & 1 & 0 & 0 & 0 \\ -1 & 0 & 0 & 0 & 0 & 0 & 0 & 0 & 0 & 0 & 0 & 0 & 0 & 0 \\ 0 & -I_{dco} & 0 & 0 & V_{sdo} & V_{sqo} & 0 & 0 & 0 & 0 & 0 & 0 & 0 & 0 \\ 0 & 0 & -1 & 0 & 1 & 0 & -1 & 0 & 0 & 0 & 0 & 0 & 0 & 0 \\ 0 & 0 & 0 & -1 & 0 & 1 & 0 & -1 & 0 & 0 & 0 & 0 & 0 & 0 \\ 0 & 0 & 0 & 0 & 0 & 0 & 0 & 0 & 1/R_l & 0 & 0 & 0 & 0 & 0 \\ 0 & 0 & 0 & 0 & 0 & 0 & 0 & 0 & 0 & 1/R_l & 0 & 0 & 0 & 0 \\ 0 & 0 & 0 & 0 & \omega_o * L_s & 0 & 0 & 0 & 0 & 1 & 0 & 1 & 0 & 0 \\ 0 & 0 & 0 & 0 & -V_{qo} & V_{do} & 0 & 0 & I_{qo} & -I_{do} & 0 & 0 & 0 & 0 \\ 0 & 0 & 0 & 0 & 0 & 0 & 0 & 0 & 0 & 0 & 0 & 0 & 0 & 0 \end{bmatrix}$$

$$A_4 = \begin{bmatrix} 0 & 0 & 0 & 0 & 0 & 0 & 0 & 0 & 0 & 0 & 0 & 0 \\ 0 & 1 & 0 & 0 & 0 & 0 & 0 & 0 & 0 & 0 & 0 & 0 \\ 0 & -L_s * I_{qo} & 0 & 0 & 0 & -1 & 0 & 0 & 0 & 0 & 0 & 0 \\ 0 & 0 & 0 & K_{mp} & 0 & 0 & 0 & 0 & 0 & 0 & 0 & 0 \\ 0 & 0 & 0 & 0 & -V_{dco} & I_{do} & I_{qo} & 0 & 0 & 0 & 0 & 0 \\ 0 & 0 & 0 & 0 & 0 & 0 & 0 & -1 & -1 & 0 & 0 & 0 \\ 0 & 0 & 0 & 0 & 0 & 0 & 0 & 0 & 0 & -1 & -1 & 0 \\ 0 & 0 & 0 & 0 & 0 & 0 & 0 & -1 & 0 & 0 & 0 & 0 \\ 0 & 0 & 0 & 0 & 0 & 0 & 0 & 0 & 0 & -1 & 0 & 0 \\ 0 & L_s * I_{do} & 0 & 0 & 0 & 0 & -1 & 0 & 0 & 0 & 0 & 0 \\ -1 & 0 & 0 & 0 & 0 & 0 & 0 & 0 & 0 & 0 & 0 & 0 \\ 0 & 0 & 0 & 0 & 0 & 0 & 0 & 0 & 0 & 0 & 0 & -1 \end{bmatrix}$$

The values for the following variables in the A matrix is defined in the following:

$$K = \frac{q}{n * N_s * k * T}$$

$$K_{mp} = -66 * I_o * \left(K + K^2 V_{mpo}\right)$$

By constructing these matrices we can conduct the small-signal stability analysis of the grid connected PV system with power system stabilizer. The eigenvalues can be obtained in MATLAB 2014b with the use of simple commands which involve the use of the two matrices E and A.

Bibliography

[1] G. M. Masters, *Renewable and Efficient Electric Power Systems*, 2nd ed., New York: John Wiley & Sons Inc., 2013, p.277.

[2] J. R. Katiraei, F. Agueero, "Solar PV integration challenges," IEEE power and energy magazine, vol. 9, pp. 62-71, JUN 2011.

[3] Z. Shahan. "World Solar Power Capacity Increased 35% in 2013 (Charts)". Internet: http://cleantechnica.com/2014/04/13/world-solar-power-capacity-increased-35-2013-charts/ , April 13, 2014.

[4] A. James "Total Global Solar PV Capacity Now Approaching or Over 100 GW". Internet: http://cleantechnica.com/2013/04/11/total-global-solar-pv-capacity-approaching-100-gw/, April 11, 2013.

[5] M. A. Eltawil, Z. Zhao, "Grid-connected photovoltaic power systems: technical and potential problems—A review", *Elsevier*, vol. 14, pp. 112-129, 2010.

[6] M.G. Villalva, E.R. Filho, J.R. Gazoli, "Comprehensive approach to modeling and simulation of photovoltaic arrays", *IEEE Transactions on Power Electronics,* vol. 24, no. 5, pp. 1198-1208, March 2009.

[7] H. Asano, K. Yajima, Y Kaya, "Influence of photovoltaic power generation on required capacity for load frequency control", *IEEE Transactions on Energy conversion,* vol. 11, no. 1, pp. 188-193, March 1996.

[8] V. Quezada, J. Abbad, T. S. Roman, "Assessment of energy distribution losses for increasing penetration of distributed generation", *IEEE Transactions on Power Systems,* vol. 21, no. 2, pp. 533-540, May 2006.

[9] T. Hoff, D.S. Shugar, "The value of grid-support photovoltaics in reducing distribution system losses," *IEEE Transactions on Energy Conversion,* vol. 10, no. 3, pp. 569-579, Sep. 1995.

[10] B.S. Rigby, R.G. Harley, N.S. Chonco, "Analysis of a power oscillation damping scheme using a voltage source inverter." *IEEE Transactions on Industry Applications,* vol. 38, no. 4, pp. 0093-9994, Jul/Aug 2002.

[11] Li Wang, Yuan-Yih, "Damping of a parallel ac-dc power system using PID power system stabilizers and rectifier current regulators," *IEEE Transactions on Energy Conversion,* vol. 3 no. 3, pp. 0885-8969, Sep. 1988.

[12] P Kundur, M. Klein, G. J. Rogers, M. S. Zywno, "Application of power system stabilizers for enhancement of overall system stability." *IEEE Transactions on Power Systems*, vol. 4, no. 2, pp. 614-621, May 1989.

[13] S. Ravichandran, S.G. Bharathi Dasan, Dr. R.P. Kumudini Devi, "Small signal stability analysis of grid connected photovoltaic distributed generator system," in *Proc.* 2011 *IEEE International Conf. on Power and Energy Sys.*, pp. 1-6.

[14] M.A Pai, D.P Sen Gupta, K.R Padiyar, "Small signal analysis of power systems", Narosa Publishing House, New Delhi, 2004.

[15] Li Wang, Ying-Hao Lin, "Dynamic stability analyses of a photovoltaic array connected to a large utility grid", in: *Proc. 2000 IEEE Power Eng. Soc. Winter Meeting*, vol. 1, pp. 476-480.

[16] Y. T. Tan, D. S. Kirschen and N. Jenkins, "A model of PV generation suitable for stability analysis", *IEEE Trans. Energy Convers.*, vol. 19, no, 4, pp. 748-755, Dec 2004.

[17] Rodriguez, G. A. J. Amaratunga, "Dynamic stability of a grid connected photovoltaic

systems", in: *Proc. 2004 IEEE Power Eng. Soc. Gen. Meeting,* Denver CO, USA, vol. 2, pp. 2193-2199.

[18] P. M. Anderson and A. A. Fouad, "Power System Control and Stability," Iowa State University Press, Ames, Iowa, 1978.

[19] R. Shah, N Mithulananthan and K. Y. Lee, "Design of robust power oscillation damping controller for large-scale PV plant," in: *Proc. 2012 IEEE Power and Energy Society Gen. Meeting* San Diego CA, USA, pp. 1-8.

[20] S. Y. Ruan, G. J. Li, B. T. Ooi and Y. Z. Sun, "Power system damping from real and reactive power modulations of voltage source converter station," *Generation, Transmission & Distribution*, *IET,* vol. 2, no. 3, 2008, pp. 311-320.

[21] A. Dysko, W. E. Leithead and J. O'Reily, "Enhanced power system stability coordinated by the PSS design," *IEEE Trans. on Power Systems*, vol. 25, no. 1, pp. 413-422, Feb. 2010.

[22] A. C. Zolostas, B. Chaudhuri, I. M. Jaimoukha and P. Korba, "A study on LQG/LTR control for damping inter-area oscillations in power systems," *IEEE Trans. Control Syst. Technol.*, vol. 15, no. 1, pp. 151-160, Jan. 2007.

[23] M. H. Khan and M. A. Abido, "Controller design of PV system to enhance the dynamic stability of smart grid network.", in Proc. *2011 IEEE PES Conf. Innovative Smart Grid Technologies-Middle East (ISGT Middle East),* pp. 1-5.

[24] P. Kundur, *Power system stability and control*, California: McGraw-Hill Inc., 1994.

[25] N. E. El-Kharbawe and S. O. Faried, "Damping inter-area oscillations using a static phase shifter," *2009 Canadian Conference on Electrical and Computer Engineering , St. John's NL*, pp. 575-578.

[26] G. Li, "Implementation of coordinated multiple facts controllers for damping

oscillations," *International Journal of Electrical Power & Energy Systems*, vol. 22, no. 2, pp. 79-92, Feb. 2000.

[27] M. Joorabian, M. Razzaz, M. Ebadi, M. Moghaddasian,"Employing fuzzy logic in damping power system oscillations using SVC," *2008 Second International Conf. on Electrical Engineering, Lahore,* pp. 1-5.

[28] M. Sedighizadeh, M. S. Toulabi, A. Rezazadeh, M. Khatibi, and B. Allahverdi-Charandabi, "Damping improvement by SSSC and STATCOM in a part of Iran electrical network," *2008 43rd International Universities Power Engineering Conference, Padova,* pp. 1-5.

[29] S. Ju Lee, H. Yong Park, G. Hun Kim, H. Ryong Seo, and M. H. Ali, "The experimental analysis of the grid-connected PV system applied by POS MPPT," *ICEMS, 2007 International Conference on Electrical Machines and Systems*, Seoul, pp. 1786-1791.

[30] X. Wang, W. Freitas, "Influence of voltage positive feedback anti-islanding scheme on inverter –based distributed generator stability," *IEEE Trans. on Power Deliv.* vol. 24, no. 2, pp. 972-973, Apr. 2009.

[31] R. G. Wandhare and V. Agarwal, "A modified control strategy for centralized PV- grid systems for assisting dynamic stability to overcome penetration issues," In: *Proc. 38th* 2012 *IEEE Photovoltaics Specialists Conf.,* Austin, TX, USA, pp.540-1544.

[32] P Kundur, M. Klein, G. J. Rogers, S. Moorty, "Analytical investigation of factors influencing power system stabilizers performance." *IEEE Transactions on Energy Conversion*, vol. 7, no. 3, pp. 382-390, Sep. 1992.

[33] J. Hernandez, N. L. Diaz and G. Gordillo, "Design-dimensioning models for grid-connected photovoltaic systems," In: *Proc. of the 9th IEEE Electrical Power & Energy Conf. (EPEC 2009),* Bogota, pp. 1-5.

[34] A. VanderMeulen and J. Maurin, "Current source inverter vs. Voltage source inverter topology," Whitepaper, WP020001EN, June 2014.

[35] R. Faranda and S. Leva, "Energy comparison of MPPT techniques for PV systems," *WSEAS Trans. on Power Systems*, Issue no. 6, vol. 3, pp. 1-6, June 2008.

[36] S. L. Brunton, C. W. Rowley, S. R. Kulkarni and C. Clarkson, "Maximum power point tracking for photovoltaic optimization using ripple-based extremum seeking control," *IEEE Trans. on Power Electronics*, vol. 25, no. 10, pp. 2531-2540, Oct. 2010.

[37] Timbus A., Liserre M., Teodorescu R., Blaabjerg F, "Synchronization methods for three-phase distributed power generation systems- An overview and evaluation," in *Proc. 2005 IEEE PESC,* pp. 2474-2481.

[38] G. Hsieh and J. Hung, "Phase-locked loop techniques- A survey," *IEEE Trans. Ind. Electron.* vol. 43, no. 6, pp. 609-615, Dec. 1996.

[39] S. Buso and P. Mattavelli, "Extension to Three-Phase Inverters" *Digital Control in Power Electronics*, ed. 1, Jerry Hudgins, USA: Morgan & Claypool, 2006, pp. 81-100.

[40] B. Huang, "Stability of Distribution Systems with a Large Penetration of Distributed Generation." Phd. Thesis, University of Dortmund, Dortmund, Germany, 2006.

[41] J. Machowski, J. W. Bialek and J. R. Bumby, "Power System Dynamics and Stability", New York: John Wiley & Sons Ltd. 1997.

[42] Leonard L. Grigsby," Power System Stability", in *Power System Stability and Control*, FL: CRC Press, 2007, pp. 7-1 – 7-7.

[43] W. Du, H. Wang and R. Dunn, "Power system small-signal oscillation stability as affected by large-scale PV penetration," in 2009 *Proc. of International Conference on Sustainable Power Generation and Supply,* Nanjing, pp. 1-6.

[44] V. John, Z. Ye, A. Kolwalkar, "Investigation of anti-islanding protection of power converter based distributed-generators using frequency domain analysis." *IEEE Transactions of Power Electronics,* vol. 19, no. 5, pp. 1177-1183, Sep. 2004.

[45] H. Malek, "Control of Grid-connected Photovoltaic Systems using fractional order operators," Ph.D. dissertation, Utah State University, Logan, Utah, 2014.

[46] A. Yazdani and et al, "Modeling guidelines and a benchmark for power system simulation studies of three-phase single-stage photovoltaic systems," *IEEE Trans. on Power Del.*, vol. 26, no. 2, pp. 1247-1264, April 2011.